

1N-34
22334
114P

NASA Technical Memorandum 109069



Direct Simulation Monte Carlo Prediction Of On-Orbit Contaminant Deposit Levels For HALOE

Michael S. Woronowicz
ViGYAN, Inc., Hampton, Virginia

Didier F. G. Rault
Langley Research Center, Hampton, Virginia

(NASA-TM-109069) DIRECT SIMULATION MONTE CARLO PREDICTION OF ON-ORBIT CONTAMINANT DEPOSIT LEVELS FOR HALOE (NASA, Langley Research Center) 114 p N95-11589
Unclas

G3/34 0022334

August 1994

National Aeronautics and
Space Administration
Langley Research Center
Hampton, Virginia 23681-0001



ABSTRACT

A three-dimensional version of the direct simulation Monte Carlo method is adapted to assess the contamination environment surrounding a highly detailed model of the Upper Atmosphere Research Satellite. Emphasis is placed on simulating a realistic, worst-case set of flowfield and surface conditions and geometric orientations for the satellite in order to estimate an upper limit for the cumulative level of volatile organic molecular deposits at the aperture of the Halogen Occultation Experiment (HALOE). Results pertaining to satellite environment are presented regarding contaminant cloud structure, cloud composition, and statistics of simulated molecules impinging on the HALOE aperture, along with data related to code performance. Using procedures developed in standard contamination analyses, along with many worst-case assumptions, the cumulative upper-limit level of volatile organic deposits on the HALOE aperture over the instrument's 35-month nominal data collection period is estimated at about 13,350Å.

ACKNOWLEDGEMENTS

M. S. W. supported by NASA Contract NAS1-19237. The authors appreciate the efforts of John Wells, Al Beswick, and the Contamination Group located at NASA Goddard Space Flight Center for their input and assistance.

TABLE OF CONTENTS

ABSTRACT	i
ACKNOWLEDGEMENTS	ii
TABLE OF CONTENTS	iii
LIST OF FIGURES	v
LIST OF TABLES	vi
NOMENCLATURE	vii
1.0 INTRODUCTION	1
2.0 CONTAMINATION ISSUES	2
3.0 NUMERICAL TOOLS	3
3.1 DSMC METHOD	3
3.2 PREPROCESSOR ROUTINES	4
3.2.1 Geometry Definition	4
3.2.2 Outgassing Inputs	6
3.2.3 Vent Plume Modeling	6
3.2.4 Global Resolution	6
4.0 APPLICATION TO UARS/HALOE CONTAMINATION	7
4.1 UARS/HALOE DESCRIPTION	7
4.2 PARALLEL CODE SCHEME	7
4.3 SPECIES WEIGHTING FACTORS	8
5.0 COMPUTATIONAL CONDITIONS	9
5.1 GEOMETRIC CONSIDERATIONS	9
5.1.1 Configurations	9
5.1.2 DSMC Resolution	11
5.2 FREESTREAM PARAMETERS	11
5.3 OUTGASSING SPECIES, FLUX RATES, & TEMPERATURES	12
5.3.1 Outgassing Species	12

5.3.2	Mass Flux Rates	12
5.3.3	Temperature Variation	13
5.3.4	Species Weighting Factors	14
5.4	CODE SETUP	14
6.0	RESULTS AND DISCUSSION	15
6.1	SPECIES NUMBER DENSITY	15
6.1.1	Case 1	16
6.1.2	Case 2	17
6.1.3	Case 3	18
6.2	CAPTURED MOLECULES-PRIOR COLLISIONS	18
6.2.1	Case 1	18
6.2.2	Case 2	19
6.2.3	Case 3	19
6.3	CAPTURED MOLECULES-VELOCITY PROBABILITY DISTRIBUTION FUNCTIONS	19
6.3.1	Case 1	19
6.3.2	Case 2	20
6.3.3	Case 3	20
6.4	MASS FLUX RATES	20
6.5	CUMULATIVE DEPOSIT LEVELS	21
6.6	COMPARISON WITH PREVIOUS ANALYSES	22
6.7	CODE PERFORMANCE	23
7.0	CONCLUDING REMARKS	23
REFERENCES	24
TABLES	26
FIGURES	92

LIST OF TABLES

Table		Page
1.	Library of Geometric Primitives	26
2.	Geometry Input Data Spreadsheet	31
3.	Input Data Listing—Geometric Model	32
4.	Input Data Listing—Subassembly Rotation Data	61
5.	Typical Elemental Outgassing Data	62
6.	Input Data Listing—Outgassing Information	63
7.	Input Data Listing—Surface Temperatures	82
8.	Typical Elemental Sonic Orifice Data	85
9.	Input Data Listing—General Preprocessor Input	86
10.	Outgassing Species Information	87
11.	Gas Species Data	88
12.	Mass Flux Rates Intercepted at the HALOE Aperture	89
13.	Subassembly Contributions to Cumulative Contaminant Deposition	89
14.	Cumulative Volatile Organic Contaminant Deposition at the HALOE Aperture	90
15.	Cumulative Volatile Organic Contaminant Deposition—Run-Averaged Total Deposition	91
16.	Simulation Set-Up and Performance	91

LIST OF FIGURES

Figure	Page
1. Geometric Representation of UARS and HALOE	92
2. Schematic Representation of Parallel Computing Arrangement	93
3. Cross-Sections of Inner Domain DSMC Grid Network	93
4. Cross-Section of Discretized UARS Geometry with Surface Normals	93
5. Number of Simulated Particles vs. Elapsed Time	94
6. Distribution of Particles per Simulated Cell	94
7. Number Density Contour Map, Freestream Species <i>O</i> , Case 1	95
8. Number Density Contour Map, <i>Ne</i> , Case 1	95
9. Number Density Contour Map, <i>CO</i> ₂ , Case 1	95
10. Number Density Contour Map, <i>GMW</i> = 100 Species, Case 1	96
11. Number Density Contour Map, <i>GMW</i> = 150 Species, Case 1	96
12. Number Density Contour Map, <i>GMW</i> = 200 Species, Case 1	96
13. Number Density Contour Map, All Species, Case 1	97
14. Number Density Contour Map, All Species, Case 2	98
15. Number Density Contour Map, All Species, Case 3	99
16. Number of Surface Collisions Prior to Striking the HALOE Aperture	100
17. Species Velocity Probability Distribution Functions, Case 1	101
18. Species Velocity Probability Distribution Functions, Case 2	102
19. Species Velocity Probability Distribution Functions, Case 3	103
20. Measured On-Orbit HALOE Voltage Signal Strength vs. Elapsed Time	104

NOMENCLATURE

CCM	Coarse Cartesian Mesh
CLAES	Cryogenic Limb Array Etalon Spectrometer
CO_2	carbon dioxide
DSMC	direct simulation Monte Carlo
FCM	Fine Cartesian Mesh
$FNUM$	ratio of real to simulated molecules
GMW	gram molecular weight
HALOE	Halogen Occultation Experiment
HGA	High Gain Antenna
IM	Instrument Module
LDEF	Long Duration Exposure Facility
MLI	Multi-Layered Insulation
MMS	Multi-mission Modular Spacecraft
Ne	neon
NEPS	Nadir Energetic Particle Spectrometer
O	monatomic oxygen
SP	Solar Panel
SI	International System of metric units
SSPP	Solar/Stellar Positioning Platform
SWF	species weighting factor
T	absolute temperature [K]
UARS	Upper Atmosphere Research Satellite
V_x, V_y, V_z	directed velocities
X, Y, Z	coordinate directions
ZEPS	Zenith Energetic Particle Spectrometer
l	length scale [\AA]
n	number density [m^{-3}]
t	relative temperature [$^{\circ}C$]
Δt	time increment [sec]
Ω	solid angle [steradians]
α	HALOE azimuth angle

β	angle describing UARS-Sun relationship
θ	HALOE elevation angle
τ	period [<i>min</i>]
$\dot{\phi}$	mass flux rate [<i>gm/cm²/sec</i>]
ω	exponent in power-law viscosity-temperature relationship

Subscripts:

j	species index
s	satellite condition
ss	steady state condition
∞	freestream condition

1.0 INTRODUCTION

The Upper Atmosphere Research Satellite (UARS) was designed to collect data on various aspects of Earth's upper atmosphere to help characterize global atmospheric changes that are thought to be occurring. Figure 1 depicts the UARS model used in this investigation. One instrument carried on board the currently-operational satellite is the NASA Langley Halogen Occultation Experiment (HALOE). During each sunrise and sunset experienced by the satellite, the HALOE instrument peers at the Sun through the atmosphere and measures solar infrared energy absorption over a range of wavelengths. With this information, vertical distributions for concentrations of trace gases such as HF , HCl , and O_3 are deduced.¹

In order to obtain precise measurements, HALOE optical surfaces must be kept extremely clean. Experience shows that even minute amounts of contamination can seriously degrade the spectral transmissivity and reflectivity of optical surfaces.² Although atmospheric density is extremely low at the satellite orbit altitude of 600 km , there are many potential sources of contamination contained on board UARS itself, ranging from light gases to heavy, long-chain polymers. Volatiles outgassed from certain materials used in satellite construction, gases vented from the interior of the satellite and cryogenically-cooled experiments, and effluents exhausted from attitude thrusters, all contribute to a gas cloud that envelops the vehicle.

Previous analyses have indicated that the cumulative level of deposits on critical HALOE optical surfaces over its nominal 35 months of operation could exceed maximum acceptable levels by over an order of magnitude.³ While UARS instrument managers specified a goal of no more than 100 \AA of cumulative deposits at the HALOE aperture, analyses predicted for its original set of orientations that it would receive about $32,170\text{ \AA}$.³ A recommended change adopted in stowing positions for HALOE reduced that estimate to about 6188 \AA .³ These analyses utilized SPACE2⁴ and MOLFLUX,⁵ which are standard engineering codes developed for estimating fluxes on target surfaces due to outgassing. These codes either assume no intermolecular collisions within the gas cloud or employ first-collision theory.

Because of the important effect of contamination on the success of the HALOE data collection effort, detailed characteristics of the gas cloud in the vicinity of the HALOE aperture are needed to accurately estimate incident contaminant fluxes and to help define criteria for optimal operation of the instrument. In order to facilitate this goal, a study of the contamination environment surrounding UARS was performed using the direct simulation Monte Carlo (DSMC) technique.^{6,7}

This report describes details of the investigation, emphasizing methods used and assessment of input data and assumptions. First, a discussion of issues important to satellite contamination is presented, followed by a general description of the DSMC method and preprocessors specifically developed to handle various necessary input conditions and geometric orientations required for the investigation. This discussion is then followed

by a description of specific data pertinent to contamination of the HALOE instrument on board UARS. Results include simulated flowfield species number density maps describing the overall gaseous environment surrounding UARS, and statistical details regarding the fluxes intercepted at the HALOE aperture. Also, results regarding predictions of cumulative contaminant deposit levels are presented and interpreted, and code performance statistics are mentioned.

2.0 CONTAMINATION ISSUES

Satellites tend to surround themselves with their own artificial atmosphere through surface outgassing, equipment venting, and attitude thruster firing. This artificial atmosphere typically has very low density, and its overall distribution is usually anisotropic and non-Maxwellian. It is composed of species having a wide range of molecular weights, including massive, long-chain, volatile organic compounds, and is characterized by a wide range of concentrations, with some important species present only at trace levels.

The molecular flux of contaminants incident on a spacecraft surface has traditionally been subdivided into two categories: direct and return flux. Freestream or outgassing molecules directly impinging on a critical target surface that may have encountered prior collisions with other surfaces, but no intermolecular collisions with other gas species, belong to the direct flux. Outgassing molecules having undergone intermolecular collisions before reaching the target surface belong to the return flux. Direct flux computation is relatively straightforward for diffuse surfaces (geometric viewfactors or particle tracing), but return flux computation, which requires an integrated knowledge about the contaminant cloud structure and collision physics, is intrinsically more complex. It also requires that a relatively large computational domain surround the satellite to ensure that the simulation satisfactorily accounts for virtually all molecules which can return to the vehicle surface, regardless of how far they ventured away from the satellite before being scattered back.

The physics involved in contamination processes, such as surface desorption, reflection, absorption, adsorption, etc. are very complex. The experimental database is presently insufficient to devise accurate models to simulate mechanisms such as surface outgassing (flux magnitude as a function of surface temperature and material composition, emitted angular velocity distribution, and species composition), surface deposition and polymerization (effects of ultraviolet radiation, atmospheric monatomic oxygen flux, and surface material), and surface reflection (momentum and energy accommodation, reflected angular velocity distribution). Reliable estimates of the contamination environment surrounding future spacecraft will therefore require improving the present state of knowledge. The molecule-based DSMC algorithm is readily amenable to incorporate new physical models as these become available. DSMC could therefore be used to evaluate these models and foster new research in this field.

3.0 NUMERICAL TOOLS

In this section, the method used to investigate HALOE on-orbit instrument contamination is presented, along with preprocessing routines developed to assimilate data concerning geometric configurations and outgassing required to provide detailed simulations. First, a general description of the DSMC method is presented, followed by a brief presentation describing the various preprocessing routines used, many of which have been specifically developed to handle outgassing emission data.

3.1 DSMC METHOD

The direct simulation Monte Carlo method has been steadily gaining acceptance as an approach to solving problems related to fluid dynamics when the effects of rarefaction become important and the gaseous medium no longer behaves as a continuum.⁸ In contrast to the approach of Computational Fluid Dynamics (CFD), where the gas is treated as a continuum mathematical fluid, macroscopic flowfield properties are calculated based on the interactions of many thousands or millions of particles that behave as molecules at the microscopic level.⁸

In the DSMC method, the simulated flowfield volume is discretized into a network of subcells, and the ensemble of particles constituting the gas is allowed to develop in time, where time is discretized into small increments over which the processes of molecular collisions and molecular motion are decoupled. The subcells are used to help identify nearest-neighbor prospective collision partners. The flowfield evolves in time from an initial, specified configuration, and once it reaches steady state, cumulative statistics on the gas are kept by the computer for small numbers of subcells grouped together to form cells. By specifying the intermolecular potential governing the behavior of collisions between the simulated molecules, or "particles," and by using concepts of kinetic theory and statistical mechanics to sample the flowfield at the subcell or cell level, one can establish macroscopic flowfield characteristics.

Although the true intermolecular potential for most interactions are unknown, a number of simple models are available which give reasonably accurate macroscopic behavior. The potential commonly used in contemporary DSMC applications is the Variable Hard Sphere (VHS) model.⁸ In this model, the hard-sphere assumption of uniform, isotropic scattering is retained, but collision cross-sections become proportional to the relative velocities between molecules.⁸ The VHS model has been employed in this investigation.

The DSMC outgassing model has been widely used in other applications,^{9,10} and is assumed to be valid in this investigation. It assumes that molecules of an outgassing species are emitted from specified surfaces at given rates, with velocities sampled from a drifting Maxwellian velocity distribution at a given temperature.

The DSMC code used in the present study was devised by Bird¹¹ and modified by Rault.^{6,7,12} High com-

putational efficiency is achieved with this code through the use of an unstructured cell network overlaid on a cubic Cartesian subcell mesh. Two levels of subcells are employed in this particular code. A fine scale mesh (FCM) is used to resolve high flowfield gradients that often occur near windward-side surfaces, and a coarser mesh (CCM) is used farther away to conserve computational resources and to improve statistically-based calculations in regions where overall density levels are low. The individual subcells at the FCM level are referred to as "pixels." When available, comparisons between results generated with this code and experimental measurements regarding surface and flowfield properties for flows around a wide variety of vehicles have yielded excellent agreement.^{12,13} The code has recently been optimized for vector architecture supercomputers, and has been complemented with a set of utilities for diagnosis, preprocessing, postprocessing, and grid adaptation.¹² Grid adaptation of the cell network with respect to certain variables can enhance resolution of flowfield phenomena as well as surface fluxes.

Special coding has been developed to collect information regarding particles striking the HALOE aperture. Such data include particle velocity, position where the aperture plane has been struck, species type, etc. In order to distinguish molecules belonging to the direct flux or the return flux, a parameter has been added to the run code to store the number of surface and intermolecular collisions each particle encounters prior to reaching the aperture. An additional parameter, storing information identifying the originating surfaces of these outgassed molecules, helps indicate which surfaces dominated the influence of volatile species fluxes at the aperture plane.

A novel additional capability featured in this simulation is the introduction of a parallel processing technique to separate the flowfield into two domains. This option allows higher resolution in the inner domain, combined with a larger outer domain for computing return flux, than would be possible if the resources of only a single computer were available. Implementation of this technique is discussed further in Section 4.2.

3.2 PREPROCESSOR ROUTINES

3.2.1 Geometry Definition

To define and input the inherently complex geometry of typical satellites, the interactive three-dimensional CAD preprocessor developed by Rault is used.^{6,7} This preprocessing utility relies on the fact that even a very complex body geometry can be decomposed into a series of simple geometric primitives, such as spheres, cylinders, planes, etc. or portions thereof.^{6,7} The current set of 16 basic primitives is presented in Table 1. UARS is modeled using 385 of these primitive subelements, and the resulting geometric model is displayed in Fig. 1. Also shown in the figure is the relative coordinate system used in this investigation, and details of the HALOE instrument in Figs. 1b-1d. As described in Ref. 6, properties of these subelements are entered

into the preprocessor code through an input file. Typical input data are presented in Table 2. After listing data associated with the overall configuration of the flowfield volume, a series of fields describe the type of each subelement, its dimensions, location, and orientation. Since the DSMC code assumes SI units, use of any other system requires conversion using the "scale" factor. In Table 2, lengths had been measured and entered in inches, requiring "scale" to be set to 0.0254.

Other entries displayed in Table 2 also require further explanation. Certain types of geometric elements can be completely described by quadratic functions. These elements are categorized under "quadratics," and are handled analytically by the DSMC code. Other planar surfaces, such as rings and disks, where limits cannot adequately be described by quadratics, are simply referred to as "planes," and are stored as a number of points with high resolution. This resolution must be higher than that used to discretize the surfaces for incorporation into the DSMC code for high fidelity.^{11,12} In this study, these two groups encompassed all types of subelements used. In other studies, nonplanar surfaces of arbitrary complexity are defined in similar fashion to the rings and disks used here.¹²

Since subassemblies or components constituting the satellite are represented in the code by groups of geometric subelements, these subelements may be linked by a common "component number." Defining a unique color to represent each component number can be useful in geometry visualization to highlight or otherwise distinguish individual components. References to "limit planes" in Table 2 pertain to the fact that these surfaces are discretized within the DSMC framework and replaced by small cubes.¹¹ Along certain edges where surfaces should intersect, small gaps may occur as a result of the discretization process. This problem occurs most frequently where surfaces intersect at oblique angles. Since the flowfield cell network is built up in layers from surfaces, these gaps will allow the interior to be filled with flowfield cells, which consumes computational resources and may lead to confusing errors.¹² Limit plane displacement lengthens or widens the original subelement to eliminate those gaps. Finally, the entry fields identified as "F3I limits" refer to a subordinate volume contained within the flowfield where the particular subelement lies. This information is used to speed up the discretization process by telling the code to check for a particular surface only within that subvolume instead of searching the entire flowfield.

Dimensions and locations for various facets of the UARS satellite have been obtained from engineering drawings provided by HALOE instrument managers, and a complete listing of the data entered for the baseline geometric representation is presented in Table 3. Code has been developed to alter subassemblies of the geometric UARS model by taking the baseline geometry file listed in Table 3, and rotating the required subelements about a given axis at a given point. The input files for cases studied are displayed in Table 4, and the output resembles Table 3, except that values for the affected subelements have been duly altered.

3.2.2 Outgassing Inputs

Code has been developed to process information pertaining to individual outgassing surfaces for incorporation into the general DSMC run code. These input files include subelement-level information pertaining to the outgassing flux at a given reference temperature, and the molar composition of the outgassing flux. Table 5 is an example of typical outgassing information, and Table 6 is a reproduction of the input file for outgassing information used in this investigation. The values listed before each outgassing rate are species mole fractions for each of the six species modeled.

The preprocessor code contains enough flexibility to process information on whether or not an individual subelement is composed of several regions outgassing different species at different rates. This capability has been used to create vent sources on certain surfaces of the Instrument Module (IM) by superimposing vent locations, flux rates, and gas constituents on existing larger elements. An example is illustrated in the data fields associated with the first geometric element in Table 6. Since outgassing rates are strongly dependent on surface temperature, additional coding has been developed to assign a unique value to each satellite surface. A listing of subelement-level temperatures in °C is presented in Table 7.

3.2.3 Vent Plume Modeling

In addition to outgassing information, a preprocessing routine for handling jet-like vent plumes from sonic orifices has been developed. Whereas effluents outgassed from surfaces and exiting most vents diffuse into the flowfield with modeled velocity distributions resembling drifting Maxwellian distributions at T_{surface} , "jet" sources represent relatively high mass flux rates exiting small orifices as choked, uniform flow at a supplied exit temperature T_{exit} . The data necessary to recreate such sources are shown in Table 8.

3.2.4 Global Resolution

Finally, Table 9 lists inputs used by the DSMC code in order to initialize the overall simulation. Some of the input variables are simply switches used to tailor the code to the problem at hand with respect to where high grid resolution is needed, sizing maximum lengths for Fortran arrays, information required for setting reasonable estimates for DSMC simulation parameters, flow direction with respect to the body, and the like.¹²

4.0 APPLICATION TO UARS/HALOE CONTAMINATION

4.1 UARS/HALOE DESCRIPTION

UARS was placed in orbit in September 1991 to probe Earth's upper atmosphere and characterize global atmospheric changes which are thought to be taking place. It operates at a roughly circular 600km altitude orbit with a 96-minute period (τ). Depicted in Fig. 1, UARS is about 10.3m long, 5.9m high, 3.2m wide, and its solar panel (SP) measures 13.3m by 3.3m.

Several instruments have been mounted on the Instrument Module (IM), including HALOE, (an occultation viewing radiometer that requires part per million signal precision and characterization¹), the Cryogenic Limb Array Etalon Spectrometer (CLAES), and the Nadir and Zenith Energetic Particle Spectrometers (NEPS and ZEPS). The High Gain Antenna (HGA) receives signals from UARS mission controllers, and the Solar/Stellar Positioning Platform (SSPP) assists in navigating the satellite. The Multi-mission Modular Spacecraft (MMS) is used to periodically boost or maneuver the satellite in accordance with mission guidelines.

UARS is designed to always keep the side with HALOE and the SP facing the Sun when it is over the horizon, but HALOE only takes measurements during sunrise and sunset, which occur once every period. At other times, whether the Sun is above or below the horizon, HALOE is stowed facing away from the freestream direction and the bulk of the satellite. Even though HALOE's stowed position has been chosen to minimize contamination from surface outgassing, it will periodically have substantial viewfactors from the continuously-rotating solar panel.

4.2 PARALLEL CODE SCHEME

As described in Section 3.1, the flowfield has been separated into two domains in order to increase grid resolution near the satellite and to create a large outer domain for computing return flux. Figure 2 shows a schematic representation of the computing arrangement. A different processor computes the solution in each domain independently, and Parallel Virtual Machine software from Oak Ridge National Laboratories has been implemented to allow the processors to communicate data between one another.¹⁴

The potential utility of this parallel routine software has been demonstrated even though an outer domain was not considered necessary for the scope of this particular investigation. Although the effect of return flux on HALOE is deemed insignificant, this feature could be useful in other contamination studies (at lower altitudes, for instance), where the far-field effect could play a more significant role. In this investigation, the inner domain takes on the shape of a right parallelepiped with dimensions slightly larger than the maximum

dimensions of UARS, and the outer domain is a cube. During a given timestep Δt , particles reaching or passing through the interface boundary separating the domains are moved to the boundary, and information required by the other processor for these entering particles is stored in a buffer. Data include particle position and velocity information, remaining fraction of Δt , individual species codes, and individual tag parameters. The buffer file is transmitted as a message to the other processor once each timestep.

It is reasoned advantageous to size the domains using the following equation:

$$\frac{FNUM_i}{FNUM_o} = \frac{\Delta t_i}{\Delta t_o} = \frac{V_i}{V_o} \propto \left(\frac{l_i}{l_o}\right)^3. \quad (1)$$

Concentrating on the first equality in Eq. (1), the need to clone or remove particles at the interfaces to ensure correct transmitted species flux levels is obviated. The second equality is an attempt to achieve roughly equal numbers of particles in each domain, a desirable feature which could result in roughly equal processor loadings under certain circumstances. One compromise inherent in Eq. (1) requires finding suitable timesteps for the different domains, such that when adequate temporal resolution in the inner domain is obtained, particles do not travel too quickly through the outer domain. Of course, shorter timesteps translate into longer run times.

4.3 SPECIES WEIGHTING FACTORS

Due to the large variation in species concentrations within a contaminant cloud, "species weighting factors" (*SWF*) have been implemented to artificially enhance minor species concentrations. Important species, such as the organic volatiles most likely to deposit and remain on critical surfaces, are usually present in trace amounts, and statistical sample sizes concerning these molecules would therefore be inadequate without the use of these weighting factors. The DSMC code has been modified by artificially increasing the outgassing flux of trace species by a species weighting factor, which in effect enables one to specify species-dependent values of *FNUM* to obtain reasonable numbers of each representative simulated species within the flowfield for better statistical property measurement. The only aspects of the simulation affected by this artifice are collision rates and quantities associated with flowfield sampling. These aspects may be accounted for by reducing bimolecular collision probabilities and cumulative species sampling summations by the same factors within the code.

The conditions under which *SWF*'s may be applied should be considered carefully, since mean free path lengths of trace species may be artificially increased when intermolecular collisions become important. Such an approximation is not considered a problem for the simulated UARS/HALOE environment.

5.0 COMPUTATIONAL CONDITIONS

This section describes details concerning the application of the tools mentioned above to the analysis of the UARS/HALOE contamination environment. First is a description of the geometric configurations that were considered to provide realistic worst-case estimates for deposits at the HALOE aperture, followed by assumed freestream and outgassing conditions.

5.1 GEOMETRIC CONSIDERATIONS

5.1.1 Configurations

For the set of assumptions associated with this approach, a realistic, conservative estimate for the cumulative level of contaminants deposited at the HALOE aperture must recognize that certain instruments rotate with respect to the rest of UARS over time. The solar panel (SP) continuously tracks the Sun, and the Solar/Stellar Positioning Platform (SSPP) undergoes limited movement as it alternately tracks the Sun and certain stars. HALOE faces the Sun during sunrise and sunset every 96-minute orbital period. Otherwise, it is stowed facing away from the freestream direction with severely restricted views of the rest of the satellite.³ Three different configurations have been chosen, representing a realistic worst case set of orientations. Two of these represent the beginning and end of the HALOE data collection period considered most deleterious with respect to contamination, and one represents the instrument in its stowed position after this data collection period.

Since the direct flux of outgassed molecules intercepted by a target surface is strongly dependent on the solid angle Ω subtended by the originating surfaces within the target's line of sight (viewfactor), cases have been chosen where HALOE collects data facing the $-X$ -direction (toward the Multi-mission Modular Spacecraft (MMS)). In this orientation, viewfactors subtended by the SP and the bulk of the satellite are maximized. In addition, since both the SP and HALOE track the Sun during HALOE data collection periods, the SP presents a large frontal area to the oncoming freestream, which could potentially contribute to increased overall number flux levels at the HALOE aperture. Movement of the SSPP has been ignored.

The angle between the HALOE aperture normal and the UARS body axis during data collection periods is equal to β , the angle between the Earth-Sun line and the plane of the satellite orbit.³ Angle β also plays a role in outgassing, since satellite surface temperatures are directly proportional to local surface inclination with respect to the Sun. For this particular orbit ($0^\circ \leq \beta \leq 80^\circ$), temperatures of influential surfaces are generally maximized when $\beta = 80^\circ$. One important exception is that trends for the SP surface temperatures run counter to the other objects. Due to the glancing angle it makes with the Sun at $\beta = 80^\circ$, SP surface

temperatures, and hence its outgassing rates, are minimized there. Conversely, SP surface temperatures are maximized when $\beta = 0^\circ$. The large SP surface area and its orientation with respect to HALOE make it a formidable influence on the latter's contamination environment. Another influential factor is that although the temperatures of the many influential outgassing surfaces are minimized at $\beta = 0^\circ$, their viewfactors are maximized with respect to HALOE for this orientation.

The three sets of geometric orientations studied in this investigation are listed below in expected descending order of severity. Angle α represents azimuth angle with respect to the UARS X axis, and θ represents elevation. Case 1 assumed $\alpha = -180^\circ$ and $\theta = 6^\circ$ (end of sunrise data collection period); Case 2 assumed $\alpha = -180^\circ$ and $\theta = -23.6^\circ$ (beginning of sunrise data collection period); and Case 3 assumed $\alpha = 45^\circ$ and $\theta = -25^\circ$ (stow position immediately prior to $\beta = 0^\circ$ sunset data collection period). Views of the geometric configurations for these cases are depicted in Fig. 1. Note that the SP location in Fig. 1c lies behind the HALOE aperture plane. The visual absence of that large, relatively high-temperature, outgassing object nearby should have a significant impact on the Case 2 contamination environment.

During each orbit at $\beta = 0^\circ$, HALOE collects data for a maximum total of 15 minutes (7.5 min. during each sunrise and sunset), and is stowed during the remainder of that period. Assuming that only the volatile species accumulate on critical optical surfaces, the average mass flux rate $\bar{\phi}$ per orbit per species j may be estimated by

$$\bar{\phi}_{j,\text{sunrise}} = \frac{\dot{\phi}_j|_{\theta=6^\circ} + \dot{\phi}_j|_{\theta=-23.6^\circ}}{2}, \quad (2)$$

$$\begin{aligned} \bar{\phi}_{j,\text{orbit}} = & \left(\frac{\tau_{\text{sunrise}}}{\tau_{\text{orbit}}} \right) \bar{\phi}_{j,\text{sunrise}} + \left(\frac{\tau_{\text{sunset}}}{\tau_{\text{orbit}}} \right) \bar{\phi}_{j,\text{sunset}} \\ & + \left(\frac{\tau_{\text{stow}}}{\tau_{\text{orbit}}} \right) \dot{\phi}_{j,\text{stow}}. \end{aligned} \quad (3)$$

In Eq. (2), linear behavior of $\dot{\phi}_j$ is assumed between the two cases, and in Eq. (3) for conservative estimates, $\bar{\phi}_{j,\text{sunset}} = \bar{\phi}_{j,\text{sunrise}}$, even though satellite IM-area viewfactors are lower for sunset viewing periods.

The probability that a contaminant molecule adheres to a critical surface is determined by its "sticking coefficient," a probabilistic parameter dependent on the combined effects of individual contaminant/surface material pairing, energy differences between contaminant molecules and the surface, and photopolymerization,¹⁵ among other things. Multiplying Eq. (3) by the number of orbits in the 35-month nominal HALOE lifespan and the area of the HALOE aperture, an upper bound for the total mass accumulated for each species may be calculated, assuming a sticking coefficient of unity. Neglecting the effects of highly-reactive O atomic flux on removing these deposits, such an assumption may be valid during data collection periods due to photopolymerization of volatile compounds on optical surfaces, but may considerably overestimate the mass accumulated while HALOE is stowed facing away from the Sun. Assuming values for the mass and volume

associated with each species, one can make a crude estimate for the depth of deposits at the aperture for each species. The total thickness becomes the summation of the contributions from each species.

5.1.2 DSMC Resolution

Figure 3 illustrates representative cross-sections of the inner domain cell network used for the present study after grid adaptation. Figure 3b shows the extent of the solar panel along with the rest of the vehicle. The body geometry is discretized and stored at the FCM level. Each element is characterized by a wetted surface area and a set of normal direction cosines. Figure 4 shows an XY-planar slice through the discretized geometry using a diagnosis utility developed for use with the DSMC code. In Fig. 4, pixels representing the surface are displayed along with outward direction cosines. Additionally, information on different levels of subcells surrounding the geometry can be represented. To simulate the UARS geometry, about 85,000 pixels have been used (pixel dimension $\approx 5.0\text{cm}$), and the inner domain computational grid is composed of 35,000 cells. All outgassing and venting particles enter the flowfield from positions adjacent to the center of the pixel face closest to the outward normal of the outgassing pixel, about 0.2 percent the distance represented by a pixel length scale inside the flowfield volume. This has been done to eliminate position round-off error. These particles are given velocity components sampled from a drifting Maxwellian at the local outgassing surface temperature.

5.2 FREESTREAM PARAMETERS

Assumed ambient conditions at the satellite operating altitude of 600km consisted of 100 percent atomic oxygen (O) at a nominal number density n_∞ of 6×10^{12} molecules/ m^3 .¹⁶ At this altitude, the density may vary from this standard in either direction by roughly an order of magnitude due to solar activity. In addition, solar activity can cause appreciable helium concentrations to develop at this altitude. For conservative calculations, assuming 100 percent O maximizes its presence, and since O is highly corrosive to certain satellite materials, and may actually reduce the cumulative level of deposits on critical optical surfaces, instrument managers may be interested in its interactions with the satellite. Of course, ambient collision rates are affected by number density and species constituency,¹⁷ however, using a single species to represent the freestream simplifies the simulation process, and it happens that UARS is operating in a period of low solar activity. These reasons may make the assumed level for n_∞ somewhat conservative. The assumed satellite orbital velocity V_s is 7500 m/sec .

5.3 OUTGASSING SPECIES, FLUX RATES, & TEMPERATURES

5.3.1 Outgassing Species

In preliminary calculations,⁶ two fictitious outgassing species were fabricated for demonstration purposes. One, with a gram molecular weight (*GMW*) of 200, was emitted from all outgassing surfaces. The other, with *GMW* = 100, was emitted only from the Instrument Module (IM) vent, located above the CLAES experiment.⁶ The *GMW*'s are similar to those used in standard industry contamination codes, and are associated with heavy, volatile, organic compounds.⁵

Further investigation into likely types of outgassing materials covering UARS focused on four different items. These were: Mylar, used in the Multi-Layered Insulation (MLI) covering most of the satellite; Chemglaze Z306, a black paint covering portions of some instruments (as well as the interior of HALOE); S/13G/LO-V10, a white paint covering portions of some instruments as well as the back side of the SP; and adhesives possibly used to affix components to the front of the SP. A report investigating the types and mass fractions of volatile components outgassing from these materials at different temperatures identified compounds such as alkanes, alcohols, organic acids, and aldehydes.¹⁸ Many components remained unidentified; however, taking the highest mass-fraction species identified for the materials listed above, a fictitious molecule with *GMW* close to each calculated average has been generated. Moreover, a fictitious species associated with venting from internally-carried components has been created. The *GMW* assumed for this material is 100, following standard contamination procedures.⁵ Values describing each of these species and their outgassing rates are listed in Table 10.

Collision cross-sections for these species ratioed to that for monatomic oxygen have been assumed to scale with the 2/3 power of the associated mass ratio (see Table 10).¹⁷ The mean viscosity-temperature power-law exponent ω is assumed to be 0.75, a value associated with *O*, and no chemistry has been considered. This information is contained within the input gas species file used by the DSMC code, which is presented in Table 11. Due to lack of information, it is not clear how well the collision dynamics of heavy, long-chain, polyatomic organic molecules are modeled by these assumptions, but since temperatures are moderate and density levels are extremely low, collision rates are assumed to be negligible.

All surfaces reflected particles diffusely, although evidence suggests incomplete momentum and energy accommodation better represent certain surfaces exposed to the vacuum of space for extended periods.¹⁹ Such behavior could affect the statistics of true fluxes encountered at the instrument aperture.

5.3.2 Mass Flux Rates

Measured mass flux rates associated with materials covering the instruments and subassemblies have been

obtained from Ref. 3, which lists data taken from a month-long bakeout test performed at NASA Goddard Space Flight Center on the completed UARS satellite at 100 °C. In that report, rates were assumed for units lacking measured data. It was noted that the rate associated with MLI covering the satellite bus varied from a high initial level to a lower, constant level by the end of the test. In this study the lower, constant value was assumed, since the HALOE aperture remained closed for the first month in orbit as a precautionary measure against the initial, transient levels of MLI outgassing. Unfortunately, no information was given on the relative location of instruments measuring these rates with respect to the satellite, and some subassemblies feature surfaces sporting more than one type of covering. Since only one rate was listed per unit, such information had to be supplemented through judicious interpretation of photographs depicting various UARS subcomponents to determine what surfaces were covered with which material. These photographs were supplied by HALOE instrument managers and personnel at Goddard Space Flight Center. The mass flux rates for surfaces and coatings deduced from Ref. 3 are presented in Table 10.

In addition to outgassing surfaces, other gas-emitting sources have been modeled. The CLAES experiment is cryogenically cooled by gases contained in two separate reservoirs.²⁰⁻²² One reservoir contains *Ne*, the other *CO*₂. After cooling the instrument, these gases are expelled through vents. The *CO*₂ vent is located at the exit of a 1 in-diameter tube intersecting the CLAES shield plate, with direction cosines for the exit plane normal as (-.49, .64, .59) in the *X*, *Y*, *Z* coordinate system indicated in Fig. 1. The *Ne* vent is located at the end of a short, 2 in-diameter tube at the +*Z*-most section of the CLAES smaller cylinder, directed downward. The flow from these vent exits is assumed to be choked at an estimated temperature of $T_{\text{exit}} = 207\text{K}$.²² Mass flow rates for the *CO*₂ and *Ne* vents have been estimated at 3.65 and 8.39mg/sec, respectively. In this study, these sources have been modeled using the jet-like vent plume routines for sonic orifices mentioned above. Calculated outgassing rates for the CLAES vents are listed in Table 10.

Other vents, such as the IM vent, MLI blanket vents, and those associated with the MMS, released effluents at much lower flux rates, and have been modeled as regular surface-temperature dependent outgassing surfaces. Assumed *GMW*'s and outgassing rates associated with these vents are listed in Table 10.

5.3.3 Temperature Variation

Mass flux rates given in Ref. 3 for the bakeout test have been adjusted to reflect levels associated with realistic operating temperatures through use of the following empirical relationship, formulated to characterize generic mass flux behavior of polymeric materials on Skylab^{4,5} (*t* in °C):

$$\frac{\dot{\phi}_j(t)}{\dot{\phi}_j(t = 100\text{ }^\circ\text{C})} = \exp\left(\frac{t - 100}{29}\right). \quad (4)$$

This formula has been used to adjust all volatile organic compound outgassing rates. Although actual material outgassing rates probably deviate from Eq. (4), this formula is the only one available for use in

this investigation. Surface temperatures associated with various components have been estimated using data contained within Ref. 3, with one exception. UARS instrument managers provided solar panel operating temperatures which were measured in orbit. For $\beta = 0^\circ$, SP temperatures oscillate on orbit between -60°C and 30°C . The maximum SP temperature has been assumed for all cases, and values for other subassembly surfaces are listed in Table 7.

5.3.4 Species Weighting Factors

Upon commencement of the first DSMC computations, problems were encountered obtaining volatile fluxes at the HALOE aperture, because the outgassing rates associated with those species created flowfield number density levels orders of magnitude lower than those associated with the freestream and the CLAES vent species.⁷ In a single timestep, about 3300 simulated monatomic oxygen molecules would enter the upstream boundary (area $\cong 110\text{m}^2$), 30 simulated volatile, organic molecules of all types outgassed from the satellite (surface area $\cong 230\text{m}^2$), and 200,000 particles exited the CLAES vents (total vent exit area = $2.5 \times 10^{-3}\text{m}^2$). The number flux of volatiles in the inner domain is therefore about two billionths of that for the CLAES vent species. Thus, by adjusting computational resources to adequately simulate the dominant CO_2 and Ne environment, keeping the computational size of the simulation large enough to simulate $\sim 10^6$ particles, the simulation would completely lose track of the volatile species whose development was the motivation for engaging in this investigation.

The solution adopted has been to implement the species weighting factors discussed in Section 4.3. First, a simulation was run without the contributions of the CLAES vents in order to assess the ratio of volatile, organic species number density levels to the freestream. Another simulation included CLAES vent contributions in order to determine those density levels relative to those from the freestream as well. With information on the relative species number density levels, simulated fluxes of the various species have been altered using arbitrary *SWF*'s in order to obtain roughly equal orders of magnitude for numbers of each simulated species in the computational volume. The weighting factors used for O , Ne , CO_2 , and the volatile, organic species with $\text{GMW} = 100, 150, \text{ and } 200$ are 40, 1, 1, 10^3 , 10^4 , and 5×10^3 , respectively.

5.4 CODE SETUP

The methodology adopted for this study is to initially run the code for each set of conditions in a free molecule (collisionless) mode. Due to the large size of the satellite and the low thermal velocity of the heavy outgassing molecules, the approach to steady state is slow ($N_{ss} \cong 10^4 \Delta t$, where $\Delta t \approx 7\mu\text{sec}$). Figure 5 shows the number of particles in the inner and outer domains versus number of elapsed timesteps. Depending on

the type of problem being studied, the region where the curves flatten out may mark the onset of steady state. (While this rule-of-thumb may usually be adequate for measuring surface quantities, it is no panacea. For example, wakes behind bodies evolve over a long period of time without perceptible change in overall density levels.) Since exploratory calculations^{6,7} demonstrated that the global level of collisions was very low, the simulation is initially run in free molecule mode to reach an approximate steady state more quickly than if intermolecular collisions were allowed. After grid adaptation, each adapted cell contains roughly the same number of molecules (about 10 for the inner domain), as shown in Fig. 6. The code is then run with intermolecular collisions until a new steady state is reached. Subsequently, molecules incident on the HALOE aperture are counted, sampled, and written to a data file.

For the inner domain, high spatial resolution is necessary, since UARS is very complex and quite large ($\sim 10m$), and the HALOE aperture is only 22.9cm (9 in) in diameter. At the CCM level, the inner domain is composed of $74 \times 46 \times 104$ equal subdivisions of 15.1cm on a side. Each FCM subcell consisted of pixels having lengths three times smaller than the CCM level, resulting in a surface resolution of 5.0cm. Since overall density levels are lower in the outer domain, the physical domain could be simulated with much coarser resolution. The outer domain is a cube measuring 21.2m on a side, composed of $70 \times 70 \times 70$ subcells at the CCM level, with each FCM subcell having resolution equal to the CCM level.

6.0 RESULTS AND DISCUSSION

The wealth of information obtainable within a DSMC simulation will clearly be demonstrated in this section, as surface flux information is obtained along with flowfield behavior within the three-dimensional solution volume. First species number density contour maps will be presented, describing concentration levels surrounding the satellite, followed by results characterizing the fluxes incident on the HALOE aperture. The latter includes statistics concerning prior collisions, velocity distribution functions, and mass flux rates associated with simulated molecules impinging upon the aperture. This last item is manipulated to obtain a cumulative contamination deposit level. Finally, this cumulative level is compared to that of Ref. 3, and some code performance measurements are presented.

6.1 SPECIES NUMBER DENSITY

Figures 7-15 depict number density contour maps for each of the six gaseous species in the entire simulated flowfield surrounding UARS, ratioed to the freestream ambient number density, $n_{O,\infty}$ using a \log_{10} scale. This information is presented in two planes that capture information concerning the majority of the flowfield physics in the three-dimensional volume. One plane runs longitudinally, parallel to the main body axis, while

the other runs normal to it and the freestream direction.

For the first set of figures concerning Case 1 (Figs. 7-12), a longitudinal solution plane has been chosen that runs through the vehicle coincident with its main body axis (X -axis), while the transverse solution plane coincides with the streamwise location of the center of the CLAES Ne vent in order to capture a cross-section of the plume emanating from it. These planes have been picked to present the overall physical environment. For the remainder of these number density maps, planes have been chosen that better reflect the environment in the vicinity of the HALOE instrument.

The black outline surrounding UARS denotes the boundary separating inner and outer domains. While contributions of each species are presented separately, they co-exist simultaneously within the simulation.

6.1.1 Case 1

In Figs. 7a and 7b, contours for freestream species monatomic oxygen are presented for Case 1. In Fig. 7a, an expected buildup of O is observed on UARS windward side components. However, in initial DSMC calculations omitting the CLAES vents,⁶ and in subsequent calculations prior to grid adaptation, when intermolecular collisions have been disallowed, the maximum density level peaked at about 25 times the freestream level on the cylindrical face of the MMS.⁶ After grid adaptation and allowing intermolecular collisions to occur, the maximum density ratio there becomes roughly 50 times the freestream level. It seems apparent that this density level increase is due to interaction of the freestream with the gases emitted from the CLAES vents. Even though the global level of intermolecular collisions is low (about 130 collisions per timestep over 740,000 simulated molecules), the CLAES vent plumes create an effectively larger frontal area for UARS with respect to the freestream and scatter O out of the streamwise direction. An advantage of presenting these maps with a logarithmic scale is that the diminished levels of O in the wake of the vehicle are clearly evident. Figure 7b depicts the same set of contours viewed from the opposite side of the domain. The large, dark parallelogram jutting out from behind the transverse plane is the SP, canted 6° upward for this case.

In Figs. 8 and 9, number density contour maps are depicted for CLAES Ne and CO_2 vent gases. In Fig. 8a, the plume developing from the Ne vent exit is clearly captured. In the transverse plane, one can observe a sizable amount of upward scattering although the vent is pointed directly downward. This is likely the result of diffuse surface scattering from surfaces of the CLAES experiment, due to its proximity to the Ne vent. Figure 8b reveals that very little of the Ne plume extends into the $-Z$ regions. In Figs. 9a and 9b, the plume associated with the CO_2 vent is also clearly defined, although its axis is directed at oblique angles to both the streamwise and transverse planes.

In Figs. 10-12, number density contour maps are presented for the outgassing species. In Figs. 10a and 10b,

the entire vehicle is surrounded by outgassing of species with $GMW = 100$. The streamwise plane contour map above UARS is dominated by outgassing from the IM vent (located just above CLAES on the $+Z$ side of the satellite bus and angled 45° upward), although much of the concentration extending in front of the satellite is due to outgassing of adhesive material from the cell side of the SP (see Fig. 10b). The minor contribution to the flowfield from surfaces outgassing Chemglaze Z306 is shown in Figs. 11a and 11b ($GMW = 150$). These clouds originate chiefly from surfaces located on NEPS and ZEPS, although the interior of HALOE outgasses this material through its aperture. In Figs. 12a and 12b, $GMW = 200$ concentrations are presented. In the streamwise plane, the highest density levels are found near the HGA dish, although most of the outgassed material originates from the back side of the SP (Fig. 12b).

Results for this identical case are shown using two other planes that better depict the HALOE environment. The HALOE instrument is located in the center of each figure. In Fig. 13a, a buildup of O is clearly seen in front of HALOE and its mount. One also notices that the highest levels are found before the SP as it plows through the rarefied atmosphere. In Fig. 13b, even though the vast majority of Ne is directed downward on UARS' other side, there is a slight presence of that species in the vicinity of HALOE through a combination of surface and intermolecular collisions. As for CO_2 , in comparing streamwise plane results for Fig. 13c with Fig. 9b, where the former is displaced approximately $1m$ closer to HALOE than the latter in Fig. 9b, density levels for that species have abated by roughly an order of magnitude. No CO_2 flux was detected at the HALOE aperture.

Comparing streamwise planes from Fig. 13d with Fig. 10b for the $GMW = 100$ material, it becomes clear that the influence of the IM vent is greatly diminished over that $1m$ separation distance, and the local flowfield is dominated by the influence of the SP. In Fig. 13e, the contribution of the $GMW = 150$ material is globally quite minor, yet there is a relatively high concentration of it at the HALOE aperture, thanks to its own contribution. Finally, the concentrations of $GMW = 200$ material at the aperture are shown in Fig. 13f to be about an order of magnitude higher than for the previous figure, which is a consequence of the high concentrations of this material from the back side of the solar panel and the $-Z$ side of the Instrument Module.

6.1.2 Case 2

Planes chosen to represent the Case 2 flowfield solution (Figs. 14a-14f) are identical to those depicted in the last subsection, emphasizing the HALOE environment. The number density contour maps for this case are similar to those presented in the preceding two paragraphs. Besides the obvious repositioning of the SP and the HALOE instrument (-23° inclination versus 6° above), the most striking difference is in the map for the $GMW = 200$ material (Fig. 14f vs. Fig. 13f). The difference in SP inclination accounts for a dramatic

decrease of this material in the vicinity of HALOE.

6.1.3 Case 3

The general features presented in Figs. 15a through 15f are similar to the other two cases. Although the SP front face and HALOE no longer face the freestream, the SP rear face now opposes it. In Fig. 15a, the solar panel still impedes the motion of freestream O , but the position of the transverse planar solution cut reveals the wake behind it. In Fig. 15b, Ne is still present around HALOE, but HALOE's orientation 25° away from the body axis toward $-Z$ effectively shields its aperture from this gas. No Ne or CO_2 was detected at the aperture for this case (Figs. 15b and 15c).

Because the SP is roughly aligned with the $+X$ direction, the $GMW = 100$ contour density map in Fig. 15d shows a striking difference from the analogous Case 1 solution depicted in Fig. 13d above, where it is roughly aligned in the opposite direction. There is a reversal of which portions of the flowfield are densely and sparsely populated with this material. Even though HALOE is stowed, its viewfactor of the SP approaches that for Case 1 ($\Omega_{SP}|_{Case\ 3} = 0.412$ steradians versus $\Omega_{SP}|_{Case\ 1} = 0.527$ steradians). It will be shown shortly that in this configuration, there is still a surprisingly significant level of contaminant flux at the instrument aperture, mostly due to the SP. Fig. 15e shows the contribution from $GMW = 150$ material for this case, with local concentration maxima emanating from the HALOE aperture, NEPS, and ZEPS. Finally, in Fig. 15f, number density contours for the $GMW = 200$ material are presented, where once again, a reversal in high and low concentrations of this material are evident compared to Case 1 results in Fig. 13f.

6.2 CAPTURED MOLECULES—PRIOR COLLISIONS

There are a variety of statistics one can glean from simulated molecules striking the HALOE aperture. Two sets of information are presented in this section and the next. First, for each case, the history of each impinging simulated molecule is presented with respect to number of prior collisions it has suffered before reaching the aperture. Second, histograms are generated, representing the X , Y , and Z velocity probability distribution functions (PDF) for these same particles.

6.2.1 Case 1

In Figs. 16a-16c, plots are presented depicting the number of surface collisions prior to reaching the aperture for each species in each case. For Case 1, depicted in Fig. 16a, nearly 90 percent of O atoms reach the aperture directly from the freestream with no prior surface collisions. In contrast, all Ne atoms suffer at least two surface collisions before reaching this location. Outgassing molecules with $GMW = 100$ and 150 tend to encounter multiple surfaces before arrival, while most $GMW = 200$ material deposits directly from the back side of the SP and the $-Z$ side of the IM.

6.2.2 Case 2

In Fig. 16b, Case 2 collision history statistics for *O* are similar to those for Case 1. However, *Ne* atoms collected encountered at least five prior surface collisions before impinging on HALOE. This could be because the solar panel lies behind it in this run, and in its visual absence (zero viewfactor from the HALOE perspective), many other surfaces are required to facilitate the presence of neon. Again, outgassing molecules tend to encounter multiple reflections before arriving at the aperture, except for the *GMW* = 200 material. This material tends to collect from direct viewing of the $-Z$ side of the IM.

6.2.3 Case 3

Figure 16c shows that no *O* atoms directly encounter the aperture; most reflect once off the SP instead. Also, due to HALOE instrument orientation, no *Ne* is detected at all. *GMW* = 100 and 150 materials also tend to reflect once off the SP before impinging, but as in Case 1, *GMW* = 200 material emitted from the back side of the SP tends to arrive directly.

These figures do not reveal all information pertinent to *O*, whose distributions contain a rather long tail of multiply-reflected particles. The highest number recorded is 114 prior surface collisions for Case 1.

6.3 CAPTURED MOLECULES-

VELOCITY PROBABILITY DISTRIBUTION FUNCTIONS

6.3.1 Case 1

Figure 17 depicts Case 1 histograms representing the *X*, *Y*, and *Z* PDF for particles striking the aperture. Only *Ne* contributes any return flux; all other species have been deposited as the result of direct flux. Beginning with the *X*, or streamwise direction in Fig. 17a, notice that PDF(V_x) for *O* is bimodal. One mode, a full Maxwellian distribution centered at $V_x = V_s$, represents molecules having suffered no previous surface collisions. The other mode, corresponding to a drifting Maxwellian distribution near $V_x = 0$, represents molecules having previously collided with the satellite at least once. Figure 17b shows PDF behavior for V_x near the origin for better detail. In this figure, the volatile outgassing species have a streamwise PDF corresponding to drifting Maxwellian distributions whose shapes differ from one another due to individual *GMW*'s. These distributions have been checked and compare favorably with theoretical calculations, but for clarity's sake the theoretical functions for PDF(V_x) have been omitted from the figure. However, the *Ne* distribution does not conform to any simple theoretical model because the majority of *Ne* samples had experienced intermolecular collisions. In Figs. 17c and 17d, probability density functions are presented for the *Y* and *Z*, or transverse, directions. The *O* distributions behave as expected, as they are dominated by contributions from the freestream mode, and compare quite well with theory. Due to the complicated

nature of the geometric setup, no comparisons between these histograms and theoretical PDF's have been attempted in these directions.

6.3.2 Case 2

Figure 18 depicts Case 2 velocity PDF histograms. The X direction plot (Fig. 18a), generally appears similar to that for Case 1. However, the origin detail displayed in Fig. 18b shows that some portion of the flux has $V_x < 0$. Figs. 18c and 18d show that although O behaves as in Case 1, other species PDF's tend to be narrower and more peaked than in the previous case. This may be because overall viewfactors for HALOE are lower than Case 1, and impinging molecules come from a smaller, more select group of surfaces.

6.3.3 Case 3

In Case 3, there is no contribution from directly-impinging, freestream O atoms, so the distinct, bell-shaped Maxwellian mode associated with that species for Figs. 17a and 18a is not present in Fig. 19a. Although the mass flux associated with O still dominates the HALOE aperture environment, it is nearly two orders of magnitude lower than for the first two cases. The contribution from $GMW = 150$ molecules come entirely from the aperture itself, where emitted molecules reflect off the SP back towards HALOE. In Figs. 19b and 19c, most of the O flux has $V_y < 0$ and $V_z > 0$, indicating that it is constituted mostly from simulated atoms scattered downward and toward UARS from the SP, since that is the only assembly occupying $-Z$ space relative to HALOE.

6.4 MASS FLUX RATES

Individual species mass flux rates impinging on the HALOE aperture are presented in Table 12. Accuracy of these results rests heavily on the reliability of values for surface outgassing flux rates at the bakeout temperature, the use of Eq. (4) to adjust those rates for surface temperature, and the relative orientation and proximity of HALOE to the contributing surfaces. The rate for O has been subdivided into those atoms coming directly from the freestream and those having suffered prior surface collisions. Since a substantial portion of impinging Ne is attributed to return flux, while the rest reaches HALOE through surface collisions alone, two entries have been listed for Ne as well. Notice that fluxes from the outgassing species are orders of magnitude less than the others. Without using SWF 's, much longer run times would be required to achieve a reasonable sample sizes—possibly by a factor of many thousand.

Tables 13a-13c relate the relative contributions of different surfaces to the mass flux rates presented in Table 12. The SP is the chief progenitor of the HALOE contamination environment for all three cases. This is because it apparently attains the highest temperatures of any surface expected on the satellite for $\beta = 0^\circ$ (see Table 7), it is large, and it is located relatively near the HALOE aperture. The $-Z$ side of the IM

(second largest contributor), also represents a large outgassing surface near HALOE, but its contributions are diminished because its outgassing rates are lower than those of the SP, and its surface normal does not oppose the HALOE aperture.

Flux rates for Case 2 are significantly less than Case 1 due to reduced viewfactors of the main contributing outgassing surfaces. Included in Tables 13a-13c are viewfactors ([solid angle Ω] = steradians out of 2π) of the SP and the $-Z$ side of the IM experienced by the HALOE aperture. Ironically, Case 3 demonstrates that while a stowed HALOE instrument is exposed to very little direct flux from the bulk of UARS, it is sometimes prone to relatively high viewfactors of the continuously-rotating SP, periodically enhancing the pernicious contamination environment surrounding HALOE.

Also enhancing this environment is a contribution from the Chemglaze-painted surfaces within its interior, whose effluents are allowed to escape out through the aperture. Some of these molecules strike other surfaces and return to the HALOE aperture, and are counted along with the other contaminants.

6.5 CUMULATIVE DEPOSIT LEVELS

Eqs. (2) and (3) may be used to estimate an upper-bound cumulative total level of deposits at the HALOE aperture. Assuming that only volatile, organic molecules accumulate (with a sticking coefficient of unity), and each occupies the space of a cube of length l , where l equals the particular species diameter listed in Table 10, a deposit depth of $\approx 3550\text{\AA}$ is estimated. If standard contamination procedures are followed, and $l = 10\text{\AA}$ is assumed regardless of species diameter,³ that estimate increases to $\approx 13,350\text{\AA}$. If the contribution HALOE receives while stowed is disregarded (sticking coefficient of zero), these estimates fall to $\approx 650\text{\AA}$ and $\approx 2650\text{\AA}$, respectively.

Tables 14 and 15 show the species-level contributions from each run to the final, averaged estimates quoted above. It is interesting to observe how *GMW* factors into the second estimate described, which is a standard procedure in the contamination community.³ A greater number of lighter *GMW* species molecules are required for a mass flux equal to that of a heavier *GMW* species. Since the deposit depth of contaminant molecules only depends on the number that accumulate, it becomes important to accurately assess the *GMW*'s of the accumulated molecules. Also, the true sticking coefficient is not known, and can be much less than unity under certain conditions (small gas/surface temperature differences, absence of direct sunlight, etc.).¹⁵ Finally, the effects of scrubbing from the high monatomic oxygen flux on reducing the level of accumulants is not clear.

The effect of this predicted cumulative buildup on instrument performance is not clear. At this time, UARS has been in orbit for over two years, and the instrument has shown negligible loss in performance.

HALOE instrument managers have provided figures quantifying performance degradation in terms of signal strength attenuation for different species concentration measurements over the first year of operation. Signal voltages obtained over the first two months of operation were used to compute a standard expected signal voltage strength per channel, with instrument temperature corrections. Subsequent voltage strengths were measured and compared to the standard. Figures 20a and 20b show signal loss correlations for *HF* and *HCl* channel measurements, respectively. For initial standard voltages of ≈ 3.3 volts and ≈ 3.45 volts, after one year's operation, *HF* and *HCl* signal strengths have apparently been attenuated by 0.02 volts and 0.004 volts, respectively. This level of voltage attenuation is indicative of measurements made for the other channels used by HALOE as well. This may suggest that the concentrations of contaminants in the vicinity of the HALOE instrument have been overestimated in this as well as in previous studies, or that the effects of contamination from the types of outgassing materials carried on board UARS are relatively benign. Perhaps better understanding of volatile *GMW*'s, outgassing rates, temperature dependence on outgassing rates, gas/surface sticking coefficients, the cleansing effects of atomic oxygen, and light attenuation and scattering due to outgassing contaminants will come from the current examination of samples carried aboard the Long Duration Exposure Facility (LDEF).²³

6.6 COMPARISON WITH PREVIOUS ANALYSES

It is difficult to make detailed comparisons with the results described in Ref. 3 for a number of reasons. First, in Ref. 3, the orientations of the SP and HALOE were decoupled. The SP cellside surface was pointed downward at HALOE, minimizing the distance between the two objects. Meanwhile, HALOE was allowed to assume various orientations associated with data collection periods as well as possible stow positions. In reality, HALOE would be stowed pointing away from the SP when its cell side faces downward. Second, the earlier contamination analyses³ assumed a constant solar array surface temperature of 100 °C. This investigation benefitted from on-orbit data measured directly on the SP which indicate that $\beta = 0^\circ$ surface temperatures are cyclic with each orbit over a range of -60 °C to 30 °C. For the 30 °C value used in this study, Eq. (4) predicts that the SP would outgas only 9 percent of the value expected at 100 °C. Third, the earlier analyses assumed only one outgassing species ($GMW = 100$) to relate cumulative depth to mass fluxes. Obscuring detailed comparisons further, the earlier analyses could not take into account the fact that after the Goddard bakeout test, MLI blankets covering the instrument module surface on the $-Z$ side had themselves been covered with panels of S/13G/LO-V10 (which outgasses at mass flux rates one to two orders of magnitude higher than MLI—see Table 10). This had the impact of increasing assumed flux levels from those surfaces to HALOE. Finally, the geometry used in Ref. 3 was somewhat less detailed than in the

present study. Taking these differences into consideration, it seems that the results of this investigation tend to confirm those contained within Ref. 3 nevertheless.

6.7 CODE PERFORMANCE

The DSMC code is run simultaneously on two Sun SPARC 2 workstations with 64MBytes memory (RAM) each. Statistics concerning memory requirements, number of particles, weighting factor $FNUM$, timestep Δt , and overall computational volumes for the cases studied are listed in Table 16.

Regarding values for CPU time spent processing each region, it should be noted that $FNUM$ and Δt could have been adjusted to create better load balancing between the inner and outer domain processors. This was not a major goal of the study, however.

Computational performance for simulations using particle methods is often measured in terms of average CPU time taken to process the state of an average particle per timestep. Using this metric, levels of approximately 29 $\mu\text{sec}/\text{particle}/\text{timestep}$ and 44 $\mu\text{sec}/\text{particle}/\text{timestep}$ have been obtained in the outer and inner domains, respectively, with the difference chiefly due to handling outgassing surfaces in the latter. This is a fairly exotic application for DSMC however, and it may be difficult to compare this performance estimate to other results in a straightforward, detailed manner.

7.0 CONCLUDING REMARKS

This report describes the development and application of a DSMC code to study contamination problems on satellites and estimate the effect of outgassing on sensitive instruments. Discussion is included on the development of a number of specially-developed preprocessor routines to incorporate detailed information regarding geometry, outgassing rates and temperature data, different types of outgassing sources, and the use of species weighting factors to enhance the statistical representation of important trace species. In estimating the amount of volatile organic molecular deposits collected at the HALOE aperture, special attention has been given to accurately account for outgassing species characteristics, surface temperatures, and geometric orientation of UARS subassemblies deemed critical to this endeavor. Using the best information available, and neglecting the scouring effects of monatomic oxygen, an upper bound on the cumulative contaminant deposition level at the HALOE aperture has been estimated at 13,350Å. If there is negligible tendency for volatile species to accumulate while HALOE is stored, this value falls to 2650Å. Notwithstanding consideration of important differences in geometric orientation, outgassing species weights and flux rates, and other specific influential input data, it appears that these results tend to confirm the earlier work described in Ref. 3.

Although the model for outgassing contained in DSMC has often been compared to other methods,^{9,10,24} it could be instructive to make direct comparisons between results obtained using the DSMC method described in this report for a simple geometry over different ambient conditions with results from industry-standard codes and experimental data when they become available. Also, this study would benefit from better characterization of outgassing materials in terms of average molecular weights, mass flux rates, temperature dependence on mass flux rates, etc.

REFERENCES

- ¹ Gordley, Larry L., Russell, James M. III, and Hesketh, W. Donald, "Calibration, Testing and Orbital Performance of the Halogen Occultation Experiment (HALOE) on the Upper Atmosphere Research Satellite," *AIAA Paper 93-0128*, Jan. 1993.
- ² Robertson, S. J., "BGK Model Solution of Back Scattering of Outgas Flow from Spherical Spacecraft," *Progress in Astronautics and Aeronautics*, Vol. 51, Part I, July 1976.
- ³ Hatef, J. B., "Predicted Contamination of the HALOE," Goddard Space Flight Center Transmittal Memo 732-91-011, May 1991.
- ⁴ Anon., "Shuttle/Payload Contamination Evaluation Program—The Space Computer Program User's Manual," Martin Marietta Aerospace, *MCR-81-509*, Jan. 1981.
- ⁵ Anon., "MOLFLUX—Molecular Flux User's Manual," Structures and Mechanics Division, Materials Branch, Rev. 1, NASA Lyndon B. Johnson Space Center, Houston, Texas, *JSC-22496*, Feb. 1989.
- ⁶ Rault, D. F. G., and Woronowicz, M. S., "A Study of Instrument Contamination Aboard UARS Using Direct Simulation Monte Carlo," *AIAA Paper 93-0724*, Jan. 1993.
- ⁷ Woronowicz, M. S., and Rault, D. F. G., "On Predicting Contamination Levels of HALOE Optics Aboard UARS Using Direct Simulation Monte Carlo," *AIAA Paper 93-2869*, July 1993.
- ⁸ Bird, G. A., *Molecular Gas Dynamics and the Direct Simulation of Gas Flows*, 1st ed., Clarendon Press, Oxford, 1994.
- ⁹ Rantanen, R. O., and Gordon, T. D., "Contaminant buildup on ram facing spacecraft surfaces," *Proceedings of SPIE, Optical System Contamination: Effects, Measurement, Control*, ed. Peter Glassford, Vol. 777, May 1987.
- ¹⁰ Justiz, C., Sega, R., Dalton, C., and Ignatiev, A., "Return Flux Contamination of an Outgassing Spacecraft in Low Earth Orbit," *AIAA Paper 93-0725*, Jan. 1993.

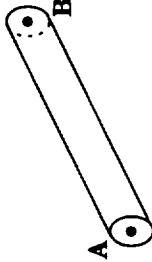
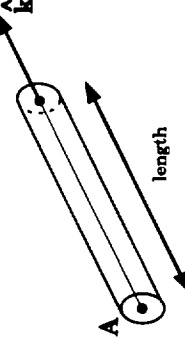
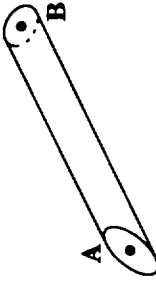
- ¹¹ Bird, G. A., "Application of the Direct Simulation Monte Carlo Method to the Full Shuttle Geometry," *AIAA Paper 90-1962*, June 1990.
- ¹² Rault, D. F. G., "Aerodynamics of Shuttle Orbiter at High Altitudes," *AIAA Paper 93-2815*, July 1993.
- ¹³ Rault, D. F. G., Wilmoth, R. G., and Bird, G. A., "An Efficient DSMC Algorithm Applied to a Delta Wing," *AIAA Paper 91-1916*, June 1991.
- ¹⁴ Beguelin, Adam, Dongarra, Jack, Geist, Al, Manchek, Robert, and Sunderam, Vaidy, "A Users' Guide to PVM Parallel Virtual Machine," *ORNL/TM-11826*, Oak Ridge National Laboratories, July 1991.
- ¹⁵ Bettini, Ronald G., "Shuttle environment effects on coated mirrors," *Proceedings of SPIE, Optical System Contamination: Effects, Measurement, Control*, ed. Peter Glassford, Vol. 777, May 1987.
- ¹⁶ *U. S. Standard Atmosphere, 1976*, U. S. Government Printing Office, Washington 25, D.C., 1976.
- ¹⁷ Vincenti, Walter G., and Kruger, Charles H., Jr., *Introduction to Physical Gas Dynamics*, 1st ed., Robert E. Krieger Publishing Company, Malabar, Florida, 1982.
- ¹⁸ Glassford, A. P. M., and Garrett, J. W., *WRDC-TR-89-4114*, "Characterization of Contamination Generation Characteristics of Satellite Materials," Materials Laboratory, Wright Research and Development Center, Air Force Systems Command, Wright-Patterson Air Force Base, Ohio, Nov. 1989.
- ¹⁹ Fredo, Richard M., and Kaplan, Marshall H., "Procedure for Obtaining Aerodynamic Properties of Spacecraft," *Journal of Spacecraft and Rockets*, Vol. 18, No. 4, 1981, pp. 366-373.
- ²⁰ Bortner, Dr. M. H., "Effect of Vented CO₂ and Neon on Performance of UARS Instruments," General Electric Astro Space Division, Valley Forge Space Center Program Information Release, *U-1K21-UARS-853*, June 1987.
- ²¹ Thames, M., "Spatial Density Distributions for UARS CLAES Ne and CO₂ Vents," General Electric Astro Space Division, Valley Forge Space Center Program Information Release, *U-1K20-UARS-878*, July 1987.
- ²² Neste, S. L., "Effect of CLAES Venting on UARS Performance," General Electric Astro Space Division, Valley Forge Space Center Program Information Release, *U-1K21-UARS-919*, Aug. 1987.
- ²³ "LDEF-69 Months in Space, Second Post-Retrieval Symposium," sponsored by LDEF Science Office, NASA Langley Research Center, and the American Institute of Aeronautics and Astronautics, ed. Arlene S. Levine, *NASA CP 9194*, June 1992.
- ²⁴ Fan, C., Gee, C., and Fong, M. C., "Monte Carlo Simulation of Molecular Flux on Simple Spacecraft Surfaces due to Self- and Ambient-Scatter of Outgassing Molecules," *AIAA Paper 93-2867*, July 1993.

Table 1: Library of Geometric Primitives (5 pgs.)

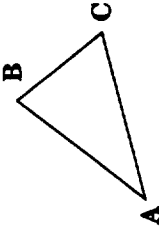
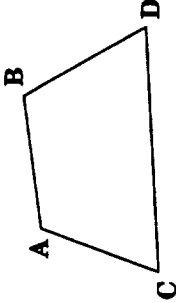
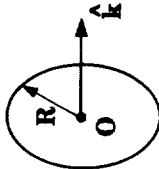
Geometry Definition for X Program: Cones

Name	Definition	Variables	Shape
ConeA	straight cone	half angle α apex A dir. cosine length	
ConeB	straight cone	apex A dir. cosine length exit radius	
ConeC	frustum	half angle α point A length dir. cosine radius at A	
ConeD	frustum	point A length dir. cosine radius at A radius at B	

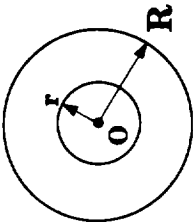
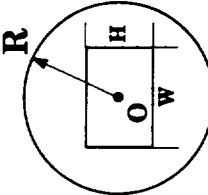
Geometry Definition for X Program: Cylinders

Name	Definition	Variables	Shape
CylinderA	straight cylinder	point A point B radius	
CylinderB	straight cylinder	point A radius dir. cosine length	
CylinderC	skewed cylinder	point A point B radius dir. cosine A dir. cosine B	

Geometry Definition for X Program: Plates

Name	Definition	Variables	Shape
PlateA	triangular plate	point A point B point C	
PlateB	four-sided plate (note order of successive pts.)	point A point B point C point D	
Disk			
Disk	circular disk	centerpoint dir. cosine radius R	

Geometry Definition for X Program: Rings

Name	Definition	Variables	Shape
RingA	concentric circular ring	centerpoint inner radius r outer radius R dir. cosine	
RingB	circular ring with centered rectangular hole	centerpoint radius R dir. cosine half height $H / 2$ half width $W / 2$	

Geometry Definition for X Program: Spheres

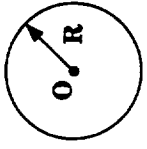
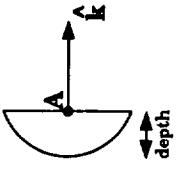
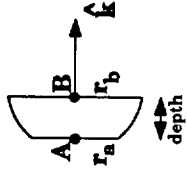
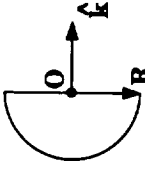
Name	Definition	Variables	Shape
SphereA	complete sphere	centerpoint radius R	
SphereC	portion of sphere	point A depth dir. cosine	
SphereD	spherical section (A & B same side as center)	point A depth dir. cosine radius at A radius at B	
SphereE	hemispherical cap	centerpoint dir. cosine radius R	

Table 2: Geometry Input Data Spreadsheet

Data	Description
27 347 0.0254 100. 1. -20. -80. 327. -100. 110. -515. 90. 100. 1. -20. 10000. 300.	no. of data planes, quadrics scale origin of axis parallelepiped around body center of gravity reference area and length
'Main block top plate ABCD1'	Quadric 1
1	component to which this quadric belongs
PlateB	flow is outward, inward, or on both sides
1	pointA
3. 48.1 -42.5	pointB
218. 48.1 -42.5	pointC
3. 48.1 2.1	pointD
218. 48.1 2.1	exterior point
100. 50. -20.	displacement of limit planes (in pixels)
0. 0. 0. 0.	
. . . .	
'CLAES small cylinder'	Quadric 15
3	component to which this quadric belongs
CylinderA	flow is outward, inward, or on both sides
1	pointA
64.5 2.7 30.6	pointB
97.1 2.7 30.6	radius
20.0	displacement of limit planes (in pixels)
0. 0.	F3I limits
0. 65. -30. 30. 0. 60.	
'CLAES Ring'	Plane 1
3	component to which this quadric belongs
RingA	pointA
64.5 2.7 30.6	direction cosine perpendicular to plane
1. 0. 0.	radius A
20.0	radius B
25.9	
'CLAES small cap'	Quadric 16
3	component to which this quadric belongs
SphereE	flow is outward, inward, or on both sides
1	pointA
97.1 2.7 30.6	direction cosine perpendicular to plane
-1. 0. 0.	radius
20.0	displacement of limit plane (in pixels)
0.5	F3I limits
64. 118. -20. 25. 0. 55.	

Component no.
4 PlateB
flow on ext., int. or both
pointA: actual point O3
pointB: actual point P3
pointC: actual point Q3
pointD: actual point R3
Exterior point
limit plane disp. (in pixels)
0. 0. 0. 0.

'Battery package ORAB3'
4
Quadric 26
Component no.
1 PlateB
flow on ext., int. or both
pointA: actual point O3
pointB: actual point P3
pointC: actual point Q3
pointD: actual point R3
Exterior point
limit plane disp. (in pixels)
0. 0. 0. 0.

'Battery package side AGCE3 lower X'
4
Quadric 27
Component no.
1 PlateB
flow on ext., int. or both
pointA: actual point A3
pointB: actual point G3
pointC: actual point M3
pointD: actual point E3
Exterior point
limit plane disp. (in pixels)
0. 0. 0. 0.

'Battery package side GIMK3 lower X'
4
Quadric 28
Component no.
1 PlateB
flow on ext., int. or both
pointA: actual point G3
pointB: actual point I3
pointC: actual point M3
pointD: actual point K3
Exterior point
limit plane disp. (in pixels)
0. 0. 0. 0.

'Battery package side MOAQ3 lower X'
4
Quadric 29
Component no.
1 PlateB
flow on ext., int. or both
pointA: actual point M3
pointB: actual point O3
pointC: actual point A3
pointD: actual point Q3
Exterior point
limit plane disp. (in pixels)
0. 0. 0. 0.

'Battery package side BDRFP3 higher X'
4
Quadric 30
Component no.
1 PlateB
flow on ext., int. or both
pointA: actual point B3
pointB: actual point D3
pointC: actual point H3
pointD: actual point F3
Exterior point
limit plane disp. (in pixels)
0. 0. 0. 0.

'Battery package side HJNL3 higher X'
4
Quadric 31
Component no.
1 PlateB
flow on ext., int. or both
pointA: actual point H3
pointB: actual point J3
pointC: actual point N3
pointD: actual point L3
Exterior point
limit plane disp. (in pixels)
0. 0. 0. 0.

'Battery package side NPBR3 higher X'
4
Quadric 32
Component no.
1 PlateB
flow on ext., int. or both
pointA: actual point N3
pointB: actual point P3
pointC: actual point B3
pointD: actual point R3
Exterior point
limit plane disp. (in pixels)
0. 0. 0. 0.

'Battery package side AGM3 lower X'
4
Quadric 33
Component no.
1 PlateB
flow on ext., int. or both
pointA: actual point A3
pointB: actual point G3
pointC: actual point M3
pointD: actual point E3
Exterior point
limit plane disp. (in pixels)
0. 0. 0. 0.

'Battery cylindrical MMS'
5
CylinderB
flow on ext., int. or both
pointA
radius
dircos
Rlength
limit plane disp. (in pixels)
-58.3 0. 0. 0.
25.0 0. 0. 0.
-1. 0. 0. 0.
21.1 0. 0. 0.
0. 0. 0. 0.
-80.0 -55.0 -25.0 25.0 -25.0 25.0

'Battery MMS plane bottom'
5
Disk
pointA
direction cosine normal to disk
radius
-79.4 0. 0. 0.
-1. 0. 0. 0.
25.0 0. 0. 0.

'HALOE mount ABC4'
6
PlateA
flow on ext., int. or both
pointA: actual point A4
pointB: actual point B4
pointC: actual point C4
Exterior point
limit plane disp. (in pixels)
0. 0. 0. 0.

'HALOE mount ACD4'
6
PlateA
flow on ext., int. or both
pointA: actual point A4
pointB: actual point C4
pointC: actual point D4
Exterior point
limit plane disp. (in pixels)
0. 0. 0. 0.

'HALOE mount CDE4'
6
PlateA
flow on ext., int. or both
pointA: actual point C4
pointB: actual point E4
pointC: actual point D4
Exterior point
limit plane disp. (in pixels)
0. 0. 0. 0.

0	flow on ext., int. or both	100.	-90.	-10.	Exterior point
136.3	pointA: actual point C4	0.	0.	0.	limit plane disp. (in pixels)
101.2	pointB: actual point D4	'Thin box under main block ABCD6'			
101.2	pointC: actual point E4	8			
150.	Exterior point	PlateB			
0.	limit plane disp. (in pixels)	1			
0.	0.	Quadric 38			
0.	0.	Component no.			
'HALOE mount BCE4'		flow on ext., int. or both			
6		pointA: actual point B4			
PlateA		pointB: actual point C4			
0		pointC: actual point E4			
171.4	pointA: actual point B4	49.3	-30.2	-25.5	Exterior point
136.3	pointB: actual point C4	49.3	-30.2	-42.5	limit plane disp. (in pixels)
101.2	pointC: actual point E4	49.3	-38.7	-25.5	Quadric 44
150.	Exterior point	49.3	-38.7	-42.5	Component no.
0.	limit plane disp. (in pixels)	0.	-35.	-20.	flow on ext., int. or both
0.	0.	pointA: actual point A6			
0.	0.	pointB: actual point B6			
0.	0.	pointC: actual point C6			
0.	0.	pointD: actual point D6			
0.	0.	Exterior point			
0.	0.	limit plane disp. (in pixels)			
0.	0.	Quadric 45			
0.	0.	Component no.			
'NEPS ABCDS'		flow on ext., int. or both			
7		pointA: actual point C6			
PlateB		pointB: actual point D6			
1		pointC: actual point G6			
83.7	pointA: actual point A5	49.3	-38.7	2.1	Exterior point
59.4	pointB: actual point B5	176.3	-38.7	2.1	limit plane disp. (in pixels)
79.6	pointC: actual point C5	176.3	-38.7	-42.5	Quadric 46
63.7	pointD: actual point D5	100.	-50.	-20.	Component no.
70.	Exterior point	flow on ext., int. or both			
0.	limit plane disp. (in pixels)	pointA: actual point D6			
0.	0.	pointB: actual point H6			
0.	0.	pointC: actual point F6			
0.	0.	pointD: actual point F6			
0.	0.	Exterior point			
0.	0.	limit plane disp. (in pixels)			
0.	0.	Quadric 47			
0.	0.	Component no.			
'NEPS BFDHS'		flow on ext., int. or both			
7		pointA: actual point E6			
PlateB		pointB: actual point H6			
1		pointC: actual point A6			
59.4	pointA: actual point B5	176.3	-38.7	-42.5	Exterior point
59.4	pointB: actual point F5	49.3	-30.2	-42.5	limit plane disp. (in pixels)
63.7	pointC: actual point D5	176.3	-30.2	-42.5	Quadric 48
63.7	pointD: actual point H5	0.	-35.	-50.	Component no.
50.	Exterior point	flow on ext., int. or both			
0.	limit plane disp. (in pixels)	pointA: actual point E6			
0.	0.	pointB: actual point A6			
0.	0.	pointC: actual point G6			
0.	0.	pointD: actual point C6			
0.	0.	Exterior point			
0.	0.	limit plane disp. (in pixels)			
0.	0.	Quadric 49			
0.	0.	Component no.			
'NEPS FEFGS'		flow on ext., int. or both			
7		pointA: actual point A7			
PlateB		pointB: actual point E7			
1		pointC: actual point C7			
59.4	pointA: actual point F5	176.3	-38.7	2.1	Exterior point
83.7	pointB: actual point E5	49.3	-38.7	2.1	limit plane disp. (in pixels)
63.7	pointC: actual point H5	100.	-35.	10.	Quadric 48
79.6	pointD: actual point G5	0.	0.	0.	Component no.
70.	Exterior point	flow on ext., int. or both			
0.	limit plane disp. (in pixels)	pointA: actual point A7			
0.	0.	pointB: actual point E7			
0.	0.	pointC: actual point C7			
0.	0.	pointD: actual point G7			
0.	0.	Exterior point			
0.	0.	limit plane disp. (in pixels)			
0.	0.	Quadric 49			
0.	0.	Component no.			
'NEPS EAGCS'		flow on ext., int. or both			
7		pointA: actual point A7			
PlateB		pointB: actual point E7			
1		pointC: actual point G7			
83.7	pointA: actual point E5	176.3	-30.2	2.1	Exterior point
83.7	pointB: actual point A5	218.0	-30.2	2.1	limit plane disp. (in pixels)
79.6	pointC: actual point G5	176.3	-51.0	2.1	Quadric 49
79.6	pointD: actual point C5	218.0	-51.0	2.1	Component no.
100.	Exterior point	flow on ext., int. or both			
0.	limit plane disp. (in pixels)	pointA: actual point E7			
0.	0.	pointB: actual point F7			
0.	0.	pointC: actual point G7			
0.	0.	pointD: actual point H7			
0.	0.	Exterior point			
0.	0.	limit plane disp. (in pixels)			
0.	0.	Quadric 49			
0.	0.	Component no.			
'NEPS JLIKS'		flow on ext., int. or both			
7		pointA: actual point E7			
PlateB		pointB: actual point F7			
1		pointC: actual point G7			
79.6	pointA: actual point J5	218.0	-30.2	2.1	Exterior point
79.6	pointB: actual point I5	218.0	-51.0	2.1	limit plane disp. (in pixels)
63.7	pointC: actual point L5	218.0	-51.0	-42.5	Quadric 49
63.7	pointD: actual point K5	250.	-35.	-20.	Component no.
0.	0.	flow on ext., int. or both			
0.	0.	pointA: actual point E7			
0.	0.	pointB: actual point F7			
0.	0.	pointC: actual point G7			
0.	0.	pointD: actual point H7			
0.	0.	Exterior point			
0.	0.	limit plane disp. (in pixels)			
0.	0.	Quadric 49			
0.	0.	Component no.			

'cylindrical truss #5 at X = 0.0' Quadric 63
 11 Component no.
 Cylinder
 1 flow on ext., int. or both
 pointA 0. 32.2 0.
 pointB 0. 94.0 0.
 radius 1.5
 limit plane disp. (in pixels) 0.
 2.0 FJI limits 2.0 2.0 30.0 100.0 -2.0
 'cylindrical truss #6 at X = 0.0' Quadric 64
 11 Component no.
 Cylinder
 1 flow on ext., int. or both
 pointA 0. 31.0 -37.8
 pointB 0. 94.0 0.
 radius 1.5
 limit plane disp. (in pixels) 0.
 2.0 FJI limits 2.0 2.0 30.0 100.0 -50.0
 'Sphere junctn betwn trusses 1-2(X=0)' Quadric 65
 11 Component no.
 SphereA
 1 flow on ext., int. or both
 pointA 0. -94.0 0.
 radius 5.0
 'Sphere junctn betwn trusses 3-4(X=0)' Quadric 66
 11 Component no.
 SphereA
 1 flow on ext., int. or both
 pointA 0. 0. -94.0
 radius 5.0
 'Sphere junctn betwn trusses 5-6(X=0)' Quadric 67
 11 Component no.
 SphereA
 1 flow on ext., int. or both
 pointA 0. 94.0 0.
 radius 5.0
 'left-hand HGA-end box AFD110' Quadric 68
 12 Component no.
 PlateB
 1 flow on ext., int. or both
 pointA: actual point A10 218.0 31.1 18.6
 pointB: actual point F10 218.0 31.1 2.1
 pointC: actual point D10 218.0 -30.2 18.6
 pointD: actual point I10 218.0 -30.2 2.1
 Exterior point 200. 35. 25.
 limit plane disp. (in pixels) 0.
 0. 0. 0.
 'left-hand HGA-end box ABDE10' Quadric 69
 12 Component no.
 PlateB
 1 flow on ext., int. or both
 pointA: actual point A10 218.0 31.1 18.6
 pointB: actual point B10 232.5 31.1 18.6
 pointC: actual point D10 218.0 -30.2 18.6
 pointD: actual point E10 225.5 -30.2 25.
 Exterior point 220. 15. 25.
 limit plane disp. (in pixels) 0.
 0. 0. 0.
 'left-hand HGA-end box BCE10' Quadric 70
 12 Component no.
 PlateA
 1 flow on ext., int. or both
 pointA: actual point B10 232.5 31.1 18.6

256.9 19.6 18.6 pointB: actual point C10
 225.5 -30.2 18.6 pointC: actual point E10
 250. 15. 25. Exterior point
 0. 0. 0. limit plane disp. (in pixels)

'left/right-hand HGA-end box ABFG10' Quadric 71
 12 Component no.
 PlateB
 1 flow on ext., int. or both
 pointA: actual point A10 218.0 31.1 18.6
 pointB: actual point B10 232.5 31.1 18.6
 pointC: actual point G11 218.0 31.1 -42.5
 pointD: actual point H11 232.5 31.1 -42.5
 Exterior point 220. 50. 0.
 limit plane disp. (in pixels) 0.
 0. 0. 0.

'left/right-hand HGA-end box BCGH10' Quadric 72
 12 Component no.
 PlateB
 1 flow on ext., int. or both
 pointA: actual point B10 232.5 31.1 18.6
 pointB: actual point C10 256.9 19.6 18.6
 pointC: actual point H11 232.5 31.1 -42.5
 pointD: actual point I11 256.9 19.6 -42.5
 Exterior point 250. 75. 0.
 limit plane disp. (in pixels) 0.
 0. 0. 0.

'left-hand HGA-end box CHEJ10' Quadric 73
 12 Component no.
 PlateB
 1 flow on ext., int. or both
 pointA: actual point C10 256.9 19.6 18.6
 pointB: actual point H10 256.9 19.6 2.1
 pointC: actual point E10 225.5 -30.2 18.6
 pointD: actual point J10 225.5 -30.2 2.1
 Exterior point 260. -30. 25.
 limit plane disp. (in pixels) 0.
 0. 0. 0.

'left/right-hand HGA-end box DEIJ10' Quadric 74
 12 Component no.
 PlateB
 1 flow on ext., int. or both
 pointA: actual point D10 218.0 -30.2 18.6
 pointB: actual point E10 225.5 -30.2 18.6
 pointC: actual point J11 218.0 -30.2 -42.5
 pointD: actual point K11 225.5 -30.2 -42.5
 Exterior point 220. -50. 0.
 limit plane disp. (in pixels) 0.
 0. 0. 0.

'right-hand HGA-end box GHJK11' Quadric 75
 12 Component no.
 PlateB
 1 flow on ext., int. or both
 pointA: actual point G11 218.0 31.1 -42.5
 pointB: actual point H11 232.5 31.1 -42.5
 pointC: actual point J11 218.0 -30.2 -42.5
 pointD: actual point K11 225.5 -30.2 -42.5
 Exterior point 220. 0. -50.
 limit plane disp. (in pixels) 0.
 0. 0. 0.

'right-hand HGA-end box CEF11' Quadric 76
 12 Component no.
 PlateA
 1 flow on ext., int. or both
 pointA: actual point C11 256.9 19.6 2.1
 pointB: actual point E11 225.5 -30.2 2.1
 pointC: actual point F11 256.9 -15.9 2.1
 Exterior point 250. 35. 25.
 limit plane disp. (in pixels) 0.
 0. 0. 0.

0.	0.	limit plane disp. (in pixels)	1.	0.	dircos
100.	150.	F3I limits	2.4	0.	radius
'solar panel support J12'					
13		Component no.	70.	200.	limit plane disp. (in pixels)
SphereE					
1	136.1	56.3	-55.5		flow on ext., int. or both
0.	0.	1.			pointA
3.5	0.	0.			dircos
0.	100.	150.	0.	70.0	radius
					limit plane disp. (in pixels)
					F3I limits
'solar panel support JK12'					
13					Component no.
CylinderA					
1	136.1	56.3	-55.5		flow on ext., int. or both
	136.1	105.79	-70.63		pointA
2.4					pointB
0.	0.	0.			radius
80.	185.	0.	110.	-100.	limit plane disp. (in pixels)
					F3I limits
'solar panel support JL12'					
13					Component no.
CylinderA					
1	136.1	56.3	-55.5		flow on ext., int. or both
	106.28	105.79	-70.63		pointA
1.4					pointB
0.	0.	0.			radius
70.	200.	-5.	120.	-100.	limit plane disp. (in pixels)
					F3I limits
'solar panel support JM12'					
13					Component no.
CylinderA					
1	136.1	56.3	-55.5		flow on ext., int. or both
	165.92	105.79	-70.63		pointA
1.4					pointB
0.	0.	0.			radius
70.	200.	-5.	120.	-100.	limit plane disp. (in pixels)
					F3I limits
'solar panel support JN12'					
13					Component no.
CylinderA					
1	136.1	56.3	-55.5		flow on ext., int. or both
	165.92	105.79	-70.63		pointA
1.4					pointB
0.	0.	0.			radius
70.	200.	-5.	120.	-100.	limit plane disp. (in pixels)
					F3I limits
'solar panel, N0PQ12'					
13					Component no.
PlateB					
0	200.5	105.79	-70.63		flow on ext., int. or both
	71.7	105.79	-70.63		pointA: actual point N12
200.5					pointB: actual point O12
71.7					pointC: actual point P12
150.	100.	-150.			pointD: actual point Q12
					Exterior point
					limit plane disp. (in pixels)
'solar panel support RS12'					
13					Component no.
CylinderA					
1	106.28	105.79	-70.63		flow on ext., int. or both
	165.92	105.79	-70.63		pointA
2.4					pointB
0.	0.	0.			radius
70.	200.	-5.	120.	-100.	limit plane disp. (in pixels)
					F3I limits
'solar panel support R12'					
13					Component no.
SphereE					
1	106.28	105.79	-70.63		flow on ext., int. or both

'HRDI telescope mount JKLM13'					
14					
PlateB					
1	132.1	-54.6	-15.1	0.7	flow on ext., int. or both
	140.5	-54.6	-15.1	-1.3	pointA: actual point J13
	132.1	-55.6	-15.1	0.7	pointB: actual point K13
	140.5	-55.6	-15.1	-1.3	pointC: actual point L13
	135.	-55.	-20.	0.	pointD: actual point M13
	0.	0.	0.	0.	Exterior point
					limit plane disp. (in pixels)
					Quadic 104
					Component no.
'HRDI telescope mount GIM13'					
14					
PlateB					
1	140.5	-54.6	0.7	0.7	flow on ext., int. or both
	140.5	-55.6	0.7	0.7	pointA: actual point G13
	140.5	-54.6	-15.1	-1.3	pointB: actual point H13
	140.5	-55.6	-15.1	-1.3	pointC: actual point I13
	150.	-55.	-20.	0.	pointD: actual point K13
	0.	0.	0.	0.	Exterior point
					limit plane disp. (in pixels)
					Quadic 105
					Component no.
'HRDI telescope mount FHJL13'					
14					
PlateB					
1	132.1	-54.6	0.7	0.7	flow on ext., int. or both
	132.1	-55.6	0.7	0.7	pointA: actual point F13
	132.1	-54.6	-15.1	-1.3	pointB: actual point H13
	132.1	-55.6	-15.1	-1.3	pointC: actual point J13
	100.	-55.	-20.	0.	pointD: actual point L13
	0.	0.	0.	0.	Exterior point
					limit plane disp. (in pixels)
					Quadic 106
					Component no.
'HRDI telescope mount HIRS13'					
14					
PlateB					
1	132.1	-55.6	0.7	0.7	flow on ext., int. or both
	140.5	-55.6	0.7	0.7	pointA: actual point H13
	133.8	-71.3	0.7	0.7	pointB: actual point I13
	138.8	-71.3	0.7	0.7	pointC: actual point R13
	135.	-70.	10.	0.	pointD: actual point S13
	0.	0.	0.	0.	Exterior point
					limit plane disp. (in pixels)
					Quadic 107
					Component no.
'HRDI telescope mount NOTU13'					
14					
PlateB					
1	132.1	-55.6	-1.3	-1.3	flow on ext., int. or both
	140.5	-55.6	-1.3	-1.3	pointA: actual point M13
	133.8	-71.3	-1.3	-1.3	pointB: actual point O13
	138.8	-71.3	-1.3	-1.3	pointC: actual point T13
	135.	-70.	-10.0	0.	pointD: actual point U13
	0.	0.	0.	0.	Exterior point
					limit plane disp. (in pixels)
					Quadic 108
					Component no.
'HRDI telescope mount IOSU13'					
14					
PlateB					
1	140.5	-55.6	0.7	0.7	flow on ext., int. or both
	140.5	-55.6	-1.3	-1.3	pointA: actual point I13
	138.8	-71.3	0.7	0.7	pointB: actual point O13
	138.8	-71.3	-1.3	-1.3	pointC: actual point S13
	150.	-70.	0.	0.	pointD: actual point U13
	0.	0.	0.	0.	Exterior point
					limit plane disp. (in pixels)
					Quadic 109
					Component no.
'HRDI telescope mount HNRT13'					
14					
PlateB					
1	132.1	-55.6	0.7	0.7	flow on ext., int. or both
	132.1	-55.6	-1.3	-1.3	pointA: actual point H13
	133.8	-71.3	0.7	0.7	pointB: actual point I13
	138.8	-71.3	-1.3	-1.3	pointC: actual point S13
	135.	-70.	-10.0	0.	pointD: actual point U13
	0.	0.	0.	0.	Exterior point
					limit plane disp. (in pixels)
					Quadic 110
					Component no.
'HRDI telescope mount RSTU13'					
14					
PlateB					
1	133.8	-71.3	0.7	0.7	flow on ext., int. or both
	138.8	-71.3	0.7	0.7	pointA: actual point R13
	133.8	-71.3	-1.3	-1.3	pointB: actual point S13
	138.8	-71.3	-1.3	-1.3	pointC: actual point T13
	100.	-70.	0.	0.	pointD: actual point U13
	0.	0.	0.	0.	Exterior point
					limit plane disp. (in pixels)
					Quadic 111
					Component no.
'HRDI telescope mount knob'					
14					
CylinderA					
1	136.3	-71.3	-1.3	-1.3	flow on ext., int. or both
	136.3	-71.3	3.7	3.7	pointA
	3.5				pointB
	0.	0.			radius
	100.	150.	-80.	0.	limit plane disp. (in pixels)
					F3I limits
					Plane 3
					Component no.
'HRDI telescope mount knob'					
14					
Disk					
1	136.3	-71.3	-1.3	-1.3	pointA
	0.	0.	-1.	-1.	direction cosine normal to disk
	3.5				radius
					Plane 4
					Component no.
'HRDI telescope mount knob'					
14					
Disk					
1	136.3	-71.3	3.7	3.7	pointA
	0.	0.	1.	1.	direction cosine normal to disk
	3.5				radius
					Quadic 112
					Component no.
'HRDI telescope mount PQW13'					
14					
PlateB					
1	132.1	-55.6	-13.1	-13.1	flow on ext., int. or both
	140.5	-55.6	-13.1	-13.1	pointA: actual point P13
	133.8	-71.3	-13.1	-13.1	pointB: actual point Q13
	138.8	-71.3	-13.1	-13.1	pointC: actual point V13
	135.	-70.	0.	0.	pointD: actual point W13
	0.	0.	0.	0.	Exterior point
					limit plane disp. (in pixels)
					Quadic 113
					Component no.
'HRDI telescope mount LMX13'					
14					
PlateB					
1	132.1	-55.6	-15.1	-15.1	flow on ext., int. or both
	140.5	-55.6	-15.1	-15.1	pointA: actual point L13
	133.8	-71.3	-15.1	-15.1	pointB: actual point M13
	138.8	-71.3	-15.1	-15.1	pointC: actual point X13
	135.	-70.	-50.	-50.	pointD: actual point Y13
	0.	0.	0.	0.	Exterior point
					limit plane disp. (in pixels)
					Quadic 114
					Component no.
'HRDI telescope mount QMW13'					
14					
PlateB					
1	132.1	-55.6	-15.1	-15.1	flow on ext., int. or both
	140.5	-55.6	-15.1	-15.1	pointA: actual point L13
	133.8	-71.3	-15.1	-15.1	pointB: actual point M13
	138.8	-71.3	-15.1	-15.1	pointC: actual point X13
	135.	-70.	-50.	-50.	pointD: actual point Y13
	0.	0.	0.	0.	Exterior point
					limit plane disp. (in pixels)
					Quadic 114
					Component no.

1	140.5	-55.6	-13.1	flow on ext., int. or both	radius	4.0	
	140.5	-55.6	-15.1	pointA: actual point Q13	Plane 8		
	138.8	-71.3	-13.1	pointB: actual point M13	Component no.	14	
	138.8	-71.3	-15.1	pointC: actual point W13			
	170.	-70.	-10.	pointD: actual point Y13	pointA		
	0.	0.	0.	Exterior point	dircos		
	0.	0.	0.	limit plane disp. (in pixels)	radius		
				Quadic 115	Quadic 119		
				Component no.	Component no.		
				PlateB	PlateB		
1	132.1	-55.6	-13.1	flow on ext., int. or both			
	132.1	-55.6	-15.1	pointA: actual point P13	pointA; actual point a13		
	133.8	-71.3	-13.1	pointB: actual point L13	pointB; actual point b13		
	133.8	-71.3	-15.1	pointC: actual point V13	pointC; actual point c13		
	100.	-70.	-10.	pointD: actual point X13	pointD; actual point d13		
	0.	0.	0.	Exterior point	Exterior point		
	0.	0.	0.	limit plane disp. (in pixels)	limit plane disp. (in pixels)		
				Quadic 116	Quadic 120		
				Component no.	Component no.		
				PlateB	PlateB		
1	133.8	-71.3	-13.1	flow on ext., int. or both			
	138.8	-71.3	-13.1	pointA: actual point V13	pointA; actual point e13		
	133.8	-71.3	-15.1	pointB: actual point X13	pointB; actual point f13		
	138.8	-71.3	-15.1	pointC: actual point Y13	pointC; actual point g13		
	100.	-100.	-10.	pointD: actual point Z13	pointD; actual point h13		
	0.	0.	0.	Exterior point	Exterior point		
	0.	0.	0.	limit plane disp. (in pixels)	limit plane disp. (in pixels)		
				Quadic 117	Quadic 121		
				Component no.	Component no.		
				CylinderA			
1	136.3	-71.3	-13.1	flow on ext., int. or both			
	136.3	-71.3	-18.1	pointC: actual point T13	pointA; actual point a13		
	3.5	0.	0.	radius	pointB; actual point b13		
	0.	0.	0.	limit plane disp. (in pixels)	pointC; actual point c13		
	100.	150.	-80.	F3I limits	pointD; actual point e13		
	0.	0.	0.	Plane 5	pointD; actual point g13		
				Component no.	Exterior point		
					limit plane disp. (in pixels)		
				Quadic 122	Quadic 126		
				Component no.	Component no.		
				Disk			
1	136.3	-71.3	-18.1	pointA	flow on ext., int. or both		
	0.	0.	-1.	direction cosine normal to disk	pointA; actual point d13		
	3.5	0.	0.	radius	pointB; actual point e13		
				Plane 6	pointC; actual point f13		
				Component no.	pointD; actual point h13		
				Disk	Exterior point		
1	136.3	-71.3	-13.1	pointA	limit plane disp. (in pixels)		
	0.	0.	1.	direction cosine normal to disk	Quadic 123		
	3.5	0.	0.	radius	Component no.		
				Quadic 118			
				Component no.			
				CylinderA			
1	144.7	-63.988	-7.2	flow on ext., int. or both	pointA; actual point c13		
	127.9	-78.7	-7.2	pointA	pointB; actual point d13		
	4.0	0.	0.	pointB	pointC; actual point g13		
	0.	0.	0.	radius	pointD; actual point h13		
	100.	150.	-80.	limit plane disp. (in pixels)	Exterior point		
	0.	0.	0.	F3I limits	limit plane disp. (in pixels)		
				Plane 7	Quadic 124		
				Component no.	Component no.		
				Disk			
1	144.7	-63.988	-7.2	pointA	flow on ext., int. or both		
	0.7523	0.6588	0.	dircos	pointA; actual point A14		

276.3	39.2	-93.8	pointB: actual point B14
276.3	-7.2	-61.0	pointC: actual point C14
276.3	-7.2	-93.8	pointD: actual point D14
300.	35.	-80.	Exterior point
0.	0.	0.	limit plane disp. (in pixels)
'SSPP box EFGH14'			
15			Component no.
1			PlateB
230.3	39.2	-61.0	flow on ext., int. or both
230.3	39.2	-93.8	pointA: actual point E14
230.3	-7.2	-61.0	pointB: actual point F14
230.3	-7.2	-93.8	pointC: actual point G14
230.3	-7.2	-93.8	pointD: actual point H14
200.	35.	-80.	Exterior point
0.	0.	0.	limit plane disp. (in pixels)
'SSPP box ABFE14'			
15			Component no.
1			PlateB
276.3	39.2	-61.0	flow on ext., int. or both
276.3	39.2	-93.8	pointA: actual point A14
230.3	39.2	-61.0	pointB: actual point B14
230.3	39.2	-93.8	pointC: actual point E14
230.3	39.2	-93.8	pointD: actual point F14
250.	50.	-80.	Exterior point
0.	0.	0.	limit plane disp. (in pixels)
'SSPP box CDGH14'			
15			Component no.
1			PlateB
276.3	-7.2	-61.0	flow on ext., int. or both
276.3	-7.2	-93.8	pointA: actual point C14
230.3	-7.2	-61.0	pointB: actual point D14
230.3	-7.2	-93.8	pointC: actual point G14
230.3	-7.2	-93.8	pointD: actual point H14
250.	-20.	-80.	Exterior point
0.	0.	0.	limit plane disp. (in pixels)
'SSPP box BFDH14'			
15			Component no.
1			PlateB
276.3	39.2	-93.8	flow on ext., int. or both
230.3	39.2	-93.8	pointA: actual point B14
276.3	-7.2	-93.8	pointB: actual point F14
230.3	-7.2	-93.8	pointC: actual point M14
250.	-20.	-150.	Exterior point
0.	0.	0.	limit plane disp. (in pixels)
'SSPP box AECG14'			
15			Component no.
1			PlateB
276.3	39.2	-61.0	flow on ext., int. or both
230.3	39.2	-61.0	pointA: actual point A14
276.3	-7.2	-61.0	pointB: actual point E14
230.3	-7.2	-61.0	pointC: actual point C14
230.3	-7.2	-61.0	pointD: actual point G14
250.	-20.	-20.	Exterior point
0.	0.	0.	limit plane disp. (in pixels)
'ISAMS box ABCD15'			
16			Component no.
1			PlateB
19.8	-30.2	11.6	flow on ext., int. or both
49.3	-30.2	11.6	pointA: actual point A15
19.8	-38.7	-25.5	pointB: actual point B15
49.3	-38.7	-25.5	pointC: actual point G15
19.8	-76.2	-25.5	pointD: actual point M15
50.	-20.	-80.	Exterior point
0.	0.	0.	limit plane disp. (in pixels)
'ISAMS box BDFH15'			
16			Component no.
1			PlateB
19.8	-30.2	11.6	flow on ext., int. or both
49.3	-30.2	11.6	pointA: actual point B15
49.3	-38.7	11.6	pointB: actual point F15
49.3	-38.7	2.1	pointC: actual point D15
49.3	-38.7	2.1	pointD: actual point H15
80.	-30.	0.	Exterior point
0.	0.	0.	limit plane disp. (in pixels)
'ISAMS box ABFE15'			
16			Component no.
1			PlateB
19.8	-30.2	11.6	flow on ext., int. or both
49.3	-30.2	11.6	pointA: actual point A15
49.3	-30.2	2.1	pointB: actual point B15
49.3	-30.2	2.1	pointC: actual point E15
49.3	-30.2	2.1	pointD: actual point F15
90.	-20.	80.	Exterior point
0.	0.	0.	limit plane disp. (in pixels)
'ISAMS box AKEH15'			
16			Component no.
1			PlateB
19.8	-30.2	11.6	flow on ext., int. or both
49.3	-76.2	11.6	pointA: actual point A15
19.8	-30.2	-25.5	pointB: actual point K15
19.8	-76.2	-25.5	pointC: actual point L15
19.8	-76.2	-25.5	pointD: actual point M15
0.	-80.	0.	Exterior point
0.	0.	0.	limit plane disp. (in pixels)
'ISAMS box CDKL15'			
16			Component no.
1			PlateB
19.8	-38.7	11.6	flow on ext., int. or both
44.8	-38.7	11.6	pointA: actual point C15
19.8	-76.2	11.6	pointB: actual point D15
44.8	-76.2	11.6	pointC: actual point K15
44.8	-76.2	11.6	pointD: actual point L15
50.	-20.	80.	Exterior point
0.	0.	0.	limit plane disp. (in pixels)
'ISAMS box GHMN15'			
16			Component no.
1			PlateB
19.8	-38.7	-25.5	flow on ext., int. or both
44.8	-38.7	-25.5	pointA: actual point G15
19.8	-76.2	-25.5	pointB: actual point H15
44.8	-76.2	-25.5	pointC: actual point M15
44.8	-76.2	-25.5	pointD: actual point N15
50.	-20.	-80.	Exterior point
0.	0.	0.	limit plane disp. (in pixels)

'ISAMS box KLMN15'	Quadrac 137	'HGA antenna C16'	Plane 10
16	Component no.	17	Component no.
PlateB	flow on ext., int. or both	Disk	pointA
1	pointA: actual point I15	278.7	40.4
19.8	pointB: actual point L15	-1.	0.
44.8	pointC: actual point M15	4.6	
19.8	pointD: actual point N15		
44.8	Exterior point		
50.	limit plane disp. (in pixels)		
0.			
'ISAMS box IJPR15'	Quadrac 138	'HGA antenna D16'	Quadrac 143
16	Component no.	17	Component no.
PlateB	flow on ext., int. or both	SphereE	flow on ext., int. or both
1	pointA: actual point I15	301.5	40.4
57.3	pointB: actual point J15	-1.	0.
57.3	pointC: actual point P15	4.6	
57.3	pointD: actual point R15	0.	
100.	Exterior point	250.	350.
0.	limit plane disp. (in pixels)	0.	60.
		0.	20.
'ISAMS box DHIJ15'	Quadrac 139	'HGA antenna E16'	Quadrac 144
16	Component no.	17	Component no.
PlateB	flow on ext., int. or both	CylinderA	flow on ext., int. or both
1	pointA: actual point D15	301.5	40.4
49.3	pointB: actual point H15	301.5	60.4
49.3	pointC: actual point I15	2.5	
57.3	pointD: actual point J15	0.	
100.	Exterior point	250.	350.
0.	limit plane disp. (in pixels)	0.	100.
		0.	0.
'HGA antenna AB16'	Quadrac 140	'HGA antenna E16'	Quadrac 145
17	Component no.	17	Component no.
CylinderA	flow on ext., int. or both	SphereC	flow on ext., int. or both
1	pointA	301.5	71.4
279.7	pointB	0.	1.
279.7	radius	11.	0.
2.8	limit plane disp. (in pixels)	25.5	
0.	F3I limits	0.	
250.		250.	400.
0.		0.	100.
60.			-50.
-30.			50.
20.			
'HGA antenna A16'	Quadrac 141	'CLAES lower mount, ABC17'	Quadrac 146
17	Component no.	18	Component no.
SphereE	flow on ext., int. or both	PlateA	flow on ext., int. or both
1	pointA	102.4	-29.2
279.7	pointB	41.9	-29.2
0.	radius	63.2	-26.2
2.8	limit plane disp. (in pixels)	100.	-35.
0.	F3I limits	0.	50.
250.		0.	0.
0.			0.
60.			
-30.			
20.			
'HGA antenna B16'	Plane 9	'CLAES lower mount, DEF17'	Quadrac 147
17	Component no.	18	Component no.
Disk	flow on ext., int. or both	PlateA	flow on ext., int. or both
1	pointA	102.4	-26.2
279.7	pointB	41.9	-26.2
0.	radius	63.2	-23.2
2.8	limit plane disp. (in pixels)	100.	-20.
0.	F3I limits	0.	50.
250.		0.	0.
0.			0.
60.			
-30.			
20.			
'HGA antenna CD16'	Quadrac 142	'CLAES lower mount, ACD17'	Quadrac 148
17	Component no.	18	Component no.
CylinderA	flow on ext., int. or both	PlateB	flow on ext., int. or both
1	pointA	102.4	-29.2
278.7	pointB	63.2	-26.2
301.5	pointC	102.4	-26.2
4.6	radius	63.2	-23.2
0.	limit plane disp. (in pixels)	100.	-30.
0.	F3I limits	0.	50.
250.		0.	0.
350.			0.
0.			
60.			
0.			
20.			

'CLAES lower mount, BCEF17' 18 PlateB 1	173.8 -30.2 9.3 173.8 -30.2 2.1 123.8 -30.2 9.3 123.8 -30.2 2.1 200. -100. 50. 2. 2.	pointA: actual point O18 pointB: actual point P18 pointC: actual point Q18 pointD: actual point R18 Exterior point limit plane disp. (in pixels)
Quadric 149 Component no.		
flow on ext., int. or both pointA: actual point B17 pointB: actual point C17 pointC: actual point E17 pointD: actual point F17 Exterior point limit plane disp. (in pixels)		
Quadric 150 Component no.		
flow on ext., int. or both pointA: actual point G17 pointB: actual point H17 pointC: actual point I17 Exterior point limit plane disp. (in pixels)		
Quadric 151 Component no.		
flow on ext., int. or both pointA: actual point J17 pointB: actual point K17 pointC: actual point L17 Exterior point limit plane disp. (in pixels)		
Quadric 152 Component no.		
flow on ext., int. or both pointA: actual point G17 pointB: actual point I17 pointC: actual point J17 pointD: actual point L17 Exterior point limit plane disp. (in pixels)		
Quadric 153 Component no.		
flow on ext., int. or both pointA: actual point H17 pointB: actual point I17 pointC: actual point K17 pointD: actual point L17 Exterior point limit plane disp. (in pixels)		
Quadric 154 Component no.		
flow on ext., int. or both pointA: actual point A18 pointB: actual point B18 pointC: actual point C18 pointD: actual point D18 Exterior point limit plane disp. (in pixels)		
Quadric 155 Component no.		
flow on ext., int. or both pointA: actual point A18 pointB: actual point B18 pointC: actual point C18 pointD: actual point D18 Exterior point limit plane disp. (in pixels)		
'CLAES lower mount, BCEF17' 18 PlateB 1	173.8 -30.2 9.3 173.8 -30.2 2.1 123.8 -30.2 9.3 123.8 -30.2 2.1 200. -100. 50. 2. 2.	pointA: actual point O18 pointB: actual point P18 pointC: actual point Q18 pointD: actual point R18 Exterior point limit plane disp. (in pixels)
Quadric 156 Component no.		
flow on ext., int. or both pointA: actual point D18 pointB: actual point B18 pointC: actual point O18 pointD: actual point P18 Exterior point limit plane disp. (in pixels)		
Quadric 157 Component no.		
flow on ext., int. or both pointA: actual point A18 pointB: actual point C18 pointC: actual point R18 pointD: actual point Q18 Exterior point limit plane disp. (in pixels)		
Quadric 158 Component no.		
flow on ext., int. or both pointA: actual point D18 pointB: actual point E18 pointC: actual point O18 pointD: actual point Q18 Exterior point limit plane disp. (in pixels)		
Quadric 159 Component no.		
flow on ext., int. or both pointA: actual point C18 pointB: actual point E18 pointC: actual point Q18 Exterior point limit plane disp. (in pixels)		
Quadric 160 Component no.		
flow on ext., int. or both pointA: actual point F18 pointB: actual point N18 pointC: actual point O18 Exterior point limit plane disp. (in pixels)		
Quadric 161 Component no.		
flow on ext., int. or both pointA: actual point E18 pointB: actual point M18 pointC: actual point Q18 Exterior point limit plane disp. (in pixels)		
'CLAES upper mount, GH117' 18 PlateA 1	'WINDII base, DBOP18' 19 PlateB 1 167.4 0. 27.3 167.4 0. 2.1 173.8 -30.2 9.3 173.8 -30.2 2.1 200. 100. 50. 2. 2.	pointA: actual point O18 pointB: actual point P18 pointC: actual point Q18 pointD: actual point R18 Exterior point limit plane disp. (in pixels)
'CLAES upper mount, JK117' 18 PlateA 1	'WINDII base, ACRQ18' 19 PlateB 1 130.8 0. 2.1 130.8 0. 27.3 123.8 -30.2 2.1 123.8 -30.2 9.3 100. 100. 50. 2. 2.	pointA: actual point A18 pointB: actual point C18 pointC: actual point R18 pointD: actual point Q18 Exterior point limit plane disp. (in pixels)
'CLAES upper mount, GIJL17' 18 PlateB 1	'WINDII base, DFO18' 19 PlateA 1 167.4 0. 27.3 167.4 -22.8 27.3 173.8 -30.2 9.3 200. 50. 50. 2. 2.	pointA: actual point D18 pointB: actual point E18 pointC: actual point O18 Exterior point limit plane disp. (in pixels)
'CLAES upper mount, HIKL17' 18 PlateB 1	'WINDII base, CFO18' 19 PlateA 1 130.8 0. 27.3 130.8 -22.8 27.3 123.8 -30.2 9.3 100. 50. 50. 2. 2.	pointA: actual point C18 pointB: actual point E18 pointC: actual point Q18 Exterior point limit plane disp. (in pixels)
'CLAES upper mount, ABCD18' 19 PlateB 1	'WINDII base, FNO18' 19 PlateA 1 167.4 -22.8 27.3 162.0 -36.4 21.8 173.8 -30.2 9.3 200. -50. 50. 2. 2.	pointA: actual point F18 pointB: actual point N18 pointC: actual point O18 Exterior point limit plane disp. (in pixels)
'CLAES upper mount, OPQR18' 19 PlateB 1	'WINDII base, EMO18' 19 PlateA 1 130.8 -22.8 27.3 136.0 -36.4 21.8 123.8 -30.2 9.3 100. -50. 50. 2. 2.	pointA: actual point E18 pointB: actual point M18 pointC: actual point Q18 Exterior point limit plane disp. (in pixels)

'WINDII base, HFNI18'									pointB: actual point J18
19									pointC: actual point K18
PlateA									pointD: actual point L18
1									Exterior point
157.9	-22.8	27.3	173.4	-31.9	46.4	0.			limit plane disp. (in pixels)
167.4	-22.8	27.3	119.7	-45.0	46.4				
162.0	-36.4	21.8	200.	-45.0	46.4				
200.	-50.	100.	0.	-40.	80.				
2.	2.	2.		0.	0.				
									Quadic 169
'WINDII base, GEM18'									Component no.
19									
PlateA									
1									
140.4	-22.8	27.3	157.9	-22.8	27.3				flow on ext., int. or both
130.8	-22.8	27.3	173.4	-31.9	46.4				pointA: actual point H18
136.0	-36.4	21.8	162.0	-36.4	21.8				pointB: actual point J18
100.	-50.	100.	179.7	-45.0	46.4				pointC: actual point N18
2.	2.	2.	200.	100.	50.				pointD: actual point L18
			2.	2.	2.				Exterior point
									limit plane disp. (in pixels)
									Quadic 170
'WINDII base, CDEF18'									Component no.
19									
PlateB									
1									
130.8	0.	27.3	124.9	-31.9	46.4				flow on ext., int. or both
167.4	0.	27.3	140.4	-22.8	27.3				pointA: actual point I18
130.8	-22.8	27.3	119.7	-45.0	46.4				pointB: actual point G18
167.4	-22.8	27.3	136.0	-36.4	21.8				pointC: actual point K18
200.	-10.	50.	100.	100.	50.				pointD: actual point M18
2.	2.	2.	2.	2.	2.				Exterior point
									limit plane disp. (in pixels)
									Quadic 171
'WINDII base, MNQO18'									Component no.
19									
PlateB									
1									
136.0	-36.4	21.8	269.8	-34.6	36.4				flow on ext., int. or both
162.0	-36.4	21.8	247.1	-34.6	36.4				pointA: actual point A19
123.8	-30.2	9.3	263.9	-34.6	16.8				pointB: actual point B19
173.8	-30.2	9.3	253.0	-34.6	16.8				pointC: actual point C19
200.	-100.	50.	250.	-50.	50.				pointD: actual point D19
2.	2.	2.	0.	0.	0.				Exterior point
									limit plane disp. (in pixels)
									Quadic 172
'WINDII base, MNKL18'									Component no.
19									
PlateB									
1									
136.0	-36.4	21.8	269.8	-32.3	36.4				flow on ext., int. or both
162.0	-36.4	21.8	247.1	-32.3	36.4				pointA: actual point E19
119.7	-45.0	46.4	263.9	-32.3	16.8				pointB: actual point F19
179.7	-45.0	46.4	253.0	-32.3	16.8				pointC: actual point G19
200.	-100.	0.	250.	50.	50.				pointD: actual point H19
2.	2.	2.	0.	0.	0.				Exterior point
									limit plane disp. (in pixels)
									Quadic 173
'WINDII base, GHIJ18'									Component no.
19									
PlateB									
1									
140.4	-22.8	27.3	269.8	-34.6	36.4				flow on ext., int. or both
157.9	-22.8	27.3	269.8	-32.3	36.4				pointA: actual point A19
124.9	-31.9	46.4	263.9	-34.6	16.8				pointB: actual point E19
173.4	-31.9	46.4	263.9	-32.3	16.8				pointC: actual point G19
200.	100.	50.	300.	-30.	20.				pointD: actual point H19
2.	2.	2.	0.	0.	0.				Exterior point
									limit plane disp. (in pixels)
									Quadic 174
'WINDII base, IJLK18'									Component no.
19									
PlateB									
1									
124.9	-31.9	46.4	247.1	-34.6	36.4				flow on ext., int. or both
			247.1	-32.3	36.4				pointA: actual point B19
			253.0	-34.6	16.8				pointB: actual point F19
			253.0	-32.3	16.8				pointC: actual point D19
									pointD: actual point H19

200. -30. 20.
0. 0. 0. Exterior point
limit plane disp. (in pixels)

Quadric 175
Component no.
1
flow on ext., int. or both
pointA: actual point C19
pointB: actual point D19
pointC: actual point G19
pointD: actual point H19
Exterior point
limit plane disp. (in pixels)

Quadric 176
Component no.
20
flow on ext., int. or both
pointA: actual point A19
pointB: actual point E19
pointC: actual point B19
pointD: actual point F19
Exterior point
limit plane disp. (in pixels)

Quadric 177
Component no.
1
flow on ext., int. or both
pointA: actual point K19
pointB: actual point L19
pointC: actual point M19
pointD: actual point N19
Exterior point
limit plane disp. (in pixels)

Quadric 178
Component no.
20
flow on ext., int. or both
pointA: actual point O19
pointB: actual point P19
pointC: actual point Q19
pointD: actual point R19
Exterior point
limit plane disp. (in pixels)

Quadric 179
Component no.
1
flow on ext., int. or both
pointA: actual point K19
pointB: actual point L19
pointC: actual point M19
pointD: actual point N19
Exterior point
limit plane disp. (in pixels)

Quadric 180
Component no.
20
flow on ext., int. or both
pointA: actual point L19
pointB: actual point P19
pointC: actual point M19
pointD: actual point R19
Exterior point
limit plane disp. (in pixels)

'PEM-AXIS base, CDGH19'
20
PlateB
1
263.9 -34.6 16.8
253.0 -34.6 16.8
263.9 -32.3 16.8
253.0 -32.3 16.8
250. -30. 0.
0. 0. 0. Exterior point
limit plane disp. (in pixels)

'PEM-AXIS base, ABBF19'
20
PlateB
1
269.8 -34.6 36.4
269.8 -32.3 36.4
247.1 -34.6 36.4
247.1 -32.3 36.4
250. -30. 50.
0. 0. 0. Exterior point
limit plane disp. (in pixels)

'PEM-AXIS base, KLMM19'
20
PlateB
1
253.0 -34.6 31.5
263.9 -34.6 31.5
253.0 -48.3 31.5
263.9 -48.3 31.5
260. -40. 50.
0. 0. 0. Exterior point
limit plane disp. (in pixels)

'PEM-AXIS base, OPQR19'
20
PlateB
1
253.0 -34.6 20.9
263.9 -34.6 20.9
253.0 -48.3 20.9
263.9 -48.3 20.9
250. -40. 0.
0. 0. 0. Exterior point
limit plane disp. (in pixels)

'PEM-AXIS base, KOMQ19'
20
PlateB
1
253.0 -34.6 31.5
253.0 -34.6 20.9
253.0 -48.3 31.5
253.0 -48.3 20.9
200. -60. 30.
0. 0. 0. Exterior point
limit plane disp. (in pixels)

'PEM-AXIS base, LPNR19'
20
PlateB
1
263.9 -34.6 31.5
263.9 -34.6 20.9
263.9 -48.3 31.5
263.9 -48.3 20.9
300. -60. 30.
0. 0. 0. Exterior point
limit plane disp. (in pixels)

'PEM-AXIS base, MNQR19'
20
PlateB
1
253.0 -48.3 31.5
263.9 -48.3 31.5
253.0 -48.3 20.9
263.9 -48.3 20.9
250. -60. 30.
0. 0. 0. Exterior point
limit plane disp. (in pixels)

Quadric 182
Component no.
20
flow on ext., int. or both
pointA: radiusA
radiusB
12.3
Rlength
15.2
dircos
0. 0.5 0.866
limit plane disp. (in pixels)
F3I limits
200. 300. -80. 0. 0. 80.
Plane 11
Component no.
20
pointA
258.3 -44.4 38.8
dircos
0. 0.5 0.866
radius
6.3
Quadric 183
Component no.
20
flow on ext., int. or both
pointA
255.8 19.6 10.4
pointB
258.3 -33.0 26.6
radius
2.
0. -0.5
200. 300. -50. 50. 0. 50.
limit plane disp. (in pixels)
F3I limits

Quadric 184
Component no.
21
PlateA
1
5.9 48.1 -42.5
28.7 48.1 -51.4
42.8 48.1 -42.5
30. 100. -50.
0. 0. 0. Exterior point
limit plane disp. (in pixels)

Quadric 185
Component no.
21
PlateA
1
5.9 48.1 -42.5
28.7 48.1 -51.4
5.9 36.4 -42.5
10. 50. -100.
0. 0. 0. Exterior point
limit plane disp. (in pixels)

Quadric 186
Component no.
21
PlateA
1
28.7 48.1 -51.4
42.8 48.1 -42.5
42.8 36.4 -42.5
80. 50. -100.
0. 0. 0. Exterior point
limit plane disp. (in pixels)

'PEM-ZEPS base, BDE20'	13.0	138.6	-43.7	pointD: actual point N20
21	0.	100.	-50.	Exterior point
PlateA	0.	0.	0.	limit plane disp. (in pixels)
1	'PEM-ZEPS box HILM20'			
21	Component no.			
PlateB	flow on ext., int. or both			
1	30.7	150.0	-55.1	pointA: actual point H20
21	41.2	150.0	-36.9	pointB: actual point I20
PlateB	30.7	138.6	-55.1	pointC: actual point L20
1	41.2	138.6	-36.9	pointD: actual point M20
21	100.	100.	-50.	Exterior point
CylinderA	0.	0.	0.	limit plane disp. (in pixels)
1	'PEM-ZEPS base, FG20'			
21	27.3	48.1	-39.8	pointA
PlateB	27.3	55.1	-39.8	pointB
1	10.	0.	0.	radius
21	0.	50.	80.	limit plane disp. (in pixels)
CylinderA	0.	0.	-90.	F3I limits
1	Plane 12			
21	Component no.			
RingA	27.3	55.1	-39.8	pointA
0.	1.	0.	0.	dircos
2.8	0.	0.	0.	radius1
10.0	0.	0.	0.	radius2
'PEM-ZEPS base, G20'	13.0	138.6	-43.7	pointA: actual point G20
21	0.	100.	-50.	Exterior point
PlateB	0.	0.	0.	limit plane disp. (in pixels)
1	'PEM-ZEPS shaft (approx.) PQ20'			
21	Component no.			
CylinderA	27.1	138.6	-40.65	pointA
1	27.1	55.1	-40.65	pointB
2.8	0.	0.	0.	radius
0.	0.	50.	150.	limit plane disp. (in pixels)
0.	100.	100.	-26.2	F3I limits
'MLS gizmo box ABCD21'	13.0	138.6	-43.7	pointA: actual point ABCD21
22	0.	100.	-50.	Exterior point
PlateB	0.	0.	0.	limit plane disp. (in pixels)
1	'PEM-ZEPS base, IJK20'			
21	30.7	150.0	-55.1	pointA: actual point I20
PlateB	41.2	150.0	-36.9	pointB: actual point J20
1	13.0	138.6	-43.7	pointC: actual point K20
21	24.3	138.6	-26.2	pointD: actual point L20
100.	200.	0.	0.	Exterior point
0.	0.	0.	0.	limit plane disp. (in pixels)
'PEM-ZEPS base, LMNO20'	13.0	138.6	-43.7	pointA: actual point LMNO20
21	0.	100.	-50.	Exterior point
PlateB	0.	0.	0.	limit plane disp. (in pixels)
1	'PEM-ZEPS base, OPQ20'			
21	30.7	150.0	-55.1	pointA: actual point OPQ20
PlateB	41.2	150.0	-36.9	pointB: actual point R20
1	13.0	138.6	-43.7	pointC: actual point S20
21	24.3	138.6	-26.2	pointD: actual point T20
100.	200.	0.	0.	Exterior point
0.	0.	0.	0.	limit plane disp. (in pixels)
'PEM-ZEPS base, RST20'	13.0	138.6	-43.7	pointA: actual point R20
21	0.	100.	-50.	Exterior point
PlateB	0.	0.	0.	limit plane disp. (in pixels)
1	'PEM-ZEPS base, UVW20'			
21	30.7	150.0	-55.1	pointA: actual point UVW20
PlateB	41.2	150.0	-36.9	pointB: actual point X20
1	13.0	138.6	-43.7	pointC: actual point Y20
21	24.3	138.6	-26.2	pointD: actual point Z20
100.	200.	0.	0.	Exterior point
0.	0.	0.	0.	limit plane disp. (in pixels)
'PEM-ZEPS base, XYZ20'	13.0	138.6	-43.7	pointA: actual point XYZ20
21	0.	100.	-50.	Exterior point
PlateB	0.	0.	0.	limit plane disp. (in pixels)
1	'PEM-ZEPS base, ABCD21'			
21	175.2	73.7	20.0	pointA: actual point ABCD21
PlateB	217.0	73.7	20.0	pointB: actual point B21
1	175.2	48.1	20.0	pointC: actual point C21
21	217.0	48.1	20.0	pointD: actual point D21
200.	50.	40.	0.	Exterior point
0.	0.	0.	0.	limit plane disp. (in pixels)
'MLS gizmo box EFGH21'	13.0	138.6	-43.7	pointA: actual point EFGH21
22	0.	100.	-50.	Exterior point
PlateB	0.	0.	0.	limit plane disp. (in pixels)
1	'PEM-ZEPS base, IJKL20'			
21	30.7	150.0	-55.1	pointA: actual point IJKL20
PlateB	41.2	150.0	-36.9	pointB: actual point J20
1	13.0	138.6	-43.7	pointC: actual point K20
21	24.3	138.6	-26.2	pointD: actual point L20
100.	200.	0.	0.	Exterior point
0.	0.	0.	0.	limit plane disp. (in pixels)
'PEM-ZEPS base, MNOP20'	13.0	138.6	-43.7	pointA: actual point MNOP20
21	0.	100.	-50.	Exterior point
PlateB	0.	0.	0.	limit plane disp. (in pixels)
1	'PEM-ZEPS base, QRST20'			
21	30.7	150.0	-55.1	pointA: actual point QRST20
PlateB	41.2	150.0	-36.9	pointB: actual point R20
1	13.0	138.6	-43.7	pointC: actual point S20
21	24.3	138.6	-26.2	pointD: actual point T20
100.	200.	0.	0.	Exterior point
0.	0.	0.	0.	limit plane disp. (in pixels)
'PEM-ZEPS base, UVWX20'	13.0	138.6	-43.7	pointA: actual point UVWX20
21	0.	100.	-50.	Exterior point
PlateB	0.	0.	0.	limit plane disp. (in pixels)
1	'PEM-ZEPS base, YZAB20'			
21	30.7	150.0	-55.1	pointA: actual point YZAB20
PlateB	41.2	150.0	-36.9	pointB: actual point Z20
1	13.0	138.6	-43.7	pointC: actual point A20
21	24.3	138.6	-26.2	pointD: actual point B20
100.	200.	0.	0.	Exterior point
0.	0.	0.	0.	limit plane disp. (in pixels)

<p>Quadric 199 Component no. 1 PlateB 22 1 217.0 73.7 20.0 217.0 73.7 2.1 217.0 48.1 20.0 217.0 48.1 2.1 250. 50. 40. 0. 0. 0. 0.</p> <p>'MLS gizmo box BFDH21' 22 PlateB 1 217.0 73.7 20.0 217.0 73.7 2.1 217.0 48.1 20.0 217.0 48.1 2.1 250. 50. 40. 0. 0. 0. 0.</p> <p>'MLS cylinder QR21' 22 CylinderA 1 172.7 24.5 16.0 218.0 24.5 16.0 5.9 0. 0. 150. 250. 0. 50. 0. 40.</p> <p>'MLS cylinder end' 22 Disk 1 218.0 24.5 16.0 1. 0. 0. 5.9</p> <p>'MLS LHS box ABCD22' 22 PlateB 1 150.4 44.1 35.3 172.7 44.1 35.3 150.4 3.2 35.3 172.7 3.2 35.3 200. 50. 40. 0. 0. 0.</p> <p>'MLS LHS box ABEF22' 22 PlateB 1 150.4 44.1 35.3 172.7 44.1 35.3 150.4 44.1 21.4 172.7 44.1 21.4 200. 50. 40. 0. 0. 0.</p> <p>'MLS LHS box CDGH22' 22 PlateB 1 150.4 3.2 35.3 172.7 3.2 35.3 150.4 3.2 21.4 172.7 3.2 21.4 200. -10. 40. 0. 0. 0.</p> <p>'MLS LHS box BFDH22' 22 PlateB 1 172.7 44.1 35.3 172.7 44.1 21.4 172.7 3.2 35.3 172.7 3.2 21.4 200. -10. 40. 0. 0. 0.</p> <p>'MLS LHS box IJKL21' 22 PlateB 1 172.7 3.2 9.5 172.7 3.2 2.1 218.0 3.2 9.5 218.0 3.2 2.1 250. 30. 40. 0. 0. 0.</p> <p>'MLS box behind antenna IJMN21' 22 PlateB 1 172.7 3.2 9.5 172.7 3.2 2.1 218.0 3.2 9.5 218.0 3.2 2.1 250. 30. 40. 0. 0. 0.</p> <p>'MLS box behind antenna IJMN21' 22 PlateB 1 172.7 3.2 9.5 172.7 3.2 2.1 218.0 3.2 9.5 218.0 3.2 2.1 250. 30. 40. 0. 0. 0.</p>	<p>flow on ext., int. or both pointA: actual point I21 pointB: actual point J21 pointC: actual point M21 pointD: actual point N21 Exterior point limit plane disp. (in pixels)</p> <p>Quadric 206 Component no. 22 flow on ext., int. or both pointA pointB radius limit plane disp. (in pixels) F3I limits Plane 13 Component no.</p> <p>pointA direction cosine normal to disk radius</p> <p>Quadric 207 Component no. 22 flow on ext., int. or both pointA: actual point A22 pointB: actual point B22 pointC: actual point C22 pointD: actual point D22 Exterior point limit plane disp. (in pixels)</p> <p>Quadric 208 Component no. 22 flow on ext., int. or both pointA: actual point A22 pointB: actual point B22 pointC: actual point E22 pointD: actual point F22 Exterior point limit plane disp. (in pixels)</p> <p>Quadric 209 Component no. 22 flow on ext., int. or both pointA: actual point C22 pointB: actual point D22 pointC: actual point G22 pointD: actual point H22 Exterior point limit plane disp. (in pixels)</p> <p>Quadric 210 Component no. 22 flow on ext., int. or both pointA: actual point B22 pointB: actual point F22 pointC: actual point D22 pointD: actual point H22 Exterior point limit plane disp. (in pixels)</p> <p>Quadric 205 Component no. 22 flow on ext., int. or both pointA: actual point K21 pointB: actual point O21 pointC: actual point L21 pointD: actual point P21 Exterior point limit plane disp. (in pixels)</p> <p>Quadric 203 Component no. 22 flow on ext., int. or both pointA: actual point J21 pointB: actual point N21 pointC: actual point L21 pointD: actual point P21 Exterior point limit plane disp. (in pixels)</p> <p>Quadric 204 Component no. 22 flow on ext., int. or both pointA: actual point K21 pointB: actual point O21 pointC: actual point L21 pointD: actual point P21 Exterior point limit plane disp. (in pixels)</p> <p>Quadric 205 Component no. 22 flow on ext., int. or both pointA: actual point K21 pointB: actual point O21 pointC: actual point L21 pointD: actual point P21 Exterior point limit plane disp. (in pixels)</p>
---	---

1	'MLS LHS box AEGG22'	169.3	29.1	9.5	flow on ext., int. or both
22	PlateB	172.7	29.1	9.5	pointA: actual point Q22
1	150.4	44.1	35.3	pointB: actual point K22	pointC: actual point Q22
150.4	44.1	21.4	pointD: actual point M22	Exterior point	
150.4	3.2	35.3	limit plane disp. (in pixels)		
150.4	3.2	21.4			
100.	-10.	40.			
0.	0.	0.			
22	'MLS LHS box BFG22'				
22	PlateB	169.3	3.2	9.5	flow on ext., int. or both
1	172.7	3.2	9.5	pointA: actual point R22	
150.4	44.1	21.4	pointB: actual point L22	pointC: actual point P22	
172.7	44.1	21.4	pointD: actual point N22	Exterior point	
150.4	29.1	21.4	limit plane disp. (in pixels)		
172.7	29.1	21.4			
200.	50.	0.			
0.	0.	0.			
22	'MLS LHS box CDE22'				
22	PlateB	169.3	29.1	9.5	flow on ext., int. or both
1	172.7	29.1	2.1	pointA: actual point Q22	
150.4	29.1	21.4	pointB: actual point O22	pointC: actual point R22	
172.7	29.1	9.5	pointD: actual point P22	Exterior point	
169.3	29.1	9.5	limit plane disp. (in pixels)		
172.7	29.1	9.5			
200.	50.	0.			
0.	0.	0.			
22	'MLS LHS box DEHI22'				
22	PlateB	185.0	15.9	26.9	flow on ext., int. or both
1	217.3	15.9	34.8	pointA: actual point B24	
150.4	3.2	21.4	pointB: actual point C24	pointC: actual point D24	
172.7	3.2	21.4	pointD: actual point E24	Exterior point	
169.3	3.2	9.5	limit plane disp. (in pixels)		
172.7	3.2	9.5			
200.	-50.	0.			
0.	0.	0.			
22	'MLS LHS box FGH22'				
22	PlateB	186.1	29.8	41.0	flow on ext., int. or both
1	216.3	29.8	33.7	pointA: actual point E24	
150.4	3.2	21.4	pointB: actual point F24	pointC: actual point G24	
172.7	3.2	21.4	pointD: actual point H24	Exterior point	
169.3	3.2	9.5	limit plane disp. (in pixels)		
172.7	3.2	9.5			
200.	-50.	0.			
0.	0.	0.			
22	'MLS LHS box GHI22'				
22	PlateB	186.1	29.8	33.7	flow on ext., int. or both
1	216.3	29.8	41.0	pointA: actual point D24	
150.4	3.2	21.4	pointB: actual point E24	pointC: actual point F24	
172.7	3.2	21.4	pointD: actual point G24	Exterior point	
169.3	3.2	9.5	limit plane disp. (in pixels)		
172.7	3.2	9.5			
200.	-50.	0.			
0.	0.	0.			
22	'MLS LHS box HIL24'				
22	PlateB	190.6	37.3	38.7	flow on ext., int. or both
1	210.7	37.3	44.0	pointA: actual point H24	
150.4	29.1	21.4	pointB: actual point I24	pointC: actual point L24	
172.7	29.1	21.4	pointD: actual point M24	Exterior point	
169.3	3.2	9.5	limit plane disp. (in pixels)		
172.7	3.2	9.5			
200.	-50.	0.			
0.	0.	0.			
22	'MLS LHS box IJK22'				
22	PlateB	190.6	37.3	38.7	flow on ext., int. or both
1	210.7	37.3	44.0	pointA: actual point H24	
150.4	29.1	21.4	pointB: actual point I24	pointC: actual point L24	
172.7	29.1	21.4	pointD: actual point M24	Exterior point	
169.3	3.2	9.5	limit plane disp. (in pixels)		
172.7	29.1	21.4			
200.	-50.	0.			
0.	0.	0.			
22	'MLS LHS box JKL22'				
22	PlateB	190.6	37.3	38.7	flow on ext., int. or both
1	210.7	37.3	44.0	pointA: actual point H24	
150.4	29.1	21.4	pointB: actual point I24	pointC: actual point L24	
172.7	29.1	21.4	pointD: actual point M24	Exterior point	
169.3	3.2	9.5	limit plane disp. (in pixels)		
172.7	29.1	21.4			
200.	-50.	0.			
0.	0.	0.			
22	'MLS LHS box QK22'				
22	PlateB	185.0	15.9	26.9	flow on ext., int. or both
1	217.3	15.9	34.8	pointA: actual point B24	
150.4	3.2	21.4	pointB: actual point C24	pointC: actual point D24	
172.7	3.2	21.4	pointD: actual point E24	Exterior point	
169.3	3.2	9.5	limit plane disp. (in pixels)		
172.7	3.2	9.5			
200.	-50.	0.			
0.	0.	0.			

216.3	5.5	30.5			pointD: actual point G24
200.	50.	100.			Exterior point
0.	0.	0.	0.		limit plane disp. (in pixels)
Quadratic 224					
Component no.					
flow on ext., int. or both					
186.1	5.5	32.2			pointA: actual point F24
216.3	5.5	30.5			pointB: actual point G24
189.5	-6.1	20.9			pointC: actual point J24
213.9	-6.1	26.8			pointD: actual point K24
200.	50.	100.			Exterior point
0.	0.	0.	0.		limit plane disp. (in pixels)
Quadratic 225					
Component no.					
flow on ext., int. or both					
189.5	-6.1	20.9			pointA: actual point J24
213.9	-6.1	26.8			pointB: actual point K24
201.6	-16.8	21.1			pointC: actual point M24
200.	50.	100.			Exterior point
0.	0.	0.	0.		limit plane disp. (in pixels)
Back face Quadratic 226					
Component no.					
flow on ext., int. or both					
185.0	16.4	24.2			pointA: actual point B24
217.3	16.4	32.1			pointB: actual point C24
186.1	30.7	32.0			pointC: actual point D24
216.3	30.7	38.3			pointD: actual point E24
200.	50.	-100.			Exterior point
0.	0.	0.	0.		limit plane disp. (in pixels)
Back face Quadratic 227					
Component no.					
flow on ext., int. or both					
186.1	30.7	32.0			pointA: actual point D24
216.3	30.7	38.3			pointB: actual point E24
190.6	38.4	36.0			pointC: actual point H24
210.7	38.4	41.3			pointD: actual point I24
200.	50.	-100.			Exterior point
0.	0.	0.	0.		limit plane disp. (in pixels)
Back face Quadratic 228					
Component no.					
flow on ext., int. or both					
190.6	38.4	36.0			pointA: actual point H24
210.7	38.4	41.3			pointB: actual point I24
200.2	43.6	43.5			pointC: actual point L24
200.	50.	-100.			Exterior point
0.	0.	0.	0.		limit plane disp. (in pixels)
Back face Quadratic 229					
Component no.					
flow on ext., int. or both					
185.0	16.4	24.2			pointA: actual point B24
217.3	16.4	32.1			pointB: actual point C24
186.1	5.7	20.5			pointC: actual point F24
216.3	5.7	27.8			pointD: actual point G24
200.	50.	-100.			Exterior point
0.	0.	0.	0.		limit plane disp. (in pixels)
Back face Quadratic 230					
Component no.					
flow on ext., int. or both					
185.0	15.9	26.9			pointA: actual point B24
216.3	15.9	34.8			pointB: actual point C24
217.3	16.4	32.1			pointC: actual point E24
216.3	29.8	41.0			pointD: actual point E24
250.	15.	40.			Exterior point
0.	0.	0.	0.		limit plane disp. (in pixels)
Back face Quadratic 231					
Component no.					
flow on ext., int. or both					
189.5	-6.3	18.2			pointA: actual point J24
213.9	-6.3	24.1			pointB: actual point K24
201.6	-17.3	18.4			pointC: actual point M24
200.	50.	-100.			Exterior point
0.	0.	0.	0.		limit plane disp. (in pixels)
Back face Quadratic 232					
Component no.					
flow on ext., int. or both					
217.3	15.9	34.8			pointA: actual point C24
217.3	16.4	32.1			pointB: actual point C24
216.3	29.8	41.0			pointC: actual point E24
216.3	30.7	38.3			pointD: actual point E24
250.	15.	40.			Exterior point
0.	0.	0.	0.		limit plane disp. (in pixels)
Back face Quadratic 233					
Component no.					
flow on ext., int. or both					
216.3	29.8	41.0			pointA: actual point E24
216.3	30.7	38.3			pointB: actual point E24
210.7	37.3	44.0			pointC: actual point I24
210.7	38.4	41.3			pointD: actual point I24
250.	30.	40.			Exterior point
0.	0.	0.	0.		limit plane disp. (in pixels)
Back face Quadratic 234					
Component no.					
flow on ext., int. or both					
185.0	15.9	26.9			pointA: actual point B24
216.3	16.4	24.2			pointB: actual point B24
186.1	29.8	33.7			pointC: actual point D24
186.1	30.7	32.0			pointD: actual point D24
100.	15.	40.			Exterior point
0.	0.	0.	0.		limit plane disp. (in pixels)
Back face Quadratic 235					
Component no.					
flow on ext., int. or both					
186.1	29.8	33.7			pointA: actual point D24
186.1	30.7	32.0			pointB: actual point D24
190.6	37.3	38.7			pointC: actual point H24
190.6	38.4	36.0			pointD: actual point H24
100.	30.	40.			Exterior point
0.	0.	0.	0.		limit plane disp. (in pixels)
Back face Quadratic 236					
Component no.					
flow on ext., int. or both					
217.3	15.9	34.8			pointA: actual point C24

217.3 16.4 32.1 pointB: actual point C24
216.3 5.5 30.5 pointC: actual point G24
216.3 5.7 27.8 pointD: actual point G24
250. 15. 40. Exterior point
0. 0. 0. limit plane disp. (in pixels)

Quadric 237
Component no.
22
PlateB
1
'MLS large antenna GQK24'
189.5 -6.1 20.9 flow on ext., int. or both
189.5 -6.3 18.2 pointA: actual point J24
201.6 -16.8 21.1 pointB: actual point J24
201.6 -17.3 18.4 pointC: actual point M24
100. -20. 40. pointD: actual point M24
0. 0. 0. Exterior point
0. 0. 0. limit plane disp. (in pixels)

Quadric 243
Component no.
22
PlateB
1
'MLS small antenna OPQR24'
174.7 4.6 53.5 flow on ext., int. or both
183.8 4.6 55.7 pointA: actual point Q24
175.6 9.1 54.9 pointB: actual point P24
182.9 9.1 57.1 pointC: actual point Q24
200. 0. 100. pointD: actual point R24
0. 0. 0. Exterior point
0. 0. 0. limit plane disp. (in pixels)

Quadric 244
Component no.
22
PlateB
1
'MLS small antenna OPQR24'
174.7 4.6 53.5 flow on ext., int. or both
183.8 4.6 55.7 pointA: actual point Q24
175.6 9.1 54.9 pointB: actual point P24
182.9 9.1 57.1 pointC: actual point Q24
200. 0. 100. pointD: actual point R24
0. 0. 0. Exterior point
0. 0. 0. limit plane disp. (in pixels)

Quadric 245
Component no.
22
PlateA
1
'MLS small antenna QRU24'
175.6 9.1 54.9 flow on ext., int. or both
182.9 9.1 57.1 pointA: actual point Q24
179.25 13.7 57.8 pointB: actual point R24
200. 0. 100. pointC: actual point U24
0. 0. 0. Exterior point
0. 0. 0. limit plane disp. (in pixels)

Quadric 246
Component no.
22
PlateB
1
'MLS small antenna OPQR24'
174.7 4.7 50.8 flow on ext., int. or both
183.8 4.7 53.0 pointA: actual point Q24
175.6 9.4 52.2 pointB: actual point P24
182.9 9.4 54.4 pointC: actual point Q24
200. 0. -100. pointD: actual point R24
0. 0. 0. Exterior point
0. 0. 0. limit plane disp. (in pixels)

Quadric 247
Component no.
22
PlateA
1
'MLS small antenna QRU24'
175.6 9.4 52.2 flow on ext., int. or both
182.9 9.4 54.4 pointA: actual point Q24
179.25 14.1 55.1 pointB: actual point R24
200. 0. -100. pointC: actual point U24
0. 0. 0. Exterior point
0. 0. 0. limit plane disp. (in pixels)

Quadric 248
Component no.
22
PlateB
1
'MLS small antenna OFST24'
174.7 4.6 53.5 flow on ext., int. or both
183.8 4.6 55.7 pointA: actual point Q24
175.6 0. 52.1 pointB: actual point P24
182.9 0. 54.3 pointC: actual point S24
200. 0. 100. pointD: actual point T24
0. 0. 0. Exterior point
0. 0. 0. limit plane disp. (in pixels)

Quadric 249
Component no.
22
PlateB
1
'MLS small antenna STV24'
174.7 4.6 53.5 flow on ext., int. or both
183.8 4.6 55.7 pointA: actual point Q24
175.6 0. 52.1 pointB: actual point P24
182.9 0. 54.3 pointC: actual point S24
200. 0. 100. pointD: actual point T24
0. 0. 0. Exterior point
0. 0. 0. limit plane disp. (in pixels)

217.3 16.4 32.1 pointB: actual point C24
216.3 5.5 30.5 pointC: actual point G24
216.3 5.7 27.8 pointD: actual point G24
250. 15. 40. Exterior point
0. 0. 0. limit plane disp. (in pixels)

Quadric 237
Component no.
22
PlateB
1
'MLS large antenna GQK24'
189.5 -6.1 20.9 flow on ext., int. or both
189.5 -6.3 18.2 pointA: actual point J24
201.6 -16.8 21.1 pointB: actual point J24
201.6 -17.3 18.4 pointC: actual point M24
100. -20. 40. pointD: actual point M24
0. 0. 0. Exterior point
0. 0. 0. limit plane disp. (in pixels)

Quadric 238
Component no.
22
PlateB
1
'MLS large antenna BBFF24'
185.0 15.9 26.9 flow on ext., int. or both
185.0 16.4 24.2 pointA: actual point B24
186.1 5.5 23.2 pointB: actual point B24
186.1 5.7 20.5 pointC: actual point F24
100. 15. 40. pointD: actual point F24
0. 0. 0. Exterior point
0. 0. 0. limit plane disp. (in pixels)

Quadric 239
Component no.
22
PlateB
1
'MLS large antenna FRUJ24'
186.1 5.5 23.2 flow on ext., int. or both
186.1 5.7 20.5 pointA: actual point F24
189.5 -6.1 20.9 pointB: actual point J24
189.5 -6.3 18.2 pointC: actual point J24
100. 0. 40. pointD: actual point J24
0. 0. 0. Exterior point
0. 0. 0. limit plane disp. (in pixels)

Quadric 240
Component no.
22
PlateB
1
'MLS large antenna ILL24'
210.7 37.3 44.0 flow on ext., int. or both
210.7 38.4 41.3 pointA: actual point I24
200.2 42.3 46.2 pointB: actual point I24
200.2 43.6 43.5 pointC: actual point L24
250. 40. 40. pointD: actual point L24
0. 0. 0. Exterior point
0. 0. 0. limit plane disp. (in pixels)

Quadric 241
Component no.
22
PlateB
1
'MLS large antenna KQHM24'
213.9 -6.1 26.8 flow on ext., int. or both
213.9 -6.3 24.1 pointA: actual point K24
201.6 -16.8 21.1 pointB: actual point K24
201.6 -17.3 18.4 pointC: actual point M24
250. -20. 40. pointD: actual point M24
0. 0. 0. Exterior point
0. 0. 0. limit plane disp. (in pixels)

Quadric 242
Component no.
22
PlateB
1
'MLS large antenna HLL24'
190.6 37.3 38.7 flow on ext., int. or both
190.6 38.4 36.0 pointA: actual point H24
200.2 42.3 46.2 pointB: actual point H24
200.2 43.6 43.5 pointC: actual point L24
0. 0. 0. pointD: actual point L24

175.6	0.	52.1			flow on ext., int. or both					
182.9	0.	54.3			pointA: actual point S24					
179.25	-4.6	51.0			pointB: actual point T24					
200.	0.	100.			pointC: actual point V24					pointD: actual point V24
0.	0.	0.	0.		Exterior point					Exterior point
0.	0.	0.	0.		limit plane disp. (in pixels)					limit plane disp. (in pixels)
					back plate Quadric 250					
22					Component no.					
174.7	4.7	50.8			flow on ext., int. or both					
183.8	4.7	53.0			pointA: actual point O24					
175.6	0.	49.4			pointB: actual point Q24					
182.9	0.	51.6			pointC: actual point S24					
200.	0.	-100.			pointD: actual point T24					
0.	0.	0.	0.		Exterior point					
0.	0.	0.	0.		limit plane disp. (in pixels)					limit plane disp. (in pixels)
					back plate Quadric 251					
22					Component no.					
175.6	0.	49.4			flow on ext., int. or both					
182.9	0.	51.6			pointA: actual point S24					
179.25	-4.7	48.3			pointB: actual point T24					
200.	0.	-100.			pointC: actual point V24					
0.	0.	0.	0.		Exterior point					
0.	0.	0.	0.		limit plane disp. (in pixels)					limit plane disp. (in pixels)
					back plate Quadric 252					
22					Component no.					
183.8	4.6	55.7			flow on ext., int. or both					
183.8	4.7	53.0			pointA: actual point P24					
182.9	9.1	57.1			pointB: actual point Q24					
182.9	9.4	54.4			pointC: actual point R24					
200.	0.	50.			pointD: actual point T24					
0.	0.	0.	0.		Exterior point					
0.	0.	0.	0.		limit plane disp. (in pixels)					limit plane disp. (in pixels)
					back plate Quadric 253					
22					Component no.					
183.8	4.6	55.7			flow on ext., int. or both					
183.8	4.7	53.0			pointA: actual point P24					
182.9	0.	54.3			pointB: actual point Q24					
182.9	0.	51.6			pointC: actual point T24					
200.	0.	50.			pointD: actual point T24					
0.	0.	0.	0.		Exterior point					
0.	0.	0.	0.		limit plane disp. (in pixels)					limit plane disp. (in pixels)
					back plate Quadric 254					
22					Component no.					
182.9	9.1	57.1			flow on ext., int. or both					
182.9	9.4	54.4			pointA: actual point R24					
179.25	13.7	57.8			pointB: actual point T24					
179.25	14.1	55.1			pointC: actual point U24					
200.	0.	50.			pointD: actual point V24					
0.	0.	0.	0.		Exterior point					
0.	0.	0.	0.		limit plane disp. (in pixels)					limit plane disp. (in pixels)
					back plate Quadric 255					
22					Component no.					
182.9	0.	54.3			flow on ext., int. or both					
182.9	0.	51.6			pointA: actual point T24					
179.25	-4.6	51.0			pointB: actual point T24					
200.	0.	100.			pointC: actual point V24					
0.	0.	0.	0.		Exterior point					
0.	0.	0.	0.		limit plane disp. (in pixels)					limit plane disp. (in pixels)
					back plate Quadric 256					
22					Component no.					
174.7	4.6	53.5			flow on ext., int. or both					
174.7	4.7	50.8			pointA: actual point O24					
175.6	9.1	54.9			pointB: actual point Q24					
175.6	9.4	52.2			pointC: actual point Q24					
100.	0.	50.			pointD: actual point Q24					
0.	0.	0.	0.		Exterior point					
0.	0.	0.	0.		limit plane disp. (in pixels)					limit plane disp. (in pixels)
					back plate Quadric 257					
22					Component no.					
174.7	4.6	53.5			flow on ext., int. or both					
174.7	4.7	50.8			pointA: actual point O24					
175.6	0.	52.1			pointB: actual point O24					
175.6	0.	49.4			pointC: actual point S24					
100.	0.	50.			pointD: actual point S24					
0.	0.	0.	0.		Exterior point					
0.	0.	0.	0.		limit plane disp. (in pixels)					limit plane disp. (in pixels)
					back plate Quadric 258					
22					Component no.					
179.25	13.7	57.8			flow on ext., int. or both					
179.25	14.1	55.1			pointA: actual point U24					
175.6	9.1	54.9			pointB: actual point U24					
175.6	9.4	52.2			pointC: actual point Q24					
100.	50.	50.			pointD: actual point Q24					
0.	0.	0.	0.		Exterior point					
0.	0.	0.	0.		limit plane disp. (in pixels)					limit plane disp. (in pixels)
					back plate Quadric 259					
22					Component no.					
175.6	0.	52.1			flow on ext., int. or both					
175.6	0.	49.4			pointA: actual point S24					
179.25	-4.6	51.0			pointB: actual point S24					
179.25	-4.7	48.3			pointC: actual point V24					
100.	-50.	50.			pointD: actual point V24					
0.	0.	0.	0.		Exterior point					
0.	0.	0.	0.		limit plane disp. (in pixels)					limit plane disp. (in pixels)
					back plate Quadric 260					
22					Component no.					
218.0	19.7	30.9			flow on ext., int. or both					
218.0	30.4	16.0			pointA: actual point A25					
218.0	10.3	30.9			pointB: actual point B25					
218.0	18.6	16.0			pointC: actual point C25					
250.	0.	50.			pointD: actual point D25					
0.	0.	0.	0.		Exterior point					
0.	0.	0.	0.		limit plane disp. (in pixels)					limit plane disp. (in pixels)
					back plate Quadric 261					
22					Component no.					
218.0	15.0	30.9			flow on ext., int. or both					
226.8	15.0	30.9			pointA					
4.8					pointB					
0.	0.	0.			radius					
0.	0.	0.			limit plane disp. (in pixels)					limit plane disp. (in pixels)
200.	300.	0.	50.	0.	FBI limits					

Component no.	Component no.	Component no.	Component no.
22 Plane 14 CylinderA	22 Plane 14 CylinderA	22 Plane 14 CylinderA	22 Plane 14 CylinderA
1 183.1 30.7 27.7 172.5 9.1 57.0 2. 0. 150. 300. 0. 50. 0. 100.	1 183.1 30.7 27.7 172.5 9.1 57.0 2. 0. 150. 300. 0. 50. 0. 100.	1 183.1 30.7 27.7 172.5 9.1 57.0 2. 0. 150. 300. 0. 50. 0. 100.	1 183.1 30.7 27.7 172.5 9.1 57.0 2. 0. 150. 300. 0. 50. 0. 100.
'MLS antenna arm, back E25'	'MLS antenna arm, back F25'	'MLS antenna arm, back G25'	'MLS antenna arm, back H25'
22 Disk 218.0 15.0 30.9 -1. 0. 0. 4.8	22 Disk 226.8 15.0 30.9 1. 0. 0. 4.8	22 Disk 216.3 30.7 35.3 2. 0. 150. 300. 0. 50. 0. 50.	22 Disk 216.3 30.7 35.3 2. 0. 150. 300. 0. 50. 0. 50.
'MLS antenna arm, back IJ25'	'MLS antenna arm, back K25'	'MLS antenna arm, back L25'	'MLS antenna arm, back M25'
22 CylinderA 183.1 30.7 27.7 216.3 30.7 35.3 2. 0. 150. 300. 0. 50. 0. 50.	22 CylinderA 183.1 30.7 27.7 172.5 0. 54.2 2. 0. 150. 300. 0. 50. 0. 100.	22 CylinderA 183.1 30.7 27.7 172.5 0. 54.2 2. 0. 150. 300. 0. 50. 0. 100.	22 CylinderA 183.1 30.7 27.7 172.5 0. 54.2 2. 0. 150. 300. 0. 50. 0. 100.
'MLS antenna arm, back N25'	'MLS antenna arm, side O25'	'MLS antenna arm, side P25'	'MLS antenna arm, side Q25'
22 SphereA 172.5 9.1 57.0 3.	22 SphereA 172.5 9.1 57.0 3.	22 SphereA 172.5 9.1 57.0 3.	22 SphereA 172.5 9.1 57.0 3.
'HGA-side bracework AB23'	'HGA-side bracework CB23'	'HGA-side bracework DB23'	'HGA-side bracework EB23'
23 CylinderA 221.0 31.1 0. 221.0 94.0 0. 1.5 0. 150. 250. 0. 100. -100. 100.	23 CylinderA 221.0 31.1 0. 221.0 94.0 0. 1.5 0. 150. 250. 0. 100. -100. 100.	23 CylinderA 221.0 29.6 -41.0 221.0 94.0 0. 1.5 0. 150. 250. 0. 100. -100. 100.	23 CylinderA 221.0 29.6 -41.0 221.0 94.0 0. 1.5 0. 150. 250. 0. 100. -100. 100.
'MLS antenna arm, back R25'	'MLS antenna arm, back S25'	'MLS antenna arm, back T25'	'MLS antenna arm, back U25'
22 SphereA 255.4 18.1 -41.0 221.0 94.0 0.	22 SphereA 255.4 18.1 -41.0 221.0 94.0 0.	22 SphereA 255.4 18.1 -41.0 221.0 94.0 0.	22 SphereA 255.4 18.1 -41.0 221.0 94.0 0.
'MLS antenna arm, back V25'	'MLS antenna arm, back W25'	'MLS antenna arm, back X25'	'MLS antenna arm, back Y25'
22 SphereA 183.1 30.7 27.7 3.	22 SphereA 183.1 30.7 27.7 3.	22 SphereA 183.1 30.7 27.7 3.	22 SphereA 183.1 30.7 27.7 3.
'MLS antenna arm, back Z25'	'MLS antenna arm, back AA25'	'MLS antenna arm, back AB25'	'MLS antenna arm, back AC25'
22 SphereA 183.1 30.7 27.7 3.	22 SphereA 183.1 30.7 27.7 3.	22 SphereA 183.1 30.7 27.7 3.	22 SphereA 183.1 30.7 27.7 3.

131.3	-40.6	-53.2	pointB: actual point L27	147.6	-55.4	-56.3	pointC: actual point I28
141.3	-50.5	-53.2	pointC: actual point Q27	121.0	-55.4	-56.3	pointD: actual point J28
131.3	-50.5	-53.2	pointD: actual point U27	150.	-50.	0.	Exterior point
150.	-50.	-100.	Exterior point	0.	0.	0.	limit plane disp. (in pixels)
0.	0.	0.	limit plane disp. (in pixels)				
Quadic 299							
Component no.							
PlateB							
1			flow on ext., int. or both				
141.3	-38.8	-49.4	pointA: actual point N27	121.0	-52.7	-66.7	pointA: actual point B28
131.3	-38.8	-49.4	pointB: actual point R27	121.0	-55.4	-66.7	pointB: actual point D28
141.3	-50.5	-49.4	pointC: actual point P27	121.0	-52.7	-56.3	pointC: actual point H28
131.3	-50.5	-49.4	pointD: actual point T27	121.0	-55.4	-56.3	pointD: actual point J28
250.	-50.	0.	Exterior point	50.	-50.	-100.	Exterior point
0.	0.	0.	limit plane disp. (in pixels)	0.	0.	0.	limit plane disp. (in pixels)
Quadic 300							
Component no.							
PlateB							
1			flow on ext., int. or both				
136.3	-50.5	-49.4	pointA	147.6	-55.4	-66.7	pointA: actual point C28
136.3	-50.5	-56.3	pointB	121.0	-55.4	-66.7	pointB: actual point D28
5.0			radius	145.0	-61.8	-66.7	pointC: actual point E28
0.	0.		limit plane disp. (in pixels)	133.8	-61.8	-66.7	pointD: actual point F28
100.	160.	-80.	F3I limits	150.	-50.	-100.	Exterior point
0.	0.	-80.		0.	0.	0.	limit plane disp. (in pixels)
Quadic 301							
Component no.							
PlateB							
1			flow on ext., int. or both				
136.3	-50.5	-49.4	pointA	147.6	-55.4	-66.7	pointA: actual point I28
0.	0.	-1.	direction cosine normal to disk	121.0	-55.4	-56.3	pointB: actual point J28
1.1			radius1	145.0	-61.8	-56.3	pointC: actual point K28
5.0			radius2	133.8	-61.8	-56.3	pointD: actual point L28
0.	0.		limit plane disp. (in pixels)	150.	-50.	0.	Exterior point
100.	160.	-80.	F3I limits	0.	0.	0.	limit plane disp. (in pixels)
0.	0.	-80.					
Quadic 302							
Component no.							
PlateB							
1			flow on ext., int. or both				
147.6	-52.7	-66.7	pointA: actual point A28	145.0	-61.8	-66.7	pointA: actual point E28
121.0	-52.7	-66.7	pointB: actual point B28	133.8	-61.8	-66.7	pointB: actual point F28
147.6	-55.4	-66.7	pointC: actual point C28	133.8	-61.8	-56.3	pointC: actual point K28
121.0	-55.4	-66.7	pointD: actual point D28	150.	-100.	0.	pointD: actual point L28
150.	-50.	-100.	Exterior point	0.	0.	0.	Exterior point
0.	0.	0.	limit plane disp. (in pixels)	0.	0.	0.	limit plane disp. (in pixels)
Quadic 303							
Component no.							
PlateB							
1			flow on ext., int. or both				
147.6	-52.7	-56.3	pointA: actual point G28	121.0	-55.4	-66.7	pointA: actual point D28
121.0	-52.7	-56.3	pointB: actual point H28	133.8	-61.8	-66.7	pointB: actual point F28
147.6	-55.4	-56.3	pointC: actual point I28	121.0	-55.4	-56.3	pointC: actual point J28
121.0	-55.4	-56.3	pointD: actual point L28	133.8	-61.8	-56.3	pointD: actual point L28
150.	-50.	-100.	Exterior point	50.	-100.	0.	Exterior point
0.	0.	0.	limit plane disp. (in pixels)	0.	0.	0.	limit plane disp. (in pixels)

0.	0.	0.	0.	0.	limit plane disp. (in pixels)
'HALOE box MNOP28'					
26	Component no.				
PlateB					
1	147.6	-43.7	-66.7	flow on ext., int. or both	
131.3	-43.7	-66.7	pointA: actual point A29		
147.6	-52.7	-66.7	pointB: actual point B29		
131.3	-52.7	-66.7	pointC: actual point C29		
150.	-50.	-100.	pointD: actual point D29		
0.	0.	0.	Exterior point		
0.	0.	0.	limit plane disp. (in pixels)		
'HALOE box ERGH29'					
26	Component no.				
PlateB					
1	147.6	-43.7	-56.3	flow on ext., int. or both	
131.3	-43.7	-56.3	pointA: actual point E29		
147.6	-52.7	-56.3	pointB: actual point F29		
131.3	-52.7	-56.3	pointC: actual point G29		
150.	-50.	0.	pointD: actual point H29		
0.	0.	0.	Exterior point		
0.	0.	0.	limit plane disp. (in pixels)		
'HALOE box ABEP29'					
26	Component no.				
PlateB					
1	147.6	-43.7	-66.7	flow on ext., int. or both	
131.3	-43.7	-66.7	pointA: actual point A29		
147.6	-43.7	-66.7	pointB: actual point B29		
131.3	-43.7	-66.7	pointC: actual point E29		
150.	0.	-50.	pointD: actual point F29		
0.	0.	0.	Exterior point		
0.	0.	0.	limit plane disp. (in pixels)		
'HALOE box BDFH29'					
26	Component no.				
PlateB					
1	147.6	-43.7	-66.7	flow on ext., int. or both	
131.3	-43.7	-66.7	pointA: actual point A29		
147.6	-43.7	-66.7	pointB: actual point B29		
131.3	-43.7	-66.7	pointC: actual point E29		
150.	0.	-50.	pointD: actual point F29		
0.	0.	0.	Exterior point		
0.	0.	0.	limit plane disp. (in pixels)		
'HALOE box BDFH29'					
26	Component no.				
PlateB					
1	131.3	-43.7	-66.7	flow on ext., int. or both	
131.3	-52.7	-66.7	pointA: actual point B29		
131.3	-43.7	-56.3	pointB: actual point D29		
131.3	-43.7	-56.3	pointC: actual point F29		
50.	-50.	-50.	pointD: actual point H29		
0.	0.	0.	Exterior point		
0.	0.	0.	limit plane disp. (in pixels)		
'HALOE box DHLM29'					
26	Component no.				
PlateB					
1	131.3	-43.7	-66.7	flow on ext., int. or both	
131.3	-52.7	-66.7	pointA: actual point B29		
131.3	-43.7	-56.3	pointB: actual point D29		
131.3	-43.7	-56.3	pointC: actual point F29		
50.	-50.	-50.	pointD: actual point H29		
0.	0.	0.	Exterior point		
0.	0.	0.	limit plane disp. (in pixels)		
'HALOE box DHLM29'					
26	Component no.				
PlateB					
1	131.3	-52.7	-66.7	flow on ext., int. or both	
131.3	-52.7	-66.7	pointA: actual point D29		
131.3	-52.7	-66.7	pointB: actual point H29		
121.0	-52.7	-66.7	pointC: actual point L29		
150.	0.	-50.	pointD: actual point M29		
0.	0.	0.	Exterior point		
0.	0.	0.	limit plane disp. (in pixels)		
'HALOE cover IJ29'					
26	Component no.				
ConeA					
1	145.65	-48.0	-64.9	flow on ext., int. or both	
-1.	0.	0.	pointA		
25.	0.	0.	dircos		
9.65	0.	0.	Cone half angle		
110.	160.	-70.	-30.	-80.	-40.
0.	0.	0.	Rlength		
0.	0.	0.	limit plane disp. (in pixels)		
0.	0.	0.	FJI limits		
'HALOE cover JK29'					
26	Component no.				
CylinderA					
1	flow on ext., int. or both				

0.	0.	0.	0.	0.	0.	0.	limit plane disp. (in pixels)
Quadic 334							
Component no.							
flow on ext., int. or both							
pointA: actual point U15							
16	44.8	-76.2	-21.7	79.6	-73.2	-2.1	pointB: actual point H15
PlateB	57.3	-76.2	-21.7	79.6	-73.2	-2.1	pointC: actual point G15
0	44.8	-91.2	-25.5	79.6	-83.5	-2.1	pointD: actual point K15
Exterior point							
50.	57.3	-91.2	-25.5	79.6	-83.5	-2.1	pointE: actual point L15
Exterior point							
0.	0.	0.	0.	0.	0.	0.	limit plane disp. (in pixels)
Quadic 335							
Component no.							
flow on ext., int. or both							
pointA: actual point V15							
16	57.3	-61.2	11.6	79.6	-73.2	-15.9	pointB: actual point C15
PlateB	57.3	-61.2	-25.5	79.6	-73.2	-2.1	pointC: actual point G15
1	57.3	-76.2	7.8	79.6	-83.5	-15.9	pointD: actual point J15
Exterior point							
150.	57.3	-76.2	-21.7	79.6	-83.5	-2.1	pointE: actual point L15
Exterior point							
0.	0.	0.	0.	0.	0.	0.	limit plane disp. (in pixels)
Quadic 336							
Component no.							
flow on ext., int. or both							
pointA: actual point S15							
16	44.8	-76.2	7.8	63.7	-73.2	-15.9	pointB: actual point D15
PlateB	44.8	-76.2	-21.7	63.7	-73.2	-2.1	pointC: actual point H15
1	57.3	-76.2	7.8	63.7	-83.5	-15.9	pointD: actual point I15
Exterior point							
50.	57.3	-76.2	-21.7	63.7	-83.5	-2.1	pointE: actual point K15
Exterior point							
0.	0.	0.	0.	0.	0.	0.	limit plane disp. (in pixels)
Quadic 337							
Component no.							
flow on ext., int. or both							
pointA: actual point O15							
16	44.8	-61.2	11.6	97.5	47.8	15.0	pointA
PlateA	44.8	-76.2	11.6	97.5	46.0	14.0	pointB
1	44.8	-76.2	7.8	11.4			radius
Exterior point							
150.	0.	-80.	0.	0.			limit plane disp. (in pixels)
Exterior point							
0.	0.	0.	0.	0.			FBI limits
Quadic 338							
Component no.							
flow on ext., int. or both							
pointA: actual point Q15							
16	44.8	-61.2	-25.5	50.	150.	30.	pointA
PlateA	44.8	-76.2	-25.5	50.	150.	70.	pointB
1	44.8	-76.2	-21.7	0.			radius
Exterior point							
150.	0.	-80.	0.	0.			limit plane disp. (in pixels)
Exterior point							
0.	0.	0.	0.	0.			FBI limits
Quadic 339							
Component no.							
flow on ext., int. or both							
pointA: actual point N15							
16	44.8	-61.2	-25.5	258.3	-45.4	37.068	pointA
PlateA	44.8	-76.2	-25.5	0.	-0.5	-0.866	dircos
1	44.8	-76.2	-21.7	6.3			radius
Exterior point							
150.	0.	-80.	0.	0.			limit plane disp. (in pixels)
Exterior point							
0.	0.	0.	0.	0.			FBI limits
Quadic 340							
Component no.							
flow on ext., int. or both							
pointA: actual point M15							
16	63.7	-73.2	-15.9	258.3	-44.4	38.8	pointA
PlateB	79.6	-73.2	-15.9	258.3	-45.4	37.068	pointB
1	63.7	-83.5	-15.9	6.3			radius
Exterior point							
70.	79.6	-83.5	-15.9	0.	0.	0.	limit plane disp. (in pixels)
Exterior point							
0.	0.	0.	0.	200.	300.	-60.	FBI limits
Quadic 341							
Component no.							
flow on ext., int. or both							
pointA: actual point P15							
16	63.7	-73.2	-15.9	0.	0.	0.	pointA
PlateB	79.6	-73.2	-15.9	0.	0.	0.	pointB
1	63.7	-83.5	-15.9	0.	0.	0.	radius
Exterior point							
100.	79.6	-83.5	-15.9	0.	0.	0.	limit plane disp. (in pixels)
Exterior point							
0.	0.	0.	0.	0.			FBI limits
Quadic 342							
Component no.							
flow on ext., int. or both							
pointA: actual point R15							
16	63.7	-73.2	-15.9	0.	0.	0.	pointA
PlateB	63.7	-73.2	-2.1	0.	0.	0.	pointB
1	63.7	-83.5	-15.9	0.	0.	0.	pointC
Exterior point							
50.	63.7	-83.5	-15.9	0.	0.	0.	pointD
Exterior point							
0.	0.	0.	0.	0.			limit plane disp. (in pixels)
Plane 26 (back face)							
Component no.							
pointA							
16	0.	0.	0.	97.5	46.0	14.0	direction
PlateA	0.	0.	0.	0.	-0.8706	-0.4921	cosine normal to disk
1	0.	0.	0.	11.4			radius
Quadic 343							
Component no.							
flow on ext., int. or both							
pointA							
16	97.5	47.8	15.0	0.			pointA
PlateA	97.5	46.0	14.0	0.			pointB
1	11.4			0.			radius
Exterior point							
150.	0.	-80.	0.	50.	150.	30.	limit plane disp. (in pixels)
Exterior point							
0.	0.	0.	0.	0.			FBI limits
Plane 27 (back face)							
Component no.							
pointA							
16	258.3	-45.4	37.068	0.			pointA
PlateA	0.	-0.5	-0.866	6.3			dircos
1	6.3			0.			radius
Exterior point							
150.	0.	-80.	0.	0.			limit plane disp. (in pixels)
Exterior point							
0.	0.	0.	0.	200.	300.	-60.	FBI limits
Quadic 344							
Component no.							
flow on ext., int. or both							
pointA							
16	258.3	-44.4	38.8	0.			pointA
PlateB	258.3	-45.4	37.068	6.3			pointB
1	6.3			0.			radius
Exterior point							
70.	200.	300.	-60.	-30.	-30.	20.	limit plane disp. (in pixels)
Exterior point							
0.	0.	0.	0.	0.			FBI limits
Quadic 345							
Component no.							
flow on ext., int. or both							
pointA: actual point abet13							
16	133.0	-74.3	-11.2	0.			pointA
PlateB	0.			0.			pointB
1	0.			0.			radius
Exterior point							
150.	0.	-80.	0.	0.			limit plane disp. (in pixels)
Exterior point							
0.	0.	0.	0.	0.			FBI limits

Table 4: Input Data Listing—Subassembly Rotation Data

Case 1 Rotation Data:

HALOE rotation (theta = 6 deg)
 How many subelements? (List follows)
 28 325 326 327 328 329 330 331 332 333 334 335 336 337 338
 339 340 341 342 343 344 345 346 347 348 349 350 351 352
 6. Rot. angle from baseline geometry (deg)
 136.3 -50.5 -56.3
 Coords. of rotating origin
 Axis of rotation
 z

solar panel rotation (theta = 6 deg)
 How many subelements? (List follows)
 7 93 94 95 96 97 98 99
 -84.
 136.1 56.3 -55.5
 Rot. angle from baseline geometry (deg)
 Coords. of rotating origin
 Axis of rotation
 z

Case 2 Rotation Data:

HALOE rotation (theta = -23.6 deg)
 How many subelements? (List follows)
 28 325 326 327 328 329 330 331 332 333 334 335 336 337 338
 339 340 341 342 343 344 345 346 347 348 349 350 351 352
 -23.6
 136.3 -50.5 -56.3
 Coords. of rotating origin
 Axis of rotation
 z

solar panel rotation (theta = -23.6 deg)
 How many subelements? (List follows)
 7 93 94 95 96 97 98 99
 -113.6
 136.1 56.3 -55.5
 Rot. angle from baseline geometry (deg)
 Coords. of rotating origin
 Axis of rotation
 z

Case 3 Rotation Data:

HALOE rotation (theta = -25 deg)
 How many subelements? (List follows)
 28 325 326 327 328 329 330 331 332 333 334 335 336 337 338
 339 340 341 342 343 344 345 346 347 348 349 350 351 352
 -25.
 136.3 -50.5 -56.3
 Coords. of rotating origin
 Axis of rotation
 z

HALOE rotation (alpha = 45 deg)
 How many subelements? (List follows)
 43 312 313 314 315 316 317 318 319 320 321 322 323 324 325
 326 327 328 329 330 331 332 333 334 335 336 337 338 339
 340 341 342 343 344 345 346 347 348 349 350 351 352 373 374
 135.
 136.3 -41.0 -60.0
 Coords. of rotating origin
 Axis of rotation
 y

solar panel rotation (theta = 84 deg)
 How many subelements (List follows)
 7 93 94 95 96 97 98 99
 84.
 136.1 56.3 -55.5
 Rot. angle from baseline geometry (deg)
 Coords. of rotating origin
 Axis of rotation
 z

Table 5: Typical Elemental Outgassing Data

Data	Description
'Main block top plate ABCD1' 1 PlateB 1 0 0. 1. 0.6264E+17 100.	Quadric 1 number of outgassing surfaces on object shape of outgassing surface flow direction code, outgassing index, (0 if entire surface has one rate, or no. of defining points) mole fractions of outgassing species, total outgassing flux [molecules/m ² /sec], ref. temp. [°C]
'Main block side Zmax CDGH1' 2 PlateB 1 0 0. 1. 0.6264E+17 100.	Quadric 2 number of outgassing surfaces on object shape of outgassing surface #1, entire surface flow direction code, outgassing index, (0 if entire surface has one rate, or no. of defining points) mole fractions of outgassing species, total outgassing flux [molecules/m ² /sec], ref. temp. [°C]
PlateB 1 4 1. 0. 0.7649E+20 100. 12. 43.1 2.1 60. 43.1 2.1 12. 45.1 2.1 60. 45.1 2.1	shape of outgassing surface #2, vent above CLAES flow direction code, outgassing index, (number of defining points) mole fractions of outgassing species, total outgassing flux [molecules/m ² /sec], ref. temp. [°C] pointA for vent pointB for vent pointC for vent pointD for vent

Table 6: Input Data Listing—Outgassing Information (19 pgs.)

```

PlateB
1 0
0. 0. 0. 1. 0. 0. 3.62E+14 100. outgas rate
(Number/m2/sec), ref temp(C)

'Front small plate Xmax EFHG1'
PlateB
1 0
0. 0. 0. 1. 0. 0. 3.62E+14 100. outgas rate
(Number/m2/sec), ref temp(C)

'Front small plate Ymin DHCC1'
PlateB
1 0
0. 0. 0. 1. 0. 0. 3.62E+14 100. outgas rate
(Number/m2/sec), ref temp(C)

'Front small plate Zmin AEDH1'
PlateB
1 0
0. 0. 0. 1. 0. 0. 3.62E+14 100. outgas rate
(Number/m2/sec), ref temp(C)

'Front small plate Zmax BFCG1'
PlateB
1 0
0. 0. 0. 1. 0. 0. 3.62E+14 100. outgas rate
(Number/m2/sec), ref temp(C)

'CLAES big cap'
Sphere
1 0
0. 0. 0. 1. 0. 0. 4.17E+14 100. outgas rate
(Number/m2/sec), ref temp(C)

'CLAES fat cylindrical part'
Cylinder
1 0
0. 0. 0. 1. 0. 0. 4.17E+14 100. outgas rate
(Number/m2/sec), ref temp(C)

'CLAES small cylindrical part'
Cylinder
1 0
0. 0. 0. 1. 0. 0. 4.17E+14 100. outgas rate
(Number/m2/sec), ref temp(C)

'CLAES Ring'
RingA
1 0
0. 0. 0. 1. 0. 0. 4.17E+14 100. outgas rate
(Number/m2/sec), ref temp(C)

'CLAES small cap'
1
Number of different outgassing surfaces on object

Main block top plate ABCD0'
PlateB
3
Number of different outgassing surfaces on object
1 0
0. 0. 0. 1. 0. 0. 3.62E+14 100. outgas rate
(Number/m2/sec), ref temp(C)
PlateB
1 4
0. 0. 0. 1. 0. 0. 7.35E+17 100. outgas rate
(Number/m2/sec), ref temp(C)
4.0 48.1 -42.25 pointA
4.0 48.1 -42.5 pointB
14.0 48.1 -42.25 pointC
14.0 48.1 -42.5 pointD
PlateB
1 4
0. 0. 0. 1. 0. 0. 7.35E+17 100. outgas rate
(Number/m2/sec), ref temp(C)
53.0 48.1 -42.25 pointA
53.0 48.1 -42.5 pointB
63.0 48.1 -42.25 pointC
63.0 48.1 -42.5 pointD

Main block side Zmax DCHG0'
PlateB
1 0
0. 0. 0. 1. 0. 0. 3.62E+14 100. outgas rate
(Number/m2/sec), ref temp(C)

Main block side Zmin ABEF0'
PlateB
1 0
0. 0. 0. 1. 1.62E+15 100. outgas rate
(Number/m2/sec), ref temp(C)

Main block bottom EFGH0'
PlateB
1 0
0. 0. 0. 1. 0. 0. 3.62E+14 100. outgas rate
(Number/m2/sec), ref temp(C)

Main block Xmin ADEH0'
PlateB
1 0
0. 0. 0. 1. 0. 0. 3.62E+14 100. outgas rate
(Number/m2/sec), ref temp(C)

Main block Xmax BCFG0'
PlateB
2
Number of different outgassing surfaces on object
1 0
0. 0. 0. 1. 0. 0. 3.62E+14 100. outgas rate
(Number/m2/sec), ref temp(C)
PlateB
1 4
0. 0. 0. 1. 0. 0. 7.35E+17 100. outgas rate
(Number/m2/sec), ref temp(C)
218.0 43.1 -42.25 pointA
218.0 43.1 -42.5 pointB
218.0 33.1 -42.25 pointC
218.0 33.1 -42.5 pointD

Front small plate ABCD1'
PlateB
1
Number of different outgassing surfaces on object

```

1	SphereE	Number of different outgassing surfaces on object	(Number/m2/sec), ref temp(C)					
1	0		-15.47 27.67 23.6				pointA	ACS vent
0	0	1. 0. 0.	4.17E+14	100.	outgas rate		pointB	
		(Number/m2/sec), ref temp(C)					pointC	
			-15.47 26.73 23.6				pointD	
			-14.53 26.73 23.6					
		'CLAES shield plate'						
1	PlateB	Number of different outgassing surfaces on object	'Battery package IJKL3'					
0	0		Number of different outgassing surfaces on object					
0	0	0. 0. 0.	1. 1.62E+15	100.	outgas rate			
		(Number/m2/sec), ref temp(C)						
0	0	0. 0. 0.	1. 1.62E+15	100.	outgas rate			
		(Number/m2/sec), ref temp(C)						
		'Battery package ABCD3'						
2	PlateB	Number of different outgassing surfaces on object	'Battery package MNOP3'					
1	0		Number of different outgassing surfaces on object					
0	0	0. 0. 0.	1. 0.	4.17E+14	100.	outgas rate		
		(Number/m2/sec), ref temp(C)						
		PlateB						
1	4		Number of different outgassing surfaces on object					
0	0	0. 0. 0.	1. 0.	7.35E+15	100.	outgas rate		
		(Number/m2/sec), ref temp(C)						
-31.12		-33.44	10.44				pointA	MPS vent
-30.18		-33.44	10.44				pointB	
-31.12		-33.87	11.27				pointC	
-30.18		-33.87	11.27				pointD	
		'Battery package CDEF3'						
2	PlateB	Number of different outgassing surfaces on object	'Battery package QRAB3'					
1	0		Number of different outgassing surfaces on object					
0	0	0. 0. 0.	1. 0.	4.17E+14	100.	outgas rate		
		(Number/m2/sec), ref temp(C)						
		PlateB						
1	4		Number of different outgassing surfaces on object					
0	0	0. 0. 0.	1. 0.	7.35E+15	100.	outgas rate		
		(Number/m2/sec), ref temp(C)						
-31.12		-28.28	27.52				pointA	MPS vent
-30.18		-28.28	27.52				pointB	
-31.12		-29.10	27.07				pointC	
-30.18		-29.10	27.07				pointD	
		'Battery package EFCH3'						
1	PlateB	Number of different outgassing surfaces on object	'Battery package side AGCE3 lower X'					
0	0		Number of different outgassing surfaces on object					
0	0	0. 0. 0.	1. 0.	4.17E+14	100.	outgas rate		
		(Number/m2/sec), ref temp(C)						
		'Battery package GHIJ3'						
3	PlateB	Number of different outgassing surfaces on object	'Battery package side GFMK3 lower X'					
1	0		Number of different outgassing surfaces on object					
0	0	0. 0. 0.	1. 0.	4.17E+14	100.	outgas rate		
		(Number/m2/sec), ref temp(C)						
		PlateB						
1	4		Number of different outgassing surfaces on object					
0	0	0. 0. 0.	1. 0.	2.21E+15	100.	outgas rate		
		(Number/m2/sec), ref temp(C)						
-31.12		-27.67	23.6				pointA	ACS vent
-30.18		-27.67	23.6				pointB	
-31.12		-26.73	23.6				pointC	
-30.18		-26.73	23.6				pointD	
		'Battery package side MOAQ3 lower X'						
1	PlateB	Number of different outgassing surfaces on object	'Battery package side MOAQ3 lower X'					
0	0		Number of different outgassing surfaces on object					
0	0	0. 0. 0.	1. 0.	4.17E+14	100.	outgas rate		
		(Number/m2/sec), ref temp(C)						
		PlateB						
1	4		Number of different outgassing surfaces on object					
0	0	0. 0. 0.	1. 0.	2.21E+15	100.	outgas rate		
		(Number/m2/sec), ref temp(C)						

'Battery package side BDHF3 higher X'
 1 PlateB Number of different outgassing surfaces on object
 0 0
 0. 0. 0. 1. 0. 0. 1.62E+15 100. outgas rate
 (Number/m2/sec), ref temp(C)
 0. 0. 0. 1. 0. 0. 1.62E+15 100. outgas rate
 (Number/m2/sec), ref temp(C)

'Battery package side HJNL3 higher X'
 1 PlateB Number of different outgassing surfaces on object
 1 0
 0. 0. 0. 1. 0. 0. 4.17E+14 100. outgas rate
 (Number/m2/sec), ref temp(C)

'Battery package side NPBR3 higher X'
 1 PlateB Number of different outgassing surfaces on object
 1 0
 0. 0. 0. 1. 0. 0. 4.17E+14 100. outgas rate
 (Number/m2/sec), ref temp(C)

'Battery package side ACM3 lower X'
 1 PlateB Number of different outgassing surfaces on object
 1 0
 0. 0. 0. 1. 0. 0. 4.17E+14 100. outgas rate
 (Number/m2/sec), ref temp(C)

'Battery Cylindrical MMS'
 1 CylinderB Number of different outgassing surfaces on object
 1 0
 0. 0. 0. 1. 0. 0. 4.17E+14 100. outgas rate
 (Number/m2/sec), ref temp(C)

'Battery MMS plane bottom'
 1 Disk Number of different outgassing surfaces on object
 1 0
 0. 0. 0. 1. 0. 0. 4.17E+14 100. outgas rate
 (Number/m2/sec), ref temp(C)

'HALOE mount ABC4'
 1 PlateA Number of different outgassing surfaces on object
 0 0
 0. 0. 0. 1. 0. 0. 1.62E+15 100. outgas rate
 (Number/m2/sec), ref temp(C)
 0. 0. 0. 1. 0. 0. 1.62E+15 100. outgas rate
 (Number/m2/sec), ref temp(C)

'HALOE mount ACDA4'
 1 PlateA Number of different outgassing surfaces on object
 1 0
 0. 0. 0. 1. 0. 0. 1.62E+15 100. outgas rate
 (Number/m2/sec), ref temp(C)

'HALOE mount CDE4'
 1 PlateA Number of different outgassing surfaces on object
 0 0
 0. 0. 0. 1. 0. 0. 1.62E+15 100. outgas rate
 (Number/m2/sec), ref temp(C)
 0. 0. 0. 1. 0. 0. 1.62E+15 100. outgas rate
 (Number/m2/sec), ref temp(C)

'HALOE mount BCE4'
 1 PlateA Number of different outgassing surfaces on object
 0 0
 0. 0. 0. 1. 0. 0. 3.62E+14 100. outgas rate
 (Number/m2/sec), ref temp(C)
 0. 0. 0. 1. 0. 0. 3.62E+14 100. outgas rate
 (Number/m2/sec), ref temp(C)

'NEPS ABCD5'
 1 PlateB Number of different outgassing surfaces on object
 1 0
 0. 0. 0. 1. 0. 0. 3.62E+14 100. outgas rate
 (Number/m2/sec), ref temp(C)

'NEPS BFDH5'
 1 PlateB Number of different outgassing surfaces on object
 1 0
 0. 0. 0. 1. 0. 0. 3.62E+14 100. outgas rate
 (Number/m2/sec), ref temp(C)

'NEPS FEHG5'
 1 PlateB Number of different outgassing surfaces on object
 1 0
 0. 0. 0. 1. 0. 0. 3.62E+14 100. outgas rate
 (Number/m2/sec), ref temp(C)

'NEPS EAGC5'
 1 PlateB Number of different outgassing surfaces on object
 1 0
 0. 0. 0. 1. 0. 0. 3.62E+14 100. outgas rate
 (Number/m2/sec), ref temp(C)

'NEPS JLIK5'
 1 PlateB Number of different outgassing surfaces on object
 1 0
 0. 0. 0. 1. 0. 0. 3.09E+15 100. outgas rate
 (Number/m2/sec), ref temp(C)

'Thin box under main block ABCD6'
 1 PlateB Number of different outgassing surfaces on object
 1 0
 0. 0. 0. 1. 0. 0. 3.62E+14 100. outgas rate
 (Number/m2/sec), ref temp(C)

'Thin box under main block CDGH6'
 1 PlateB Number of different outgassing surfaces on object
 1 0
 0. 0. 0. 1. 0. 0. 3.62E+14 100. outgas rate
 (Number/m2/sec), ref temp(C)

'Thin box under main block DHEF6'
 1 PlateB Number of different outgassing surfaces on object
 1 0
 0. 0. 0. 1. 0. 0. 3.62E+14 100. outgas rate
 (Number/m2/sec), ref temp(C)

'Thin box under main block EAGC6'
 1 PlateB Number of different outgassing surfaces on object
 1 0
 0. 0. 0. 1. 0. 0. 3.62E+14 100. outgas rate
 (Number/m2/sec), ref temp(C)

```

(Number/m2/sec), ref temp(C)
'Box under main block AECG7'
1
PlateB
1 0
Number of different outgassing surfaces on object
0. 0. 0. 1. 0. 0. 3.62E+14 100. outgas rate
(Number/m2/sec), ref temp(C)
'Box under main block EFGH7'
1
PlateB
1 0
Number of different outgassing surfaces on object
0. 0. 0. 1. 0. 0. 3.62E+14 100. outgas rate
(Number/m2/sec), ref temp(C)
'Box under main block BFDH7'
1
PlateB
1 0
Number of different outgassing surfaces on object
0. 0. 0. 1. 0. 0. 3.62E+14 100. outgas rate
(Number/m2/sec), ref temp(C)
'Box under main block CGDH7'
1
PlateB
1 0
Number of different outgassing surfaces on object
0. 0. 0. 1. 0. 0. 3.62E+14 100. outgas rate
(Number/m2/sec), ref temp(C)
'Box under main block LCD7'
1
PlateB
1 0
Number of different outgassing surfaces on object
0. 0. 0. 1. 0. 0. 3.62E+14 100. outgas rate
(Number/m2/sec), ref temp(C)
'HRDI interferometer ABCD8'
0
'HRDI interferometer BFDH8'
0
'HRDI interferometer HGF8'
0
'HRDI interferometer AECG8'
0
'HRDI interferometer AEJH8'
0
'HRDI interferometer CDGH8'
0
'cylindrical truss #1 at X = 0.'
1
CylinderA
1 0
Number of different outgassing surfaces on object
0. 0. 0. 1. 0. 0. 3.62E+14 100. outgas rate
(Number/m2/sec), ref temp(C)
'cylindrical truss #2 at X = 0.'
1
CylinderA
1 0
Number of different outgassing surfaces on object
0. 0. 0. 1. 0. 0. 3.62E+14 100. outgas rate
(Number/m2/sec), ref temp(C)
'cylindrical truss #3 at X = 0.'
1
CylinderA
1 0
Number of different outgassing surfaces on object
0. 0. 0. 1. 0. 0. 3.62E+14 100. outgas rate
(Number/m2/sec), ref temp(C)
'cylindrical truss #4 at X = 0.'
1
CylinderA
1 0
Number of different outgassing surfaces on object
0. 0. 0. 1. 0. 0. 3.62E+14 100. outgas rate
(Number/m2/sec), ref temp(C)
'cylindrical truss #5 at X = 0.'
1
CylinderA
1 0
Number of different outgassing surfaces on object
0. 0. 0. 1. 0. 0. 3.62E+14 100. outgas rate
(Number/m2/sec), ref temp(C)
'cylindrical truss #6 at X = 0.'
1
CylinderA
1 0
Number of different outgassing surfaces on object
0. 0. 0. 1. 0. 0. 3.62E+14 100. outgas rate
(Number/m2/sec), ref temp(C)
'Sphere junctn betwn trusses 1-2(X=0)'
0
'Sphere junctn betwn trusses 3-4(X=0)'
0
'Sphere junctn betwn trusses 5-6(X=0)'
0
'left-hand HGA-end box AFDI10'
1
PlateB
1 0
Number of different outgassing surfaces on object
0. 0. 0. 1. 0. 0. 3.62E+14 100. outgas rate
(Number/m2/sec), ref temp(C)
'left-hand HGA-end box ABDE10'
1
PlateB
1 0
Number of different outgassing surfaces on object
0. 0. 0. 1. 0. 0. 3.62E+14 100. outgas rate
(Number/m2/sec), ref temp(C)
'left-hand HGA-end box BCE10'
1
PlateA
1 0
Number of different outgassing surfaces on object
1. 0. 0. 3.62E+14 0. 0. 0. 100. outgas rate
(Number/m2/sec), ref temp(C)
'left/right-hand HGA-end box AFGH10'
1
PlateB
1 0
Number of different outgassing surfaces on object
0. 0. 0. 1. 0. 0. 3.62E+14 100. outgas rate
(Number/m2/sec), ref temp(C)
'left/right-hand HGA-end box BCGH10'
1
PlateB
1 0
Number of different outgassing surfaces on object

```

```

0. 0. 0. 1. 0. 0. 3.62E+14 100. outgas rate
(Number/m2/sec), ref temp(C)
'left-hand HGA-end box CHEJ10'
PlateB
1 0
Number of different outgassing surfaces on object
0. 0. 0. 1. 0. 0. 3.62E+14 100. outgas rate
(Number/m2/sec), ref temp(C)
'left/right-hand HGA-end box DELJ10'
PlateB
1 0
Number of different outgassing surfaces on object
0. 0. 0. 1. 0. 0. 3.62E+14 100. outgas rate
(Number/m2/sec), ref temp(C)
'right-hand HGA-end box GHJK11'
PlateB
1 0
Number of different outgassing surfaces on object
0. 0. 0. 1. 0. 0. 3.62E+14 100. outgas rate
(Number/m2/sec), ref temp(C)
'right-hand HGA-end box CEF11'
PlateA
1 0
Number of different outgassing surfaces on object
0. 0. 0. 1. 0. 0. 3.62E+14 100. outgas rate
(Number/m2/sec), ref temp(C)
'right-hand HGA-end box HIKL11'
PlateB
1 0
Number of different outgassing surfaces on object
0. 0. 0. 1. 0. 0. 3.62E+14 100. outgas rate
(Number/m2/sec), ref temp(C)
'right-hand HGA-end box CIFL11'
0
Number of different outgassing surfaces on object
'right-hand HGA-end box EFKL11'
PlateB
1 0
Number of different outgassing surfaces on object
0. 0. 0. 1. 0. 0. 3.62E+14 100. outgas rate
(Number/m2/sec), ref temp(C)
'HGA-end nose box CIMN11'
PlateB
1 0
Number of different outgassing surfaces on object
0. 0. 0. 1. 0. 0. 3.62E+14 100. outgas rate
(Number/m2/sec), ref temp(C)
'HGA-end nose box MNP11'
PlateB
1 0
Number of different outgassing surfaces on object
0. 0. 0. 1. 0. 0. 3.62E+14 100. outgas rate
(Number/m2/sec), ref temp(C)
'HGA-end nose box CHF11'
PlateA
1 0
Number of different outgassing surfaces on object
0. 0. 0. 1. 0. 0. 3.62E+14 100. outgas rate
(Number/m2/sec), ref temp(C)
'HGA-end nose box INL11'
1
Number of different outgassing surfaces on object
PlateA
1 0
Number of different outgassing surfaces on object
0. 0. 0. 1. 0. 0. 3.62E+14 100. outgas rate
(Number/m2/sec), ref temp(C)
'solar panel mount ABCD12'
PlateB
1 0
Number of different outgassing surfaces on object
0. 0. 0. 1. 0. 0. 3.62E+14 100. outgas rate
(Number/m2/sec), ref temp(C)
'solar panel mount EFGH12'
1
Number of different outgassing surfaces on object
0. 0. 0. 1. 0. 0. 3.62E+14 100. outgas rate
(Number/m2/sec), ref temp(C)
'solar panel mount AECG12'
PlateB
1 0
Number of different outgassing surfaces on object
0. 0. 0. 1. 0. 0. 3.62E+14 100. outgas rate
(Number/m2/sec), ref temp(C)
'solar panel mount BFDH12'
1
Number of different outgassing surfaces on object
0. 0. 0. 1. 0. 0. 3.62E+14 100. outgas rate
(Number/m2/sec), ref temp(C)
'solar panel mount ABEF12'
PlateB
1 0
Number of different outgassing surfaces on object
0. 0. 0. 1. 0. 0. 3.62E+14 100. outgas rate
(Number/m2/sec), ref temp(C)
'solar panel support IJ12'
1
Number of different outgassing surfaces on object
CylinderA
1 0
Number of different outgassing surfaces on object
0. 0. 0. 1. 0. 0. 3.62E+14 100. outgas rate
(Number/m2/sec), ref temp(C)
'solar panel support J12'
1
Number of different outgassing surfaces on object
SphereE
1 0
Number of different outgassing surfaces on object
0. 0. 0. 1. 0. 0. 3.62E+14 100. outgas rate
(Number/m2/sec), ref temp(C)
'solar panel support JK12'
1
Number of different outgassing surfaces on object
CylinderA
1 0
Number of different outgassing surfaces on object
0. 0. 0. 1. 0. 0. 3.62E+14 100. outgas rate
(Number/m2/sec), ref temp(C)
'solar panel support JL12'
1
Number of different outgassing surfaces on object
CylinderC
1 0
Number of different outgassing surfaces on object
0. 0. 0. 1. 0. 0. 3.62E+14 100. outgas rate
(Number/m2/sec), ref temp(C)

```

```

'solar panel support JM12'
1 0 0 0 1 0 0 0 3.62E+14 100 outgas rate
  (Number/m2/sec), ref temp(C)
CylinderC
1 0
0 0 0 1 0 0 3.62E+14 100 outgas rate
  (Number/m2/sec), ref temp(C)
'solar panel NOPQ12'
1 0 0 0 1 0 0 0 3.62E+14 100 outgas rate
  (Number/m2/sec), ref temp(C)
PlateB
0 0
0 0 0 1 0 0 1.10E+16 100 outgas rate
  (Number/m2/sec), ref temp(C)
0 0 0 0 0 1 1.62E+15 100 outgas rate
  (Number/m2/sec), ref temp(C)
'solar panel support RS12'
1 0 0 0 1 0 0 0 3.62E+14 100 outgas rate
  (Number/m2/sec), ref temp(C)
CylinderA
1 0
0 0 0 1 0 0 3.62E+14 100 outgas rate
  (Number/m2/sec), ref temp(C)
'solar panel support R12'
1 0 0 0 1 0 0 0 3.62E+14 100 outgas rate
  (Number/m2/sec), ref temp(C)
SphereE
1 0
0 0 0 1 0 0 3.62E+14 100 outgas rate
  (Number/m2/sec), ref temp(C)
'solar panel support S12'
1 0 0 0 1 0 0 0 3.62E+14 100 outgas rate
  (Number/m2/sec), ref temp(C)
CylinderA
1 0
0 0 0 1 0 0 3.62E+14 100 outgas rate
  (Number/m2/sec), ref temp(C)
'HRDI telescope mount AB13'
1 0 0 0 1 0 0 0 3.62E+14 100 outgas rate
  (Number/m2/sec), ref temp(C)
ConeD
1 0
0 0 0 1 0 0 3.62E+14 100 outgas rate
  (Number/m2/sec), ref temp(C)
'HRDI telescope mount BC13'
1 0 0 0 1 0 0 0 3.62E+14 100 outgas rate
  (Number/m2/sec), ref temp(C)
'HRDI telescope mount FGJK13'
1 0 0 0 1 0 0 0 3.62E+14 100 outgas rate
  (Number/m2/sec), ref temp(C)
PlateB
1 0
0 0 0 1 0 0 3.62E+14 100 outgas rate
  (Number/m2/sec), ref temp(C)
'HRDI telescope mount HILM13'
1 0 0 0 1 0 0 0 3.62E+14 100 outgas rate
  (Number/m2/sec), ref temp(C)
PlateB
1 0
0 0 0 1 0 0 3.62E+14 100 outgas rate
  (Number/m2/sec), ref temp(C)
'HRDI telescope mount FCHI13'
1 0 0 0 1 0 0 0 3.62E+14 100 outgas rate
  (Number/m2/sec), ref temp(C)
PlateB
1 0
0 0 0 1 0 0 3.62E+14 100 outgas rate
  (Number/m2/sec), ref temp(C)
'HRDI telescope mount JKL13'
1 0 0 0 1 0 0 0 3.62E+14 100 outgas rate
  (Number/m2/sec), ref temp(C)
PlateB
1 0
0 0 0 1 0 0 3.62E+14 100 outgas rate
  (Number/m2/sec), ref temp(C)
'HRDI telescope mount GIKM13'
1 0 0 0 1 0 0 0 3.62E+14 100 outgas rate
  (Number/m2/sec), ref temp(C)
'HRDI telescope mount FHJL13'
1 0 0 0 1 0 0 0 3.62E+14 100 outgas rate
  (Number/m2/sec), ref temp(C)
PlateB
1 0
0 0 0 1 0 0 3.62E+14 100 outgas rate
  (Number/m2/sec), ref temp(C)
'HRDI telescope mount NOTU13'
1 0 0 0 1 0 0 0 3.62E+14 100 outgas rate
  (Number/m2/sec), ref temp(C)
PlateB
1 0
0 0 0 1 0 0 3.62E+14 100 outgas rate
  (Number/m2/sec), ref temp(C)
'HRDI telescope mount IOSU13'
1 0 0 0 1 0 0 0 3.62E+14 100 outgas rate
  (Number/m2/sec), ref temp(C)
PlateB
1 0
0 0 0 1 0 0 3.62E+14 100 outgas rate
  (Number/m2/sec), ref temp(C)
'HRDI telescope mount HMR13'
1 0 0 0 1 0 0 0 3.62E+14 100 outgas rate
  (Number/m2/sec), ref temp(C)
PlateB
1 0
0 0 0 1 0 0 3.62E+14 100 outgas rate
  (Number/m2/sec), ref temp(C)
'HRDI telescope mount RSTU13'
1 0 0 0 1 0 0 0 3.62E+14 100 outgas rate
  (Number/m2/sec), ref temp(C)
CylinderA
1 0
0 0 0 1 0 0 3.62E+14 100 outgas rate
  (Number/m2/sec), ref temp(C)
'HRDI telescope mount knob'
1 0 0 0 1 0 0 0 3.62E+14 100 outgas rate
  (Number/m2/sec), ref temp(C)
Disk
1 0
0 0 0 1 0 0 3.62E+14 100 outgas rate
  (Number/m2/sec), ref temp(C)

```

```

'DRDI telescope mount knob'
1
Number of different outgassing surfaces on object
Disk
0. 0. 0. 1. 0. 0. 4.17E+14 100. outgas rate
(Number/m2/sec), ref temp(C)
'DRDI telescope E13'
1
Number of different outgassing surfaces on object
Disk
1
0
'DRDI telescope box abcd13'
1
Number of different outgassing surfaces on object
PlateB
0. 0. 0. 1. 0. 0. 4.17E+14 100. outgas rate
(Number/m2/sec), ref temp(C)
'DRDI telescope box efgh13'
1
Number of different outgassing surfaces on object
PlateB
0. 0. 0. 1. 0. 0. 4.17E+14 100. outgas rate
(Number/m2/sec), ref temp(C)
'DRDI telescope box aceg13'
1
Number of different outgassing surfaces on object
PlateB
0. 0. 0. 1. 0. 0. 4.17E+14 100. outgas rate
(Number/m2/sec), ref temp(C)
'DRDI telescope box bdfh13'
1
Number of different outgassing surfaces on object
PlateB
0. 0. 0. 1. 0. 0. 4.17E+14 100. outgas rate
(Number/m2/sec), ref temp(C)
'DRDI telescope box cdgh13'
1
Number of different outgassing surfaces on object
PlateB
0. 0. 0. 1. 0. 0. 4.17E+14 100. outgas rate
(Number/m2/sec), ref temp(C)
'SSPP box ABCD14'
1
Number of different outgassing surfaces on object
PlateB
0. 0. 0. 1. 0. 0. 4.17E+14 100. outgas rate
(Number/m2/sec), ref temp(C)
'SSPP box EFGH14'
1
Number of different outgassing surfaces on object
PlateB
0. 0. 0. 1. 0. 0. 4.17E+14 100. outgas rate
(Number/m2/sec), ref temp(C)
'SSPP box ABFE14'
1
Number of different outgassing surfaces on object
PlateB
0. 0. 0. 1. 0. 0. 4.17E+14 100. outgas rate
(Number/m2/sec), ref temp(C)
'SSPP box CDGH14'
1
Number of different outgassing surfaces on object
'DRDI telescope mount knob'
1
Number of different outgassing surfaces on object
Disk
0. 0. 0. 1. 0. 0. 3.62E+14 100. outgas rate
(Number/m2/sec), ref temp(C)
'DRDI telescope mount PQW13'
1
Number of different outgassing surfaces on object
PlateB
0. 0. 0. 1. 0. 0. 3.62E+14 100. outgas rate
(Number/m2/sec), ref temp(C)
'DRDI telescope mount LMXY13'
1
Number of different outgassing surfaces on object
PlateB
0. 0. 0. 1. 0. 0. 3.62E+14 100. outgas rate
(Number/m2/sec), ref temp(C)
'DRDI telescope mount QWV13'
1
Number of different outgassing surfaces on object
PlateB
0. 0. 0. 1. 0. 0. 3.62E+14 100. outgas rate
(Number/m2/sec), ref temp(C)
'DRDI telescope mount PUVX13'
1
Number of different outgassing surfaces on object
PlateB
0. 0. 0. 1. 0. 0. 3.62E+14 100. outgas rate
(Number/m2/sec), ref temp(C)
'DRDI telescope mount VWXY13'
1
Number of different outgassing surfaces on object
CylinderA
0. 0. 0. 1. 0. 0. 3.62E+14 100. outgas rate
(Number/m2/sec), ref temp(C)
'DRDI telescope mount knob'
1
Number of different outgassing surfaces on object
Disk
0. 0. 0. 1. 0. 0. 3.62E+14 100. outgas rate
(Number/m2/sec), ref temp(C)
'DRDI telescope mount knob'
1
Number of different outgassing surfaces on object
Disk
0. 0. 0. 1. 0. 0. 3.62E+14 100. outgas rate
(Number/m2/sec), ref temp(C)
'DRDI telescope mount knob'
1
Number of different outgassing surfaces on object
Disk
0. 0. 0. 1. 0. 0. 3.62E+14 100. outgas rate
(Number/m2/sec), ref temp(C)
'DRDI telescope DE13'
1
Number of different outgassing surfaces on object
CylinderA
0. 0. 0. 1. 0. 0. 4.17E+14 100. outgas rate
(Number/m2/sec), ref temp(C)
'DRDI telescope D13'
1
Number of different outgassing surfaces on object

```

```

1      Number of different outgassing surfaces on object
PlateB
1 0
0. 0. 0. 1. 0. 0. 4.17E+14 100. outgas rate
(Number/m2/sec), ref temp(C)
'SSFP box BFDH14'
1      Number of different outgassing surfaces on object
PlateB
1 0
0. 0. 0. 1. 0. 0. 4.17E+14 100. outgas rate
(Number/m2/sec), ref temp(C)
'SSFP box AEGG14'
1      Number of different outgassing surfaces on object
PlateB
1 0
0. 0. 0. 1. 0. 0. 4.17E+14 100. outgas rate
(Number/m2/sec), ref temp(C)
'ISAMS box ABCD15'
1      Number of different outgassing surfaces on object
PlateB
1 0
0. 0. 0. 1. 0. 0. 4.17E+14 100. outgas rate
(Number/m2/sec), ref temp(C)
'ISAMS box EFGH15'
1      Number of different outgassing surfaces on object
PlateB
1 0
0. 0. 0. 1. 0. 0. 4.17E+14 100. outgas rate
(Number/m2/sec), ref temp(C)
'ISAMS box BFDH15'
1      Number of different outgassing surfaces on object
PlateB
1 0
0. 0. 0. 1. 0. 0. 4.17E+14 100. outgas rate
(Number/m2/sec), ref temp(C)
'ISAMS box ABEF15'
1      Number of different outgassing surfaces on object
PlateB
1 0
0. 0. 0. 1. 0. 0. 4.17E+14 100. outgas rate
(Number/m2/sec), ref temp(C)
'ISAMS box AKEM15'
1      Number of different outgassing surfaces on object
PlateB
1 0
0. 0. 0. 1. 0. 0. 4.17E+14 100. outgas rate
(Number/m2/sec), ref temp(C)
'ISAMS box GHIJ15'
1      Number of different outgassing surfaces on object
PlateB
1 0
0. 0. 0. 1. 0. 0. 4.17E+14 100. outgas rate
(Number/m2/sec), ref temp(C)
'ISAMS box KLMN15'
1      Number of different outgassing surfaces on object
PlateB
1 0
0. 0. 0. 1. 0. 0. 4.17E+14 100. outgas rate
(Number/m2/sec), ref temp(C)
'ISAMS box IJPR15'
1      Number of different outgassing surfaces on object
PlateB
1 0
0. 0. 0. 1. 0. 0. 4.17E+14 100. outgas rate
(Number/m2/sec), ref temp(C)
'ISAMS box DHIJ15'
1      Number of different outgassing surfaces on object
PlateB
1 0
0. 0. 0. 1. 0. 0. 4.17E+14 100. outgas rate
(Number/m2/sec), ref temp(C)
'HGA antenna AB16'
1      Number of different outgassing surfaces on object
CylinderA
1 0
0. 0. 0. 1. 0. 0. 3.62E+14 100. outgas rate
(Number/m2/sec), ref temp(C)
'HGA antenna AI16'
1      Number of different outgassing surfaces on object
SphereE
1 0
0. 0. 0. 1. 0. 0. 3.62E+14 100. outgas rate
(Number/m2/sec), ref temp(C)
'HGA antenna BI16'
1      Number of different outgassing surfaces on object
Disk
1 0
0. 0. 0. 1. 0. 0. 3.62E+14 100. outgas rate
(Number/m2/sec), ref temp(C)
'HGA antenna CD16'
1      Number of different outgassing surfaces on object
CylinderA
1 0
0. 0. 0. 1. 0. 0. 3.62E+14 100. outgas rate
(Number/m2/sec), ref temp(C)
'HGA antenna C16'
1      Number of different outgassing surfaces on object
Disk
1 0
0. 0. 0. 1. 0. 0. 3.62E+14 100. outgas rate
(Number/m2/sec), ref temp(C)
'HGA antenna D16'
1      Number of different outgassing surfaces on object
SphereE
1 0
0. 0. 0. 1. 0. 0. 3.62E+14 100. outgas rate
(Number/m2/sec), ref temp(C)
'HGA antenna DE16'
1      Number of different outgassing surfaces on object
CylinderA
1 0
0. 0. 0. 1. 0. 0. 3.62E+14 100. outgas rate
(Number/m2/sec), ref temp(C)

```



```

'HCA antenna E16'
1      Number of different outgassing surfaces on object
SphereC
0 0
0. 0. 0. 0. 1. 1.62E+15 100. outgas rate
(Number/m2/sec), ref temp(C)
0. 0. 0. 0. 1. 1.62E+15 100. outgas rate
(Number/m2/sec), ref temp(C)
'CLAES lower mount, ABC17'
1      Number of different outgassing surfaces on object
PlateA
1 0
0. 0. 0. 1. 0. 0. 3.62E+14 100. outgas rate
(Number/m2/sec), ref temp(C)
'CLAES lower mount, DEF17'
1      Number of different outgassing surfaces on object
PlateA
1 0
0. 0. 0. 1. 0. 0. 3.62E+14 100. outgas rate
(Number/m2/sec), ref temp(C)
'CLAES lower mount, ACD17'
1      Number of different outgassing surfaces on object
PlateB
1 0
0. 0. 0. 1. 0. 0. 3.62E+14 100. outgas rate
(Number/m2/sec), ref temp(C)
'CLAES lower mount, BCE17'
1      Number of different outgassing surfaces on object
PlateB
1 0
0. 0. 0. 1. 0. 0. 3.62E+14 100. outgas rate
(Number/m2/sec), ref temp(C)
'CLAES upper mount, GHI17'
1      Number of different outgassing surfaces on object
PlateA
1 0
0. 0. 0. 1. 0. 0. 3.62E+14 100. outgas rate
(Number/m2/sec), ref temp(C)
'CLAES upper mount, JKL17'
1      Number of different outgassing surfaces on object
PlateA
1 0
0. 0. 0. 1. 0. 0. 3.62E+14 100. outgas rate
(Number/m2/sec), ref temp(C)
'CLAES upper mount, GJL17'
1      Number of different outgassing surfaces on object
PlateB
1 0
0. 0. 0. 1. 0. 0. 3.62E+14 100. outgas rate
(Number/m2/sec), ref temp(C)
'CLAES upper mount, HIKL17'
1      Number of different outgassing surfaces on object
PlateB
1 0
0. 0. 0. 1. 0. 0. 3.62E+14 100. outgas rate
(Number/m2/sec), ref temp(C)
'WINDII base, ABCD18'
1      Number of different outgassing surfaces on object
PlateB
1 0
0. 0. 0. 1. 0. 0. 2.61E+13 100. outgas rate
(Number/m2/sec), ref temp(C)
'WINDII base, OPQR18'
1      Number of different outgassing surfaces on object
PlateB
1 0
0. 0. 0. 1. 0. 0. 2.61E+13 100. outgas rate
(Number/m2/sec), ref temp(C)
'WINDII base, DBOPI8'
1      Number of different outgassing surfaces on object
PlateB
1 0
0. 0. 0. 1. 0. 0. 2.61E+13 100. outgas rate
(Number/m2/sec), ref temp(C)
'WINDII base, ACRQI8'
1      Number of different outgassing surfaces on object
PlateB
1 0
0. 0. 0. 1. 0. 0. 2.61E+13 100. outgas rate
(Number/m2/sec), ref temp(C)
'WINDII base, DFOI8'
1      Number of different outgassing surfaces on object
PlateA
1 0
0. 0. 0. 1. 0. 0. 2.61E+13 100. outgas rate
(Number/m2/sec), ref temp(C)
'WINDII base, CEQI8'
1      Number of different outgassing surfaces on object
PlateA
1 0
0. 0. 0. 1. 0. 0. 2.61E+13 100. outgas rate
(Number/m2/sec), ref temp(C)
'WINDII base, FNOI8'
1      Number of different outgassing surfaces on object
PlateA
1 0
0. 0. 0. 1. 0. 0. 2.61E+13 100. outgas rate
(Number/m2/sec), ref temp(C)
'WINDII base, EMQI8'
1      Number of different outgassing surfaces on object
PlateA
1 0
0. 0. 0. 1. 0. 0. 2.61E+13 100. outgas rate
(Number/m2/sec), ref temp(C)
'WINDII base, HFNI8'
1      Number of different outgassing surfaces on object
PlateA
1 0
0. 0. 0. 1. 0. 0. 2.61E+13 100. outgas rate
(Number/m2/sec), ref temp(C)
'WINDII base, GEMI8'
1      Number of different outgassing surfaces on object
PlateA
1 0
0. 0. 0. 1. 0. 0. 2.61E+13 100. outgas rate
(Number/m2/sec), ref temp(C)
'WINDII base, CDEFI8'
1      Number of different outgassing surfaces on object
PlateB
1 0
0. 0. 0. 1. 0. 0. 2.61E+13 100. outgas rate
(Number/m2/sec), ref temp(C)

```

```

1 PlateB Number of different outgassing surfaces on object
1 0
0. 0. 0. 1. 0. 0. 2.61E+13 100. outgas rate
(Number/m2/sec), ref temp(C)
'WINDII base, MNQO18'
1 PlateB Number of different outgassing surfaces on object
1 0
0. 0. 0. 1. 0. 0. 2.61E+13 100. outgas rate
(Number/m2/sec), ref temp(C)
'WINDII base, MNKL18'
1 PlateB Number of different outgassing surfaces on object
1 0
0. 0. 0. 1. 0. 0. 2.61E+13 100. outgas rate
(Number/m2/sec), ref temp(C)
'WINDII base, GHIJ18'
1 PlateB Number of different outgassing surfaces on object
1 0
0. 0. 0. 1. 0. 0. 2.61E+13 100. outgas rate
(Number/m2/sec), ref temp(C)
'WINDII base, IJKL18'
1 PlateB Number of different outgassing surfaces on object
1 0
0. 0. 0. 1. 0. 0. 2.61E+13 100. outgas rate
(Number/m2/sec), ref temp(C)
'WINDII base, HJNL18'
1 PlateB Number of different outgassing surfaces on object
1 0
0. 0. 0. 1. 0. 0. 2.61E+13 100. outgas rate
(Number/m2/sec), ref temp(C)
'WINDII base, IGRM18'
1 PlateB Number of different outgassing surfaces on object
1 0
0. 0. 0. 1. 0. 0. 2.61E+13 100. outgas rate
(Number/m2/sec), ref temp(C)
'PEM-AXIS base, ABCD19'
1 PlateB Number of different outgassing surfaces on object
1 0
0. 0. 0. 1. 0. 0. 4.17E+14 100. outgas rate
(Number/m2/sec), ref temp(C)
'PEM-AXIS base, EFGH19'
1 PlateB Number of different outgassing surfaces on object
1 0
0. 0. 0. 1. 0. 0. 4.17E+14 100. outgas rate
(Number/m2/sec), ref temp(C)
'PEM-AXIS antenna JI19'
1 ConeD Number of different outgassing surfaces on object
0 0
0. 0. 0. 0. 0. 0. 1. 0. 100. outgas rate
(Number/m2/sec), ref temp(C)
'PEM-AXIS base, AECG19'
1 PlateB Number of different outgassing surfaces on object
1 0
0. 0. 0. 1. 0. 0. 4.17E+14 100. outgas rate
(Number/m2/sec), ref temp(C)
'PEM-AXIS antenna J19'
1 Disk Number of different outgassing surfaces on object
1 0
0. 0. 0. 0. 0. 0. 1. 1.62E+15 100. outgas rate
(Number/m2/sec), ref temp(C)
'PEM-AXIS base, BFDH19'
1 PlateB Number of different outgassing surfaces on object
1 0
0. 0. 0. 1. 0. 0. 4.17E+14 100. outgas rate
(Number/m2/sec), ref temp(C)
'PEM-AXIS base, CDGH19'
1 PlateB Number of different outgassing surfaces on object
1 0
0. 0. 0. 1. 0. 0. 4.17E+14 100. outgas rate
(Number/m2/sec), ref temp(C)
'PEM-AXIS base, AEBF19'
1 PlateB Number of different outgassing surfaces on object
1 0
0. 0. 0. 1. 0. 0. 4.17E+14 100. outgas rate
(Number/m2/sec), ref temp(C)
'PEM-AXIS base, KLMN19'
1 PlateB Number of different outgassing surfaces on object
1 0
0. 0. 0. 1. 0. 0. 4.17E+14 100. outgas rate
(Number/m2/sec), ref temp(C)
'PEM-AXIS base, OFOR19'
1 PlateB Number of different outgassing surfaces on object
1 0
0. 0. 0. 1. 0. 0. 4.17E+14 100. outgas rate
(Number/m2/sec), ref temp(C)
'PEM-AXIS base, KOMQ19'
1 PlateB Number of different outgassing surfaces on object
1 0
0. 0. 0. 1. 0. 0. 4.17E+14 100. outgas rate
(Number/m2/sec), ref temp(C)
'PEM-AXIS base, LPNR19'
1 PlateB Number of different outgassing surfaces on object
1 0
0. 0. 0. 1. 0. 0. 4.17E+14 100. outgas rate
(Number/m2/sec), ref temp(C)
'PEM-AXIS base, MNQR19'
1 PlateB Number of different outgassing surfaces on object
1 0
0. 0. 0. 1. 0. 0. 4.17E+14 100. outgas rate
(Number/m2/sec), ref temp(C)
'PEM-AXIS antenna JI19'
1 ConeD Number of different outgassing surfaces on object
0 0
0. 0. 0. 0. 0. 0. 1. 0. 100. outgas rate
(Number/m2/sec), ref temp(C)
'PEM-AXIS base, AECG19'
1 PlateB Number of different outgassing surfaces on object
1 0
0. 0. 0. 1. 0. 0. 1.62E+15 100. outgas rate
(Number/m2/sec), ref temp(C)
'PEM-AXIS antenna J19'
1 Disk Number of different outgassing surfaces on object
1 0
0. 0. 0. 0. 0. 0. 1. 1.62E+15 100. outgas rate
(Number/m2/sec), ref temp(C)

```



```

(Number/m2/sec), ref temp(C)
0. 0. 0. 1. 0. 0. 3.62E+14 100. outgas rate
(Number/m2/sec), ref temp(C)
'MLS box behind antenna KOLP21'
1
PlateB
1 0
Number of different outgassing surfaces on object
0. 0. 0. 1. 0. 0. 3.62E+14 100. outgas rate
(Number/m2/sec), ref temp(C)
'MLS box behind antenna IJMN21'
1
PlateB
1 0
Number of different outgassing surfaces on object
0. 0. 0. 1. 0. 0. 3.62E+14 100. outgas rate
(Number/m2/sec), ref temp(C)
'MLS cylinder QR21'
1
PlateB
1 0
Number of different outgassing surfaces on object
0. 0. 0. 1. 0. 0. 3.62E+14 100. outgas rate
(Number/m2/sec), ref temp(C)
'MLS cylinder end'
1
PlateB
1 0
Number of different outgassing surfaces on object
0. 0. 0. 1. 0. 0. 3.62E+14 100. outgas rate
(Number/m2/sec), ref temp(C)
'MLS LHS box ABCD22'
1
PlateB
1 0
Number of different outgassing surfaces on object
0. 0. 0. 1. 0. 0. 3.62E+14 100. outgas rate
(Number/m2/sec), ref temp(C)
'MLS LHS box ABEF22'
1
PlateB
1 0
Number of different outgassing surfaces on object
0. 0. 0. 1. 0. 0. 3.62E+14 100. outgas rate
(Number/m2/sec), ref temp(C)
'MLS LHS box CDGH22'
1
PlateB
1 0
Number of different outgassing surfaces on object
0. 0. 0. 1. 0. 0. 3.62E+14 100. outgas rate
(Number/m2/sec), ref temp(C)
'MLS LHS box BFDH22'
1
PlateB
1 0
Number of different outgassing surfaces on object
0. 0. 0. 1. 0. 0. 3.62E+14 100. outgas rate
(Number/m2/sec), ref temp(C)
'MLS LHS box AEGG22'
1
PlateB
1 0
Number of different outgassing surfaces on object
0. 0. 0. 1. 0. 0. 3.62E+14 100. outgas rate
(Number/m2/sec), ref temp(C)
'MLS LHS box EFTJ22'
1
PlateB
1 0
Number of different outgassing surfaces on object
0. 0. 0. 1. 0. 0. 3.62E+14 100. outgas rate
(Number/m2/sec), ref temp(C)
'MLS LHS box IJOK22'
1
PlateB
1 0
Number of different outgassing surfaces on object
0. 0. 0. 1. 0. 0. 3.62E+14 100. outgas rate
(Number/m2/sec), ref temp(C)
'MLS LHS box JKL22'
1
PlateB
1 0
Number of different outgassing surfaces on object
0. 0. 0. 1. 0. 0. 3.62E+14 100. outgas rate
(Number/m2/sec), ref temp(C)
'MLS LHS box IQR22'
1
PlateB
1 0
Number of different outgassing surfaces on object
0. 0. 0. 1. 0. 0. 3.62E+14 100. outgas rate
(Number/m2/sec), ref temp(C)
'MLS LHS box QKOM22'
1
PlateB
1 0
Number of different outgassing surfaces on object
0. 0. 0. 1. 0. 0. 3.62E+14 100. outgas rate
(Number/m2/sec), ref temp(C)
'MLS LHS box RLPN22'
1
PlateB
1 0
Number of different outgassing surfaces on object
0. 0. 0. 1. 0. 0. 3.62E+14 100. outgas rate
(Number/m2/sec), ref temp(C)
'MLS LHS box QORP22'
1
PlateB
1 0
Number of different outgassing surfaces on object
0. 0. 0. 1. 0. 0. 3.62E+14 100. outgas rate
(Number/m2/sec), ref temp(C)
'MLS large antenna BCDE24'
0
Number of different outgassing surfaces on object
'MLS large antenna DBHI24'
0
Number of different outgassing surfaces on object
'MLS large antenna HIL24'
0
Number of different outgassing surfaces on object
'MLS large antenna BCFG24'
0
Number of different outgassing surfaces on object
'MLS large antenna FGJK24'
0
Number of different outgassing surfaces on object
'MLS large antenna JKM24'
0
Number of different outgassing surfaces on object

```



```

(Number/m2/sec), ref temp(C)
'MLS small antenna ORU24'
1
PlateB
1 0
0. 0. 0. 1. 0. 0. 3.62E+14 100. outgas rate
(Number/m2/sec), ref temp(C)
'MLS small antenna OPST24'
0
Number of different outgassing surfaces on object
'MLS small antenna STV24'
0
Number of different outgassing surfaces on object
'MLS small antenna OPST24'
1
PlateB
1 0
0. 0. 0. 1. 0. 0. 3.62E+14 100. outgas rate
(Number/m2/sec), ref temp(C)
'MLS small antenna STV24'
1
PlateA
1 0
0. 0. 0. 1. 0. 0. 3.62E+14 100. outgas rate
(Number/m2/sec), ref temp(C)
'MLS small antenna PPR24'
1
PlateB
1 0
0. 0. 0. 1. 0. 0. 3.62E+14 100. outgas rate
(Number/m2/sec), ref temp(C)
'MLS small antenna PPT24'
1
PlateB
1 0
0. 0. 0. 1. 0. 0. 3.62E+14 100. outgas rate
(Number/m2/sec), ref temp(C)
'MLS small antenna RRU24'
1
PlateB
1 0
0. 0. 0. 1. 0. 0. 3.62E+14 100. outgas rate
(Number/m2/sec), ref temp(C)
'MLS small antenna TTV24'
1
PlateB
1 0
0. 0. 0. 1. 0. 0. 3.62E+14 100. outgas rate
(Number/m2/sec), ref temp(C)
'MLS small antenna OOO24'
1
PlateB
1 0
0. 0. 0. 1. 0. 0. 3.62E+14 100. outgas rate
(Number/m2/sec), ref temp(C)
'MLS small antenna OOS24'
1
PlateB
1 0
0. 0. 0. 1. 0. 0. 3.62E+14 100. outgas rate
(Number/m2/sec), ref temp(C)
(Number/m2/sec), ref temp(C)
'MLS small antenna QQU24'
1
PlateB
1 0
0. 0. 0. 1. 0. 0. 3.62E+14 100. outgas rate
(Number/m2/sec), ref temp(C)
'MLS small antenna SSV24'
1
PlateB
1 0
0. 0. 0. 1. 0. 0. 3.62E+14 100. outgas rate
(Number/m2/sec), ref temp(C)
'MLS antenna arm, RHS ABCD25'
1
PlateB
0 0
0. 0. 0. 1. 0. 0. 3.62E+14 100. outgas rate
(Number/m2/sec), ref temp(C)
0. 0. 0. 1. 0. 0. 3.62E+14 100. outgas rate
(Number/m2/sec), ref temp(C)
'MLS antenna arm, RHS EF25'
1
CylinderA
1 0
0. 0. 0. 1. 0. 0. 3.62E+14 100. outgas rate
(Number/m2/sec), ref temp(C)
'MLS antenna arm, RHS E25'
1
Disk
1 0
0. 0. 0. 1. 0. 0. 3.62E+14 100. outgas rate
(Number/m2/sec), ref temp(C)
'MLS antenna arm, RHS F25'
1
Disk
1 0
0. 0. 0. 1. 0. 0. 3.62E+14 100. outgas rate
(Number/m2/sec), ref temp(C)
'MLS antenna arm, back GH25'
1
CylinderA
1 0
0. 0. 0. 1. 0. 0. 3.62E+14 100. outgas rate
(Number/m2/sec), ref temp(C)
'MLS antenna arm, back IJ25'
1
CylinderA
1 0
0. 0. 0. 1. 0. 0. 3.62E+14 100. outgas rate
(Number/m2/sec), ref temp(C)
'MLS antenna arm, back H25'
1
SphereE
1 0
0. 0. 0. 1. 0. 0. 3.62E+14 100. outgas rate
(Number/m2/sec), ref temp(C)
'MLS antenna arm, back J25'
1
0. 0. 0. 1. 0. 0. 3.62E+14 100. outgas rate
(Number/m2/sec), ref temp(C)

```

```

SphereE
1 0
0. 0. 0. 1. 0. 0. 3.62E+14 100. outgas rate
(Number/m2/sec), ref temp(C)
'MLS antenna arm, back G25'
1
SphereA
1 0
0. 0. 0. 1. 0. 0. 3.62E+14 100. outgas rate
(Number/m2/sec), ref temp(C)
'MLS antenna arm, back I25'
1
SphereA
1 0
0. 0. 0. 1. 0. 0. 3.62E+14 100. outgas rate
(Number/m2/sec), ref temp(C)
'MLS antenna arm, back I25'
1
SphereA
1 0
0. 0. 0. 1. 0. 0. 3.62E+14 100. outgas rate
(Number/m2/sec), ref temp(C)
'MLS antenna arm, between GK25'
1
CylinderA
1 0
0. 0. 0. 1. 0. 0. 3.62E+14 100. outgas rate
(Number/m2/sec), ref temp(C)
'MLS antenna arm, between IL25'
1
CylinderA
1 0
0. 0. 0. 1. 0. 0. 3.62E+14 100. outgas rate
(Number/m2/sec), ref temp(C)
'MLS antenna arm, side K25'
1
SphereA
1 0
0. 0. 0. 1. 0. 0. 3.62E+14 100. outgas rate
(Number/m2/sec), ref temp(C)
'MLS antenna arm, side L25'
1
SphereA
1 0
0. 0. 0. 1. 0. 0. 3.62E+14 100. outgas rate
(Number/m2/sec), ref temp(C)
'HGA-side bracework AB23'
1
CylinderA
1 0
0. 0. 0. 1. 0. 0. 3.62E+14 100. outgas rate
(Number/m2/sec), ref temp(C)
'HGA-side bracework CB23'
1
CylinderA
1 0
0. 0. 0. 1. 0. 0. 3.62E+14 100. outgas rate
(Number/m2/sec), ref temp(C)
'HGA-side bracework EB23'
1
CylinderA
1 0
0. 0. 0. 1. 0. 0. 3.62E+14 100. outgas rate
(Number/m2/sec), ref temp(C)
'HGA-side bracework GB23'
1
SphereE
1 0
0. 0. 0. 1. 0. 0. 3.62E+14 100. outgas rate
(Number/m2/sec), ref temp(C)
'HGA-side bracework IJ23'
1
SphereA
1 0
0. 0. 0. 1. 0. 0. 3.62E+14 100. outgas rate
(Number/m2/sec), ref temp(C)
'HGA-side bracework KJ23'
1
SphereA
1 0
0. 0. 0. 1. 0. 0. 3.62E+14 100. outgas rate
(Number/m2/sec), ref temp(C)
'HGA-side bracework MJ23'
1
SphereA
1 0
0. 0. 0. 1. 0. 0. 3.62E+14 100. outgas rate
(Number/m2/sec), ref temp(C)
'HGA-side bracework NQ23'
1
SphereA
1 0
0. 0. 0. 1. 0. 0. 3.62E+14 100. outgas rate
(Number/m2/sec), ref temp(C)
'HGA-side bracework OR23'
1
SphereA
1 0
0. 0. 0. 1. 0. 0. 3.62E+14 100. outgas rate
(Number/m2/sec), ref temp(C)
'HGA-side bracework SR23'
1
SphereA
1 0
0. 0. 0. 1. 0. 0. 3.62E+14 100. outgas rate
(Number/m2/sec), ref temp(C)
'Sphere junctn B23'
0
'Sphere junctn J23'
0
'Sphere junctn R23'
0
'Dish above CLAES'
0
'Thrusters, AC26'
1
ConeA
0 0
0. 0. 0. 1. 0. 0. 3.62E+14 100. outgas rate
(Number/m2/sec), ref temp(C)
0. 0. 0. 1. 0. 0. 3.09E+15 100. outgas rate
(Number/m2/sec), ref temp(C)

```

```

'Thrusters, BD26'
1      Number of different outgassing surfaces on object
ConeA
0 0
0 0. 0. 1. 0. 0. 3.62E+14 100. outgas rate
(Number/m2/sec), ref temp(C)
'HALOE mount FGH127'
1      Number of different outgassing surfaces on object
PlateB
1 0
0 0. 0. 1. 0. 0. 3.62E+14 100. outgas rate
(Number/m2/sec), ref temp(C)
'HALOE mount A27'
1      Number of different outgassing surfaces on object
Disk
1 0
0 0. 0. 1. 0. 0. 3.62E+14 100. outgas rate
(Number/m2/sec), ref temp(C)
'HALOE mount AB27'
1      Number of different outgassing surfaces on object
CylinderA
1 0
0 0. 0. 1. 0. 0. 3.62E+14 100. outgas rate
(Number/m2/sec), ref temp(C)
'HALOE mount B27'
1      Number of different outgassing surfaces on object
RingA
1 0
0 0. 0. 1. 0. 0. 3.62E+14 100. outgas rate
(Number/m2/sec), ref temp(C)
'HALOE mount BC27'
1      Number of different outgassing surfaces on object
CylinderA
1 0
0 0. 0. 1. 0. 0. 3.62E+14 100. outgas rate
(Number/m2/sec), ref temp(C)
'HALOE mount C27'
1      Number of different outgassing surfaces on object
RingA
1 0
0 0. 0. 1. 0. 0. 3.62E+14 100. outgas rate
(Number/m2/sec), ref temp(C)
'HALOE mount CD27'
1      Number of different outgassing surfaces on object
ConeD
1 0
0 0. 0. 1. 0. 0. 3.62E+14 100. outgas rate
(Number/m2/sec), ref temp(C)
'HALOE mount D27'
1      Number of different outgassing surfaces on object
RingA
1 0
0 0. 0. 1. 0. 0. 3.62E+14 100. outgas rate
(Number/m2/sec), ref temp(C)
'HALOE mount DE27'
1      Number of different outgassing surfaces on object
CylinderA
1 0
0 0. 0. 1. 0. 0. 3.62E+14 100. outgas rate
(Number/m2/sec), ref temp(C)
'HALOE mount E27'
1      Number of different outgassing surfaces on object
Disk
1 0
0 0. 0. 1. 0. 0. 3.62E+14 100. outgas rate
(Number/m2/sec), ref temp(C)
'HALOE mount FGH127'
1      Number of different outgassing surfaces on object
PlateB
1 0
0 0. 0. 1. 0. 0. 3.62E+14 100. outgas rate
(Number/m2/sec), ref temp(C)
'HALOE mount JKLM27'
1      Number of different outgassing surfaces on object
PlateB
1 0
0 0. 0. 1. 0. 0. 3.62E+14 100. outgas rate
(Number/m2/sec), ref temp(C)
'HALOE mount FGJK27'
1      Number of different outgassing surfaces on object
PlateB
1 0
0 0. 0. 1. 0. 0. 3.62E+14 100. outgas rate
(Number/m2/sec), ref temp(C)
'HALOE mount HIJLM27'
1      Number of different outgassing surfaces on object
PlateB
1 0
0 0. 0. 1. 0. 0. 3.62E+14 100. outgas rate
(Number/m2/sec), ref temp(C)
'HALOE mount FNJR27'
1      Number of different outgassing surfaces on object
PlateB
1 0
0 0. 0. 1. 0. 0. 3.62E+14 100. outgas rate
(Number/m2/sec), ref temp(C)
'HALOE mount NFPQ27'
1      Number of different outgassing surfaces on object
PlateB
1 0
0 0. 0. 1. 0. 0. 3.62E+14 100. outgas rate
(Number/m2/sec), ref temp(C)
'HALOE mount RJTU27'
1      Number of different outgassing surfaces on object
PlateB
1 0
0 0. 0. 1. 0. 0. 3.62E+14 100. outgas rate
(Number/m2/sec), ref temp(C)
'HALOE mount HLQU27'
1      Number of different outgassing surfaces on object
PlateB
1 0
0 0. 0. 1. 0. 0. 3.62E+14 100. outgas rate
(Number/m2/sec), ref temp(C)
'HALOE mount NRPT27'
1      Number of different outgassing surfaces on object
PlateB
1 0
0 0. 0. 1. 0. 0. 3.62E+14 100. outgas rate
(Number/m2/sec), ref temp(C)
'HALOE mount VW27'
1      Number of different outgassing surfaces on object
CylinderA
1 0
0 0. 0. 1. 0. 0. 3.62E+14 100. outgas rate
(Number/m2/sec), ref temp(C)

```



```

1 0
0. 0. 0. 1. 0. 0. 3.62E+14 100. outgas rate
(Number/m2/sec), ref temp(C)
'HALOE mount V27'
1 Number of different outgassing surfaces on object
RingA
1 0
0. 0. 0. 1. 0. 0. 3.62E+14 100. outgas rate
(Number/m2/sec), ref temp(C)
'HALOE mount VX27'
1 Number of different outgassing surfaces on object
CylinderA
1 0
0. 0. 0. 1. 0. 0. 3.62E+14 100. outgas rate
(Number/m2/sec), ref temp(C)
'HALOE mount X27'
1 Number of different outgassing surfaces on object
Disk
1 0
0. 0. 0. 1. 0. 0. 3.62E+14 100. outgas rate
(Number/m2/sec), ref temp(C)
'HALOE box ABCD28'
1 Number of different outgassing surfaces on object
PlateB
1 0
0. 0. 0. 1. 0. 0. 4.17E+14 100. outgas rate
(Number/m2/sec), ref temp(C)
'HALOE box GHIJ28'
1 Number of different outgassing surfaces on object
PlateB
1 0
0. 0. 0. 1. 0. 0. 4.17E+14 100. outgas rate
(Number/m2/sec), ref temp(C)
'HALOE box BDHJ28'
1 Number of different outgassing surfaces on object
PlateB
1 0
0. 0. 0. 1. 0. 0. 4.17E+14 100. outgas rate
(Number/m2/sec), ref temp(C)
'HALOE box CDEF28'
1 Number of different outgassing surfaces on object
PlateB
1 0
0. 0. 0. 1. 0. 0. 4.17E+14 100. outgas rate
(Number/m2/sec), ref temp(C)
'HALOE box IJKL28'
1 Number of different outgassing surfaces on object
PlateB
1 0
0. 0. 0. 1. 0. 0. 4.17E+14 100. outgas rate
(Number/m2/sec), ref temp(C)
'HALOE box CEIK28'
1 Number of different outgassing surfaces on object
PlateB
1 0
0. 0. 0. 1. 0. 0. 4.17E+14 100. outgas rate
(Number/m2/sec), ref temp(C)
'HALOE box EFKL28'
1 Number of different outgassing surfaces on object
0
'HALOE box DFJL28'
0 Number of different outgassing surfaces on object
'HALOE box MNOP28'
1 Number of different outgassing surfaces on object
PlateB
0 0
0. 0. 0. 1. 0. 0. 4.17E+14 100. outgas rate
(Number/m2/sec), ref temp(C)
0. 0. 0. 1. 0. 0. 4.17E+14 100. outgas rate
(Number/m2/sec), ref temp(C)
'HALOE box QRST28'
0 Number of different outgassing surfaces on object
'HALOE box QRUW28'
0 Number of different outgassing surfaces on object
'HALOE box STWX28'
1 Number of different outgassing surfaces on object
PlateB
1 0
0. 0. 0. 1. 0. 0. 4.17E+14 100. outgas rate
(Number/m2/sec), ref temp(C)
'HALOE box RVTX28'
0 Number of different outgassing surfaces on object
'HALOE box QUSW28'
0 Number of different outgassing surfaces on object
'HALOE box ABCD29'
1 Number of different outgassing surfaces on object
PlateB
1 0
0. 0. 0. 1. 0. 0. 4.17E+14 100. outgas rate
(Number/m2/sec), ref temp(C)
'HALOE box EFGH29'
1 Number of different outgassing surfaces on object
PlateB
1 0
0. 0. 0. 1. 0. 0. 4.17E+14 100. outgas rate
(Number/m2/sec), ref temp(C)
'HALOE box ABEF29'
1 Number of different outgassing surfaces on object
PlateB
1 0
0. 0. 0. 1. 0. 0. 4.17E+14 100. outgas rate
(Number/m2/sec), ref temp(C)
'HALOE box BDFH29'
1 Number of different outgassing surfaces on object
PlateB
1 0
0. 0. 0. 1. 0. 0. 4.17E+14 100. outgas rate
(Number/m2/sec), ref temp(C)
'HALOE box DHLM29'
1 Number of different outgassing surfaces on object
PlateB
1 0
0. 0. 0. 1. 0. 0. 4.17E+14 100. outgas rate
(Number/m2/sec), ref temp(C)
'HALOE cover IJ29'
1 Number of different outgassing surfaces on object
0

```

```

ConeA
1 0
0 0. 0. 1. 0. 0. 4.17E+14 100. outgas rate
(Number/m2/sec), ref temp(C)
'HALOE cover JK29'
1 Number of different outgassing surfaces on object
CylinderA
1 0
0 0. 0. 1. 0. 0. 4.17E+14 100. outgas rate
(Number/m2/sec), ref temp(C)
'HALOE aperture K29'
1 Number of different outgassing surfaces on object
Disk
1 0
0 0. 0. 0. 1. 0. 3.09E+15 100. outgas rate
(Number/m2/sec), ref temp(C)
'HALOE sun-sensor NQPQ29'
0 Number of different outgassing surfaces on object
'HALOE sun-sensor MORS29'
1 Number of different outgassing surfaces on object
PlateB
1 0
0 0. 0. 1. 0. 0. 4.17E+14 100. outgas rate
(Number/m2/sec), ref temp(C)
'HALOE sun-sensor PQTU29'
1 Number of different outgassing surfaces on object
PlateB
1 0
0 0. 0. 1. 0. 0. 4.17E+14 100. outgas rate
(Number/m2/sec), ref temp(C)
'HALOE sun-sensor NRPT29'
1 Number of different outgassing surfaces on object
PlateB
1 0
0 0. 0. 1. 0. 0. 4.17E+14 100. outgas rate
(Number/m2/sec), ref temp(C)
'HALOE sun-sensor OSQU29'
1 Number of different outgassing surfaces on object
PlateB
1 0
0 0. 0. 1. 0. 0. 4.17E+14 100. outgas rate
(Number/m2/sec), ref temp(C)
'HALOE aperture cover L29'
0 Number of different outgassing surfaces on object
'SSPP support'
1 Number of different outgassing surfaces on object
CylinderA
1 0
0 0. 0. 1. 0. 0. 3.62E+14 100. outgas rate
(Number/m2/sec), ref temp(C)
'ISAMS box DTOP15'
1 Number of different outgassing surfaces on object
PlateB
1 0
0 0. 0. 1. 0. 0. 4.17E+14 100. outgas rate
(Number/m2/sec), ref temp(C)
'ISAMS box HQR15'
1 Number of different outgassing surfaces on object
PlateB
1 0
0 0. 0. 1. 0. 0. 4.17E+14 100. outgas rate
(Number/m2/sec), ref temp(C)
'ISAMS box OFST15'
0 Number of different outgassing surfaces on object
'ISAMS box QROV15'
0 Number of different outgassing surfaces on object
'ISAMS box STMX15'
1 Number of different outgassing surfaces on object
PlateB
0 0
0 0. 0. 1. 0. 0. 4.17E+14 100. outgas rate
(Number/m2/sec), ref temp(C)
0 0. 1. 0. 0. 4.17E+14 100. outgas rate
(Number/m2/sec), ref temp(C)
'ISAMS box UYVZ15'
1 Number of different outgassing surfaces on object
PlateB
0 0
0 0. 0. 1. 0. 0. 4.17E+14 100. outgas rate
(Number/m2/sec), ref temp(C)
0 0. 1. 0. 0. 4.17E+14 100. outgas rate
(Number/m2/sec), ref temp(C)
'ISAMS box PRTV15'
1 Number of different outgassing surfaces on object
PlateB
1 0
0 0. 0. 1. 0. 0. 4.17E+14 100. outgas rate
(Number/m2/sec), ref temp(C)
'ISAMS box SUTV15'
1 Number of different outgassing surfaces on object
PlateB
1 0
0 0. 0. 1. 0. 0. 4.17E+14 100. outgas rate
(Number/m2/sec), ref temp(C)
'ISAMS box OLS15'
1 Number of different outgassing surfaces on object
PlateA
1 0
0 0. 0. 1. 0. 0. 4.17E+14 100. outgas rate
(Number/m2/sec), ref temp(C)
'ISAMS box QNV15'
1 Number of different outgassing surfaces on object
PlateA
1 0
0 0. 0. 1. 0. 0. 4.17E+14 100. outgas rate
(Number/m2/sec), ref temp(C)
'NEPS DCIJ15'
1 Number of different outgassing surfaces on object
PlateB
1 0
0 0. 0. 0. 1. 0. 3.09E+15 100. outgas rate
(Number/m2/sec), ref temp(C)
'NEPS HGKL15'
1 Number of different outgassing surfaces on object
PlateB
1 0
0 0. 0. 0. 1. 0. 3.09E+15 100. outgas rate
(Number/m2/sec), ref temp(C)

```

```

(Number/m2/sec), ref temp(C)
'NEPS CGJL15'
1 Number of different outgassing surfaces on object
PlateB
1 0
0. 0. 0. 0. 1. 0. 3.09E+15 100. outgas rate
(Number/m2/sec), ref temp(C)
'NEPS DHIK15'
1 Number of different outgassing surfaces on object
PlateB
1 0
0. 0. 0. 0. 1. 0. 3.09E+15 100. outgas rate
(Number/m2/sec), ref temp(C)
'Dish above CLAES'
0 Number of different outgassing surfaces on object
'Dish above CLAES'
0 Number of different outgassing surfaces on object
'PEM-AXIS antenna J19'
1 Number of different outgassing surfaces on object
Disk
1 0
0. 0. 0. 0. 0. 1. 1.62E+15 100. outgas rate
(Number/m2/sec), ref temp(C)
'PEM-AXIS antenna ?119'
1 Number of different outgassing surfaces on object
CylinderA
1 0
0. 0. 0. 0. 0. 1. 1.62E+15 100. outgas rate
(Number/m2/sec), ref temp(C)
'HRDI telescope box abef13'
0 Number of different outgassing surfaces on object
'HALOE mount GIK427'
0 Number of different outgassing surfaces on object
'HALOE mount PQTU27'
0 Number of different outgassing surfaces on object
'CLAES Neon vent A30'
0 Number of different outgassing surfaces on object
'CLAES Neon vent AB30'
0 Number of different outgassing surfaces on object
'CLAES Neon vent B30'
0 Number of different outgassing surfaces on object
'CLAES CO2 vent CD30'
0 Number of different outgassing surfaces on object
'CLAES CO2 vent D30'
0 Number of different outgassing surfaces on object
'IM vent ABEF31'
1 Number of different outgassing surfaces on object
PlateB
1 0
0. 0. 0. 1. 0. 0. 9.64E+18 100. outgas rate
(Number/m2/sec), ref temp(C)
'IM vent CDEF31'
0 Number of different outgassing surfaces on object
'IM vent ACE31'
0 Number of different outgassing surfaces on object
'IM vent BDF31'
0 Number of different outgassing surfaces on object
'HALOE mount ACFG4'
2 Number of different outgassing surfaces on object
PlateB
0 0
0. 0. 0. 1. 0. 0. 3.62E+14 100. outgas rate
(Number/m2/sec), ref temp(C)
0. 0. 0. 1. 0. 0. 3.62E+14 100. outgas rate
(Number/m2/sec), ref temp(C)
PlateB
1 4
0. 0. 0. 1. 0. 0. 7.35E+17 100. outgas rate
(Number/m2/sec), ref temp(C)
140.36 -17.31 -63.83 pointA HALOE blanket vent
140.36 -17.31 -63.58 pointB
137.82 -21.24 -65.59 pointC
137.82 -21.24 -65.34 pointD
'HALOE mount CDGH4'
2 Number of different outgassing surfaces on object
PlateB
0 0
0. 0. 0. 1. 0. 0. 3.62E+14 100. outgas rate
(Number/m2/sec), ref temp(C)
0. 0. 0. 1. 0. 0. 3.62E+14 100. outgas rate
(Number/m2/sec), ref temp(C)
PlateB
1 4
0. 0. 0. 1. 0. 0. 7.35E+17 100. outgas rate
(Number/m2/sec), ref temp(C)
132.24 -17.31 -63.83 pointA HALOE blanket vent
132.24 -17.31 -63.58 pointB
134.78 -21.24 -65.59 pointC
134.78 -21.24 -65.34 pointD

```

Table 7: Input Data Listing—Surface Temperatures (3 pgs.)

-7	'Main block top plate ABCD0'	7	'left-hand HGA-end box AFDI10'
-22	'Main block side Zmax DCHG0'	-22	'left-hand HGA-end box ABDE10'
-25	'Main block side Zmin ABEF0'	-22	'left-hand HGA-end box BCE10'
4	'Main block bottom EIHJ0'	-7	'left/right-hand HGA-end box ABFG10'
7	'Main block Xmin ADEH0'	-7	'left/right-hand HGA-end box BCGH10'
9	'Main block Xmax BCFG0'	9	'left-hand HGA-end box CHEJI0'
7	'Front small plate Xmin ABCD1'	4	'left/right-hand HGA-end box DEIJ10'
9	'Front small plate Xmax EFGH1'	-25	'right-hand HGA-end box GHJK11'
4	'Front small plate Ymin DCHG1'	-22	'right-hand HGA-end box CEF11'
-7	'Front small plate Ymax ABEF1'	-25	'right-hand HGA-end box HIKL11'
-25	'Front small plate Zmin AEDH1'	9	'right-hand HGA-end box CIFL11'
-22	'Front small plate Zmax BFCG1'	9	'right-hand HGA-end box EFKL11'
-34	'CLAES big cap'	4	'HGA-end nose box CIMN11'
-60	'CLAES fat cylindrical part'	9	'HGA-end nose box MNEFL11'
-60	'CLAES small cylindrical part'	9	'HGA-end nose box CMFL11'
-60	'CLAES Ring'	9	'HGA-end nose box INL11'
-34	'CLAES small cap'	-25	'solar panel mount ARCD12'
-7	'CLAES shield plate'	-22	'solar panel mount EFGH12'
-76	'Battery package ABCD3'	9	'solar panel mount AECG12'
11	'Battery package CDEF3'	7	'solar panel mount BFDH12'
-14	'Battery package EFGH3'	-7	'solar panel mount ABEF12'
-55	'Battery package GHIJ3'	9	'solar panel support IJ12'
11	'Battery package IJKL3'	9	'solar panel support JK12'
-22	'Battery package KLMN3'	9	'solar panel support JL12'
-2	'Battery package MNOP3'	9	'solar panel support JM12'
3	'Battery package OPQR3'	30	'solar panel support NPOQ12'
-39	'Battery package QRAB3'	9	'solar panel support RS12'
-41	'Battery package side AGCE3 lower X'	9	'solar panel support RI2'
-7	'Battery package side GIMK3 lower X'	9	'solar panel support S12'
-2	'Battery package side MOAQ3 lower X'	4	'HRDI telescope mount AB13'
-37	'Battery package side BDHF3 higher X'	4	'HRDI telescope mount BC13'
1	'Battery package side HJNL3 higher X'	4	'HRDI telescope mount FGJK13'
3	'Battery package side NPBR3 higher X'	4	'HRDI telescope mount HILM13'
1	'Battery package side AGM3 lower X'	4	'HRDI telescope mount FGH113'
-75	'Battery cylindrical MMS'	4	'HRDI telescope mount JKLMI3'
-64	'Battery MMS plane bottom'	4	'HRDI telescope mount HIRSI3'
-25	'HALOE mount ABC4'	4	'HRDI telescope mount IOSU13'
-25	'HALOE mount ACD4'	4	'HRDI telescope mount HNRU13'
-25	'HALOE mount CDE4'	4	'HRDI telescope mount RSTU13'
-25	'HALOE mount BCE4'	4	'HRDI telescope mount knob'
-44	'NEPS ABCD5'	-15	'HRDI telescope mount knob'
-8	'NEPS BFDH5'	-15	'HRDI telescope mount knob'
-3	'NEPS EFGH5'	4	'HRDI telescope mount knob'
-28	'NEPS FAGG5'	4	'HRDI telescope mount knob'
6	'NEPS JLIK5'	4	'HRDI telescope mount knob'
7	'Thin box under main block ABCD6'	4	'HRDI telescope mount knob'
4	'Thin box under main block CDGH6'	4	'HRDI telescope mount knob'
-25	'Thin box under main block DHB6'	4	'HRDI telescope mount knob'
-22	'Thin box under main block EAGC6'	4	'HRDI telescope mount knob'
-22	'Box under main block AECG7'	4	'HRDI telescope mount knob'
9	'Box under main block EFGH7'	4	'HRDI telescope mount knob'
-25	'Box under main block BFDH7'	4	'HRDI telescope mount knob'
7	'Box under main block IJCD7'	4	'HRDI telescope mount knob'
4	'Box under main block CGDH7'	4	'HRDI telescope mount knob'
-29	'HRDI interferometer ABCD8'	4	'HRDI telescope mount knob'
-45	'HRDI interferometer BFDH8'	4	'HRDI telescope mount knob'
14	'HRDI interferometer AECG8'	4	'HRDI telescope mount knob'
-65	'HRDI interferometer EFGH8'	4	'HRDI telescope mount knob'
-25	'HRDI interferometer AEJ18'	4	'HRDI telescope mount knob'
-15	'HRDI interferometer CDGH8'	4	'HRDI telescope mount knob'
4	'cylindrical truss #1 at X = 0.'	4	'HRDI telescope E13'
4	'cylindrical truss #2 at X = 0.'	-35	'HRDI telescope box abcd13'
-25	'cylindrical truss #3 at X = 0.'	-35	'HRDI telescope box efgH13'
-25	'cylindrical truss #4 at X = 0.'	-35	'HRDI telescope box aceg13'
-7	'cylindrical truss #5 at X = 0.'	-35	'HRDI telescope box bdfh13'
-7	'cylindrical truss #6 at X = 0.'	-34	'HRDI telescope box cdgh13'
4	'Sphere junctn betwn trusses 1-2(X=0)'	-72	'SSPP box ABCD14'
-25	'Sphere junctn betwn trusses 3-4(X=0)'	-88	'SSPP box EFGH14'
-7	'Sphere junctn betwn trusses 5-6(X=0)'	-12	'SSPP box ABEF14'
		50	'SSPP box CDGH14'
		-11	'SSPP box BFDH14'
		-127	'ISAMS box AECG14'
			'ISAMS box ABCD15'

-41 'ISAMS box EFGH15'
 -9 'ISAMS box BFDH15'
 -2 'ISAMS box ABEF15'
 -18 'ISAMS box AKEM15'
 -127 'ISAMS box CDKL15'
 -41 'ISAMS box GHRM15'
 -14 'ISAMS box KJMN15'
 -9 'ISAMS box IJPR15'
 -2 'ISAMS box DHJ15'
 9 'HGA antenna AB16'
 11 'HGA antenna B16'
 13 'HGA antenna CD16'
 13 'HGA antenna C16'
 15 'HGA antenna D16'
 17 'HGA antenna DE16'
 20 'HGA antenna E16'
 -22 'CLAES lower mount, ABC17'
 -22 'CLAES lower mount, DEF17'
 -22 'CLAES lower mount, ACD17'
 -22 'CLAES lower mount, BCEF17'
 -22 'CLAES upper mount, GHI17'
 -22 'CLAES upper mount, JKLI17'
 -22 'CLAES upper mount, GJLI17'
 -22 'CLAES upper mount, HIKLI17'
 -9 'WINDII base, ABCD18'
 -11 'WINDII base, OPQR18'
 -24 'WINDII base, DBOPI18'
 -24 'WINDII base, ACRQ18'
 -24 'WINDII base, DFO18'
 -24 'WINDII base, CQO18'
 -24 'WINDII base, FNO18'
 -24 'WINDII base, EMQ18'
 -66 'WINDII base, HFN18'
 -66 'WINDII base, GEM18'
 -11 'WINDII base, MNOQ18'
 -11 'WINDII base, MNKL18'
 -35 'WINDII base, GHLJ18'
 -79 'WINDII base, IJKLI8'
 -30 'WINDII base, HJNLI8'
 -9 'WINDII base, IGMK18'
 -37 'PEM-AXIS base, ABCD19'
 -37 'PEM-AXIS base, EFGH19'
 -37 'PEM-AXIS base, AEGC19'
 -37 'PEM-AXIS base, BFDH19'
 -37 'PEM-AXIS base, CDGH19'
 -37 'PEM-AXIS base, AEBF19'
 -37 'PEM-AXIS base, KLMN19'
 -37 'PEM-AXIS base, OPQR19'
 -37 'PEM-AXIS base, KOMQ19'
 -37 'PEM-AXIS base, LPNR19'
 -37 'PEM-AXIS base, MMQR19'
 -37 'PEM-AXIS antenna J19'
 -43 'PEM-AXIS antenna J19'
 -37 'PEM-AXIS base, STI9'
 -7 'PEM-ZEPS base, ABC20'
 -25 'PEM-ZEPS base, ABD20'
 -25 'PEM-ZEPS base, BCE20'
 -25 'PEM-ZEPS base, BDE20'
 -7 'PEM-ZEPS base, FG20'
 -7 'PEM-ZEPS base, G20'
 -2 'PEM-ZEPS box HJK20'
 -9 'PEM-ZEPS box LMKO20'
 -2 'PEM-ZEPS box JKNO20'
 -7 'PEM-ZEPS box HJLM20'
 -1 'PEM-ZEPS box HJLM20'
 -7 'PEM-ZEPS box IKMO20'
 -7 'PEM-ZEPS shaft (approx.) PQ20'
 -85 'MLS gizmo box ABCD21'
 -40 'MLS gizmo box EFGH21'
 -32 'MLS gizmo box EFAB21'
 -46 'MLS gizmo box BFDH21'
 -45 'MLS gizmo box AEGC21'
 -66 'MLS gizmo box CDGH21'
 -37 'MLS box behind antenna IJKL21'
 -37 'MLS box behind antenna JNLP21'
 -37 'MLS box behind antenna KOLP21'
 -37 'MLS box behind antenna IJMN21'
 -37 'MLS cylinder QR21'
 -37 'MLS cylinder end'
 -77 'MLS LHS box ABCD22'
 -77 'MLS LHS box ABEF22'
 -21 'MLS LHS box CDGH22'
 -60 'MLS LHS box BFDH22'
 -40 'MLS LHS box AEGC22'
 -42 'MLS LHS box EFGH22'
 -37 'MLS LHS box EFIJ22'
 -21 'MLS LHS box IJQK22'
 -60 'MLS LHS box GHLR22'
 -40 'MLS LHS box JKHL22'
 -37 'MLS LHS box IQGR22'
 -21 'MLS LHS box QKOM22'
 -60 'MLS LHS box RLPN22'
 -42 'MLS LHS box QORP22'
 -28 'MLS large antenna BCDE24'
 -28 'MLS large antenna DEHI24'
 -28 'MLS large antenna HLL24'
 -28 'MLS large antenna BCFG24'
 -28 'MLS large antenna FGJK24'
 -28 'MLS large antenna JKM24'
 -37 'MLS large antenna BCDE24'
 -37 'MLS large antenna DEHI24'
 -37 'MLS large antenna HLL24'
 -37 'MLS large antenna BCFG24'
 -37 'MLS large antenna FGJK24'
 -37 'MLS large antenna JKM24'
 -32 'MLS large antenna CCEB24'
 -32 'MLS large antenna EEII24'
 -32 'MLS large antenna BBDD24'
 -32 'MLS large antenna DDHH24'
 -32 'MLS large antenna CCGS24'
 -32 'MLS large antenna GGGK24'
 -32 'MLS large antenna BBFF24'
 -32 'MLS large antenna FFJJ24'
 -32 'MLS large antenna IILL24'
 -32 'MLS large antenna KKMN24'
 -32 'MLS large antenna HLLI24'
 -32 'MLS large antenna JMMN24'
 -37 'MLS small antenna OPQR24'
 -37 'MLS small antenna QRU24'
 -28 'MLS small antenna OPQR24'
 -28 'MLS small antenna QRU24'
 -37 'MLS small antenna OPST24'
 -37 'MLS small antenna STV24'
 -28 'MLS small antenna OPST24'
 -28 'MLS small antenna STV24'
 -32 'MLS small antenna PPR24'
 -32 'MLS small antenna PPTT24'
 -32 'MLS small antenna RRUU24'
 -32 'MLS small antenna TTVV24'
 -32 'MLS small antenna OQQ24'
 -32 'MLS small antenna OOSS24'
 -32 'MLS small antenna QQUU24'
 -32 'MLS small antenna SSVV24'
 -28 'MLS antenna arm, RHS ABCD25'
 -28 'MLS antenna arm, RHS EF25'
 -28 'MLS antenna arm, RHS E25'
 -28 'MLS antenna arm, RHS F25'

-28 'MLS antenna arm, back GH25'
 -28 'MLS antenna arm, back IJ25'
 -28 'MLS antenna arm, back H25'
 -28 'MLS antenna arm, back J25'
 -28 'MLS antenna arm, back G25'
 -28 'MLS antenna arm, back I25'
 -28 'MLS antenna arm, between GK25'
 -28 'MLS antenna arm, between IL25'
 -28 'MLS antenna arm, side K25'
 -28 'MLS antenna arm, side L25'
 -7 'HGA-side bracework AB23'
 -7 'HGA-side bracework CB23'
 -7 'HGA-side bracework EB23'
 -7 'HGA-side bracework GB23'
 4 'HGA-side bracework IJ23'
 4 'HGA-side bracework KJ23'
 4 'HGA-side bracework MJ23'
 -25 'HGA-side bracework OJ23'
 -25 'HGA-side bracework QR23'
 -7 'Sphere junctn B23'
 4 'Sphere junctn J23'
 -25 'Sphere junctn R23'
 -7 'Dish above CLAES'
 -55 'Thrusters, AC26'
 -55 'Thrusters, BD26'
 -27 'HALOE mount A27'
 -27 'HALOE mount AB27'
 -27 'HALOE mount B27'
 -27 'HALOE mount BC27'
 -27 'HALOE mount C27'
 -27 'HALOE mount CD27'
 -27 'HALOE mount D27'
 -27 'HALOE mount DE27'
 -27 'HALOE mount E27'
 -24 'HALOE mount FGH127'
 -24 'HALOE mount JKL127'
 -24 'HALOE mount FGJK27'
 -24 'HALOE mount HILM27'
 -21 'HALOE mount FNR127'
 -21 'HALOE mount NFFQ27'
 -21 'HALOE mount RJTU27'
 -21 'HALOE mount HLQU27'
 -21 'HALOE mount NRPT27'
 -19 'HALOE mount VM27'
 -19 'HALOE mount V27'
 -19 'HALOE mount VX27'
 -19 'HALOE mount X27'
 -44 'HALOE box ABCD28'
 -19 'HALOE box GHIJ28'
 -17 'HALOE box BDNJ28'
 -44 'HALOE box CDEF28'
 -19 'HALOE box IJKL28'
 -36 'HALOE box CEIK28'
 -10 'HALOE box EFKL28'
 -17 'HALOE box DFJL28'
 -36 'HALOE box MNOP28'
 -36 'HALOE box QRST28'
 -9 'HALOE box QUVW28'
 -10 'HALOE box STWX28'
 -44 'HALOE box RVTX28'
 -19 'HALOE box QUSW28'
 -44 'HALOE box ABCD29'
 -10 'HALOE box EFGH29'
 -9 'HALOE box ABEF29'
 -17 'HALOE box BDFH29'
 -9 'HALOE box DHLM29'
 -44 'HALOE cover IJ29'
 -24 'HALOE cover JK29'
 -44 'HALOE aperture K29'
 -17 'HALOE sun-sensor NOPQ29'
 -9 'HALOE sun-sensor NORS29'
 -10 'HALOE sun-sensor PQTU29'
 -44 'HALOE sun-sensor NRPT29'
 -9 'HALOE sun-sensor OSQU29'
 -44 'HALOE aperture cover L29'
 -11 'SSPP support'
 -127 'ISAMS box DIOP15'
 -41 'ISAMS box HJQR15'
 -127 'ISAMS box OFST15'
 -41 'ISAMS box QRUV15'
 -127 'ISAMS box STWX15'
 -41 'ISAMS box UVYZ15'
 -9 'ISAMS box PRTV15'
 -14 'ISAMS box SUTV15'
 -127 'ISAMS box OLS15'
 -41 'ISAMS box QNU15'
 -44 'NEPS DCIL15'
 -3 'NEPS HGKL15'
 -28 'NEPS CGJL15'
 -8 'NEPS DHIK15'
 -7 'Dish above CLAES'
 -7 'Dish above CLAES'
 -37 'PEM-AXIS antenna J19'
 -37 'PEM-AXIS antenna J719'
 -35 'HRDI telescope box abef13'
 -21 'HALOE mount GIKM27'
 -21 'HALOE mount PQTU27'
 -66 'CLAES Neon vent A30'
 -66 'CLAES Neon vent AB30'
 -66 'CLAES Neon vent B30'
 -66 'CLAES CO2 vent CD30'
 -66 'CLAES CO2 vent D30'
 -22 'IM vent ABEF31'
 -22 'IM vent CDEF31'
 -22 'IM vent ACE31'
 -22 'IM vent BDF31'
 -27 'HALOE mount ACFG4'
 -27 'HALOE mount CDGH4'

Table 8: Typical Elemental Sonic Orifice Data

Data						Description
0.0254						scale
0.	-1.	0.				jet direction cosine, <i>Ne</i> vent
71.0	1.7	53.0				jet center
1.						jet radius
3.28E+20						jet density [molecules/m ³]
377.						jet velocity [m/sec]
207.						jet exit temperature [K]
0.	1.	0.	0.	0.	0.	species fraction in jet
-0.4924 0.6428 0.5868						jet direction cosine, <i>CO</i> ₂ vent
65.1 36.6 26.2						jet center
0.5						jet radius
4.04E+20						jet density [molecules/m ³]
244.						jet velocity [m/sec]
207.						jet exit temperature [K]
0.	0.	1.	0.	0.	0.	species fraction in jet

Table 9: Input Data Listing—General Preprocessor Input

```

*-----data to model gas around UARS
*
*-----CONVENTION:
*-----GAS species # 1: O
*-----GAS species # 2: Ne
*-----GAS species # 3: CO_2
*-----GAS species # 4: outgas # 1 molecular mass = 100
*-----GAS species # 5: outgas # 2 molecular mass = 150
*-----GAS species # 6: outgas # 3 molecular mass = 200
*-----No Internal energy, no chemistry
*
*-----IRA = 1 means chemistry is on
IRA = 0
*
*-----MVRT = maximum # of vibrational degrees of freedom in any species
MVRT = 0
*
* SP(1,L)= mass of a molecule of species L (Kg)
* SP(2,L)= diameter of a molecule of species L at T = TREF (meter)
*
* SP(3,L)= # of rotational deg. of freedom for species L
* SP(4,L)= index K pointing to the table of SPRR for rot. rel. of L
* IRROT(1)= switch for the # of collisions to relax rot. energy
* SPRR(K,1)= # of collisions to relax rotational energy
* SPRR(K,2)= polynomial coefficient; first order of temp
* SPRR(K,3)= polynomial coefficient; second order of temp
* SPRR(K,4)= polynomial coefficient; third order of temp
*
* SP(5,1)= index M pointing to the table of SPRR for vib. rel. of L
* IRVIB(1)= switch for the # of collisions to relax vib. energy
* SPRR(M,1)= # of collisions to relax vibrational energy
* SPRR(M,2)= polynomial coefficient; first order of temp
* SPRR(M,3)= polynomial coefficient; second order of temp
* SPRR(M,4)= polynomial coefficient; third order of temp
* SP(6,L)= Vibrational temperature
*
indexO = 1
indexNe = 2
indexCO2 = 3
indexO1 = 4
indexO2 = 5
indexO3 = 6
*
avogadro = 6.02252e+23
boltzmann = 1.38054e-23
*
*-----counter for internal energy table
itable = 0
*
*-----Monatomic Oxygen O
n = indexO
SP(1,n) = ( 16.0 * 1.e-3 ) / avogadro
SP(2,n) = 3.0e-10
SP(3,n) = 0.
SP(4,n) = 0.
SP(5,n) = 0.
SP(6,n) = 0.
SP(7,n) = 0.
SP(8,n) = 0.
SP(9,n) = 0.
*
*-----Neon Ne
n = indexNe
SP(1,n) = ( 20.179 * 1.e-3 ) / avogadro
SP(2,n) = 2.72e-10
SP(3,n) = 0.
SP(4,n) = 0.
*
*-----Carbon Dioxide CO_2
n = indexCO2
SP(1,n) = ( 44.01 * 1.e-3 ) / avogadro
SP(2,n) = 5.41e-10
SP(3,n) = 0.
SP(4,n) = 0.
SP(5,n) = 0.
SP(6,n) = 0.
SP(7,n) = 0.
SP(8,n) = 0.
SP(9,n) = 0.
*
*-----Outgassing gas # 1
n = indexO1
SP(1,n) = ( 100.0 * 1.e-3 ) / avogadro
SP(2,n) = SP(2,indexO)*(SP(1,n)/SP(1,indexO))**.3333
SP(3,n) = 0.
SP(4,n) = 0.
SP(5,n) = 0.
SP(6,n) = 0.
SP(7,n) = 0.
SP(8,n) = 0.
SP(9,n) = 0.
*
*-----Outgassing gas # 2
n = indexO2
SP(1,n) = ( 150.0 * 1.e-3 ) / avogadro
SP(2,n) = SP(2,indexO)*(SP(1,n)/SP(1,indexO))**.3333
SP(3,n) = 0.
SP(4,n) = 0.
SP(5,n) = 0.
SP(6,n) = 0.
SP(7,n) = 0.
SP(8,n) = 0.
SP(9,n) = 0.
*
*-----Outgassing gas # 3
n = indexO3
SP(1,n) = ( 200.0 * 1.e-3 ) / avogadro
SP(2,n) = SP(2,indexO)*(SP(1,n)/SP(1,indexO))**.3333
SP(3,n) = 0.
SP(4,n) = 0.
SP(5,n) = 0.
SP(6,n) = 0.
SP(7,n) = 0.
SP(8,n) = 0.
SP(9,n) = 0.
*
*-----max. no. of tables for rot. & vib. relaxation (SPRR)
MRCFFE= max(itable,1)
*
*-----Data for Tref, W, molecular diam.: from J. Moss
Tref=300.
W = 0.75
*
*-----
*
110 continue

```


Table 10: Outgassing Species Information

Species	GMW	d [Å]	Mass Flux Rates at 100°C [gm/cm ² /sec]
fictional organic volatile species representing products from MLI	100	5.33	4.33×10^{-13} to 6.01×10^{-12}
fictional organic volatile species representing products from solar array adhesives	100	5.33	1.83×10^{-10}
fictional organic volatile species representing products from IM and MLI vents	100	5.33	1.60×10^{-7} (IM) 1.22×10^{-8} (MLI)
fictional organic volatile species representing products from MMS vents	100	5.33	3.67×10^{-11} to 1.22×10^{-10}
fictional organic volatile species representing products from Chemglaze Z306	150	6.33	7.70×10^{-11}
fictional organic volatile species representing products from S/13G/LO-V10	200	6.96	4.30×10^{-11} to 5.39×10^{-11}
neon vented from CLAES experiment	20.18	2.72	$4.14 \times 10^{-4*}$
carbon dioxide vented from CLAES experiment	44.01	5.41	$7.20 \times 10^{-4*}$

* rate at operating temperature $T_{\text{exit}} = 207K$

Table 11: Gas Species Data

0	spatial resolution switch: body-0, gas-1
7.	max no. of Megabytes for body defn.
30000	ratio to compute mean no. of subcells/cell
0.5	ratio of cells near body
0	initially uniform freestream or vacuum
6	total no. of molecular species
2	no. of jet species (subset of total no. of species)
132	GAS?.FOR file (species-dependent gas info.)
7500.	free stream velocity
0.	angle of incidence alpha (deg)
0.	roll angle phi (deg)
6.e+12 1000.	freestream density, temp.
1. 0. 0. 0. 0. 0.	fraction of each species in freestream
300.	surface temp.
300.	mean expected temp. in flow
2 2 2 0 2 2	boundary conds. at -X, -Y, -Z, +X, +Y, +Z
1. 1. 1000.	safety factors for max no. of molecules, timestep, FNUM
20. 10. 10. 10. 10. 10.	clearances for -X, +X, -Y, +Y, -Z, +Z edges
350000	no. of subcells within computational domain
2	scale ratio between inner & outer domains
3. 0.28	anticipated density enhancements: peak, mean (used to estimate cell and subcell sizes)
1.	fraction of total volume to be used
2 50	no. of timesteps between sampling, no. of samples between saved states
2	parameter used to size pixel element arrays

Table 12: Mass Flux Rates Intercepted at HALOE Aperture

Species	Mass Flux Rates [$gm/cm^2/sec$]		
	Case #1	Case #2	Case #3
monatomic oxygen from freestream distribution	1.2×10^{-10}	1.0×10^{-10}	$< 4.2 \times 10^{-14}$ *
monatomic oxygen from surface-accommodated distribution	9.3×10^{-12}	7.5×10^{-12}	5.4×10^{-12}
neon vented from CLAES experiment (return flux)	1.9×10^{-11}	5.9×10^{-12}	$< 2.1 \times 10^{-12}$ *
neon vented from CLAES experiment (direct flux)	1.3×10^{-11}	5.9×10^{-12}	$< 2.1 \times 10^{-12}$ *
carbon dioxide vented from CLAES experiment	$< 5.8 \times 10^{-12}$ *	$< 6.5 \times 10^{-12}$ *	$< 4.6 \times 10^{-12}$ *
fictitious organic volatile species representing all $GMW = 100$ materials	9.2×10^{-14}	1.8×10^{-13}	8.4×10^{-14}
fictitious organic volatile species representing $GMW = 150$ material	3.9×10^{-15}	1.1×10^{-14}	1.4×10^{-14}
fictitious organic volatile species representing $GMW = 200$ material	4.3×10^{-13}	1.8×10^{-14}	2.7×10^{-13}

* no samples collected

Table 13a: Subassembly Contributions to Cumulative Contaminant Deposition (Case #1)

Subassembly	Percent Contribution to Contaminant Flux		
	$GMW = 100$	$GMW = 150$	$GMW = 200$
Solar Panel ($\Omega = 0.527$ steradians)	56	—	81
Instrument Module ($\Omega = 0.719$ steradians)	13	—	19
HALOE	25	73	—
NEPS	3	27	—
ISAMS	3	—	—

Table 13b: Subassembly Contributions to Cumulative Contaminant Deposition (Case #2)

Subassembly	Percent Contribution to Contaminant Flux		
	<i>GMW</i> = 100	<i>GMW</i> = 150	<i>GMW</i> = 200
Solar Panel ($\Omega = 0$ steradians)	92	—	—
Instrument Module ($\Omega = 0.292$ steradians)	—	—	100
HALOE	8	80	—
NEPS	—	20	—

Table 13c: Subassembly Contributions to Cumulative Contaminant Deposition (Case #3)

Subassembly	Percent Contribution to Contaminant Flux		
	<i>GMW</i> = 100	<i>GMW</i> = 150	<i>GMW</i> = 200
Solar Panel ($\Omega = 0.412$ steradians)	75	—	94
Instrument Module ($\Omega = 0.0354$ steradians)	13	—	6
HALOE	12	100	—

Table 14: Cumulative Volatile Organic Contaminant Deposition at HALOE Aperture (values based on d_0 in parentheses)

Species	Cumulative Depth Over 35 Months [\AA]		
	Case #1	Case #2	Case #3
fictitious organic volatile species representing all <i>GMW</i> = 100 materials	9496 (1602)	9787 (1652)	4663 (787)
fictitious organic volatile species representing <i>GMW</i> = 150 material	683 (173)	408 (103)	524 (133)
fictitious organic volatile species representing <i>GMW</i> = 200 material	13355 (4507)	489 (165)	7460 (2518)
total extrapolated accumulation per run	23534 (6282)	10684 (1920)	12647 (3438)

Table 15: Cumulative Volatile Organic Contaminant Deposition at HALOE Aperture—Arrival at Case-Averaged Total Deposition
(values based on d_O in parentheses)

Item	Amount Based On $l = 10\text{\AA}$ [\AA]	Amount Based On $d_O = 3.0\text{\AA}$ [\AA]
Average for runs #1 & #2	17109	(4101)
Avg. $\times (1 - \tau_{\text{stow}}/\tau_{\text{orbit}})$	2673	(641)
Average for run #3	12647	(3438)
Avg. $\times \tau_{\text{stow}}/\tau_{\text{orbit}}$	10671	(2901)
Case-averaged Total Deposition	13344	(3542)

Table 16: Simulation Set-Up and Performance

Item	Inner Domain	Outer Domain
Δt [sec]	1.35×10^{-5}	2.69×10^{-5}
<i>FNUM</i>	2.08×10^{13}	4.17×10^{13}
Volume [m^3]	$11.21 \times 6.97 \times 15.75$	$21.20 \times 21.20 \times 21.20$
CCM Resolution	$74 \times 46 \times 104$	$70 \times 70 \times 70$
FCM Resolution w/in CCM	$3 \times 3 \times 3$	$1 \times 1 \times 1$
No. of cells	34,900	7,530
No. of simulated molecules	329,000	404,000
Total CPU time [hrs]	191	150
Memory required [Mbytes]	60	40
Performance [$\mu\text{sec}/\text{particle}/\Delta t$]	44	29

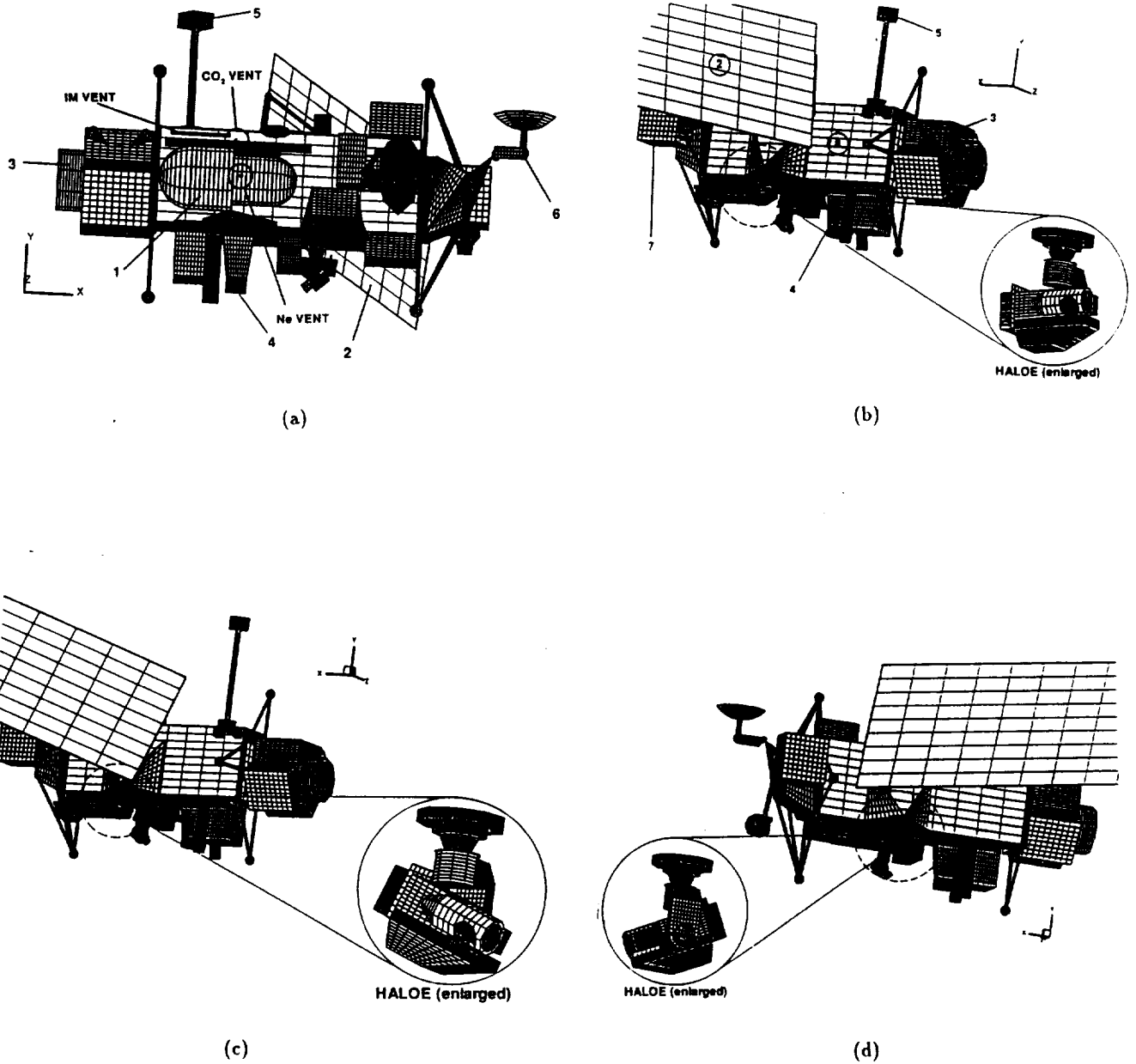


Figure 1. UARS model used in DSMC simulation: (a) +z side, Case 1; (b) -z side, Case 1; (c) -z side, Case 2; (d) -z side, Case 3. Key: 1-Cryogenic Limb Array Etalon Spectrometer (CLAES), 2-Solar panel (SP), 3-Multi-mission Modular Spacecraft (MMS), 4-Nadir Energetic Particle Spectrometer (NEPS), 5-Zenith Energetic Particle Spectrometer (ZEPS), 6-High Gain Antenna (HGA), 7-Solar/Stellar Positioning Platform (SSPP), and 8-Instrument Module (IM).

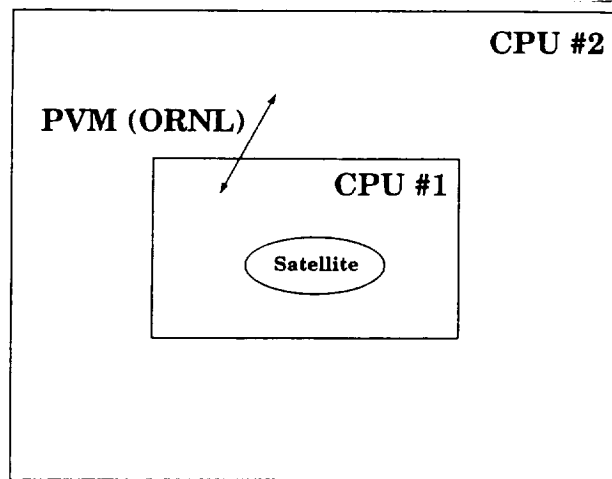


Figure 2. Schematic representation of computational flowfield volume used with parallelization routines.

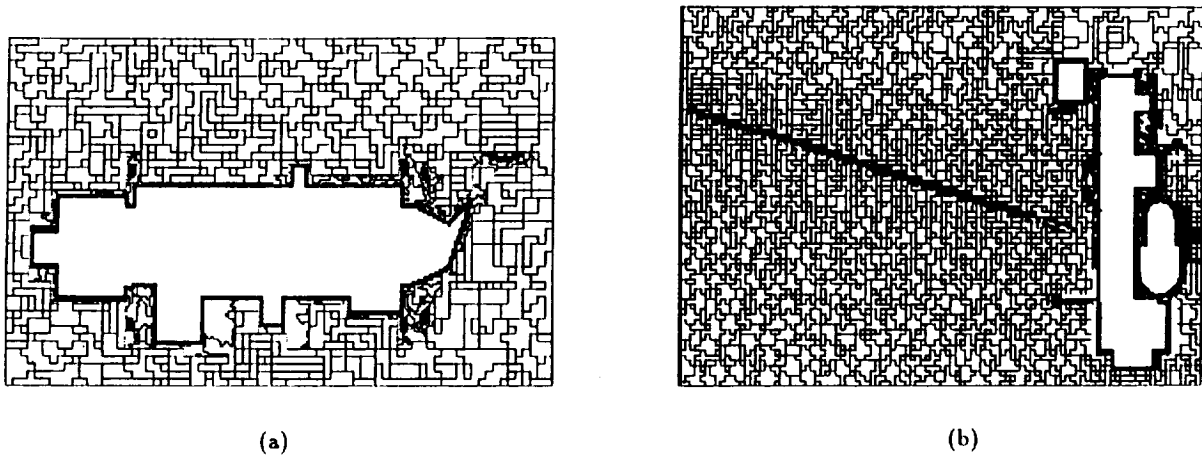


Figure 3. Representative cross-sections of computational grid for DSMC simulation; (a) inner domain at $Z = 0$, (b) inner domain at $Y = 0$.

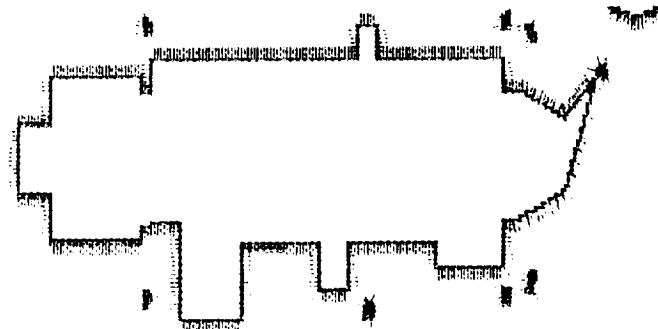


Figure 4. Representative cross-section of UARS geometric model discretized for incorporation into DSMC code. Outward-pointed normals included with surface pixel locations.

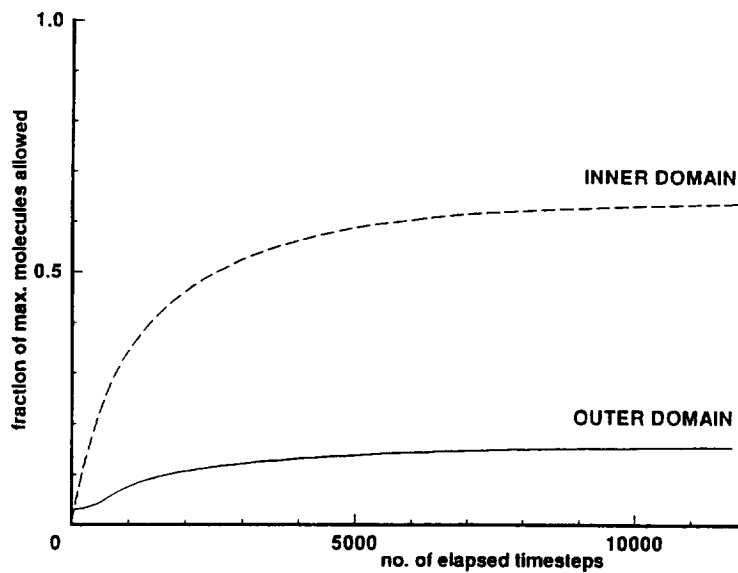


Figure 5. Typical behavior for number of particles per timestep versus simulated elapsed time as steady state is approached.

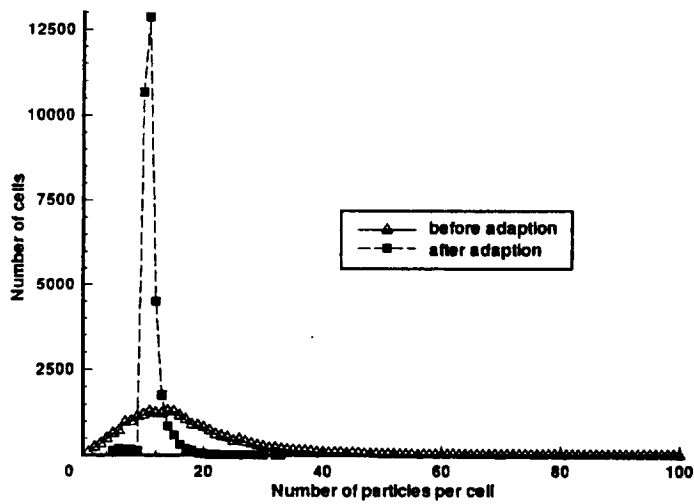


Figure 6. Typical distribution of particles per inner-domain cell before and after grid adaption.

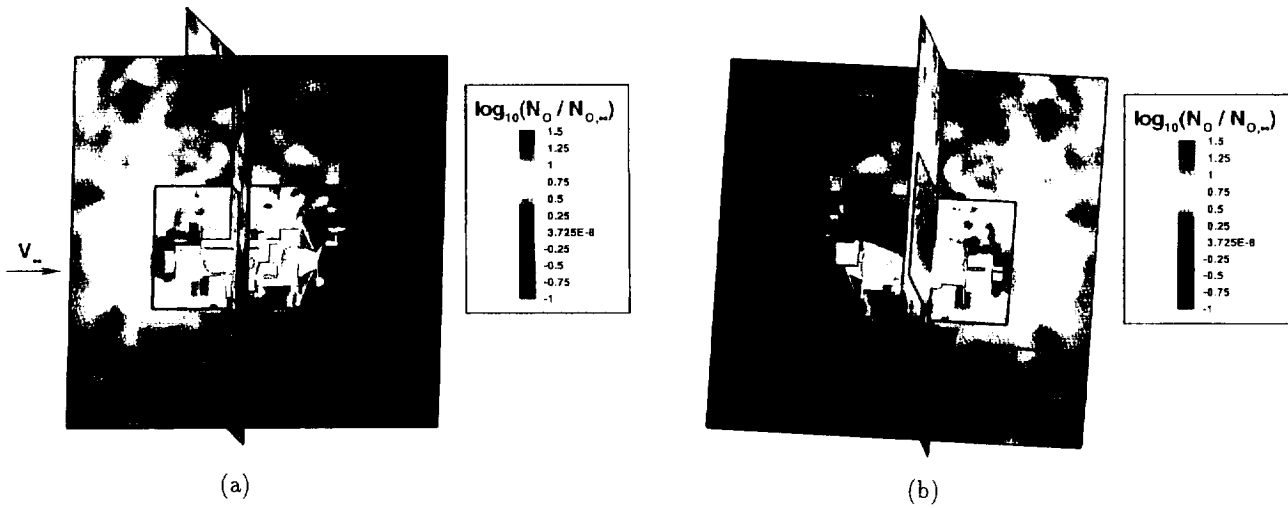


Figure 7. Case 1 number density contours of freestream species O , logarithmic scale nondimensionalized by freestream number density $[O]_\infty$: (a) +Z side, (b) -Z side.

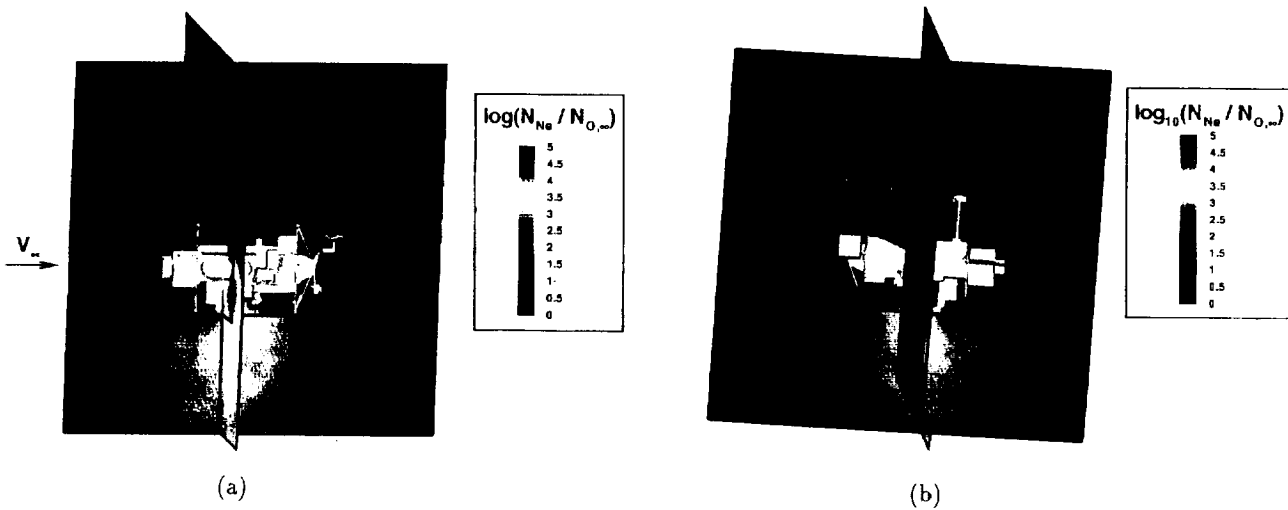


Figure 8. Case 1 number density contours of neon, logarithmic scale nondimensionalized by $[O]_\infty$: (a) +Z side, (b) -Z side.

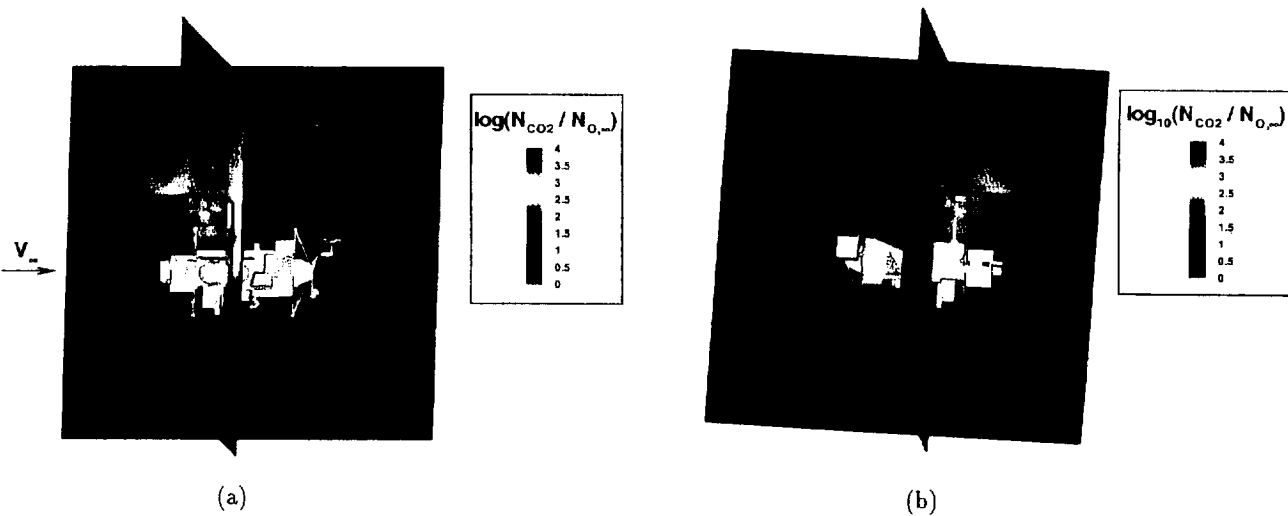


Figure 9. Case 1 number density contours of carbon dioxide, logarithmic scale nondimensionalized by $[O]_\infty$: (a) +Z side, (b) -Z side.

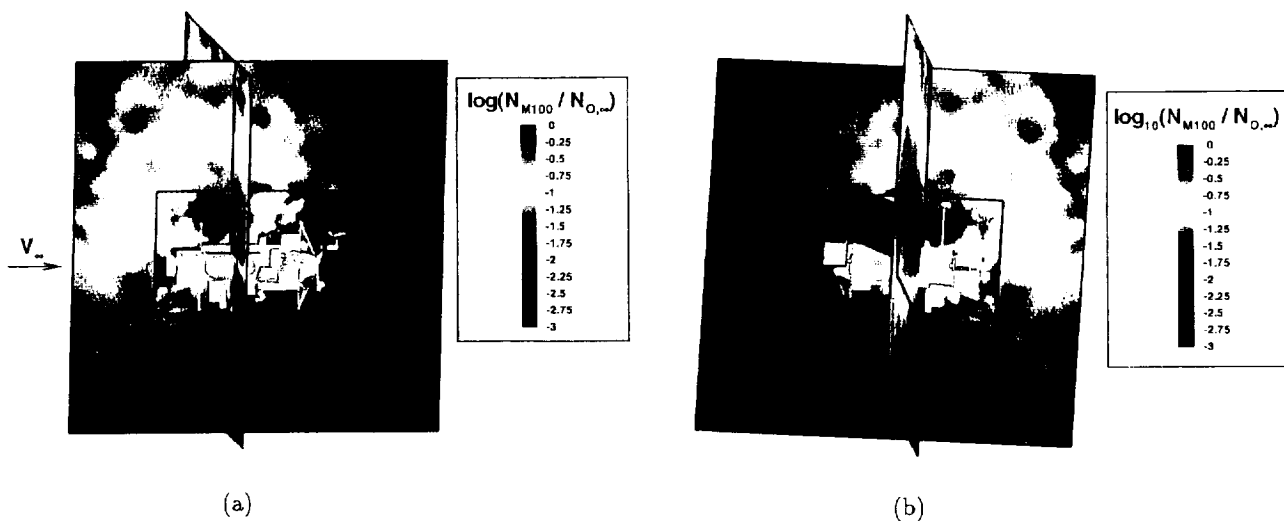


Figure 10. Case 1 number density contours of $GMW = 100$ outgassing species, logarithmic scale nondimensionalized by $[O]_\infty$: (a) $+Z$ side, (b) $-Z$ side.

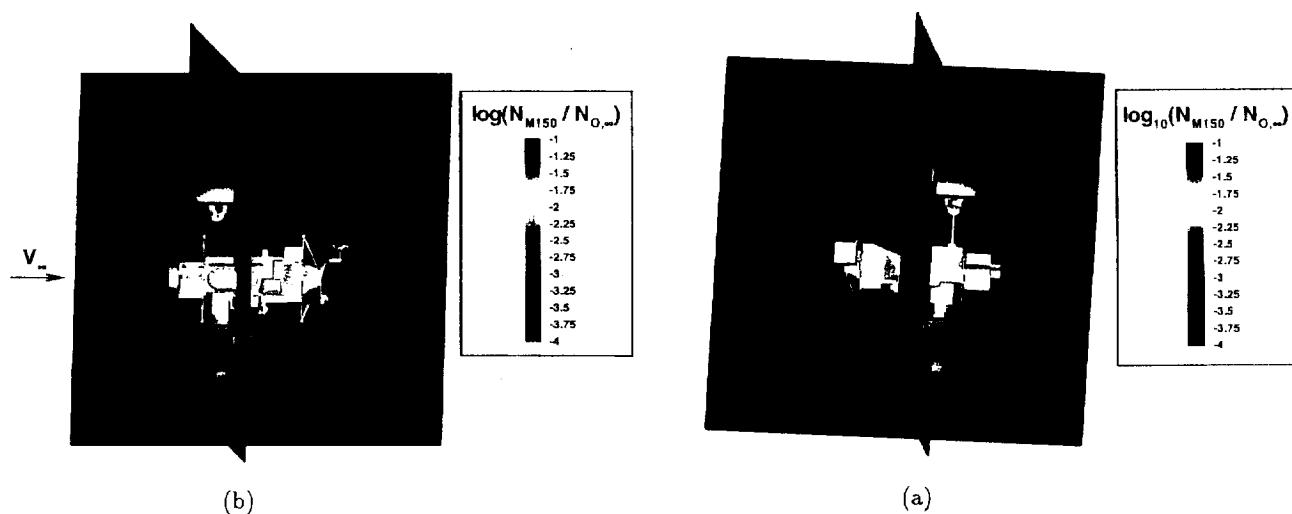


Figure 11. Case 1 number density contours of $GMW = 150$ outgassing species, logarithmic scale nondimensionalized by $[O]_\infty$: (a) $+Z$ side, (b) $-Z$ side.

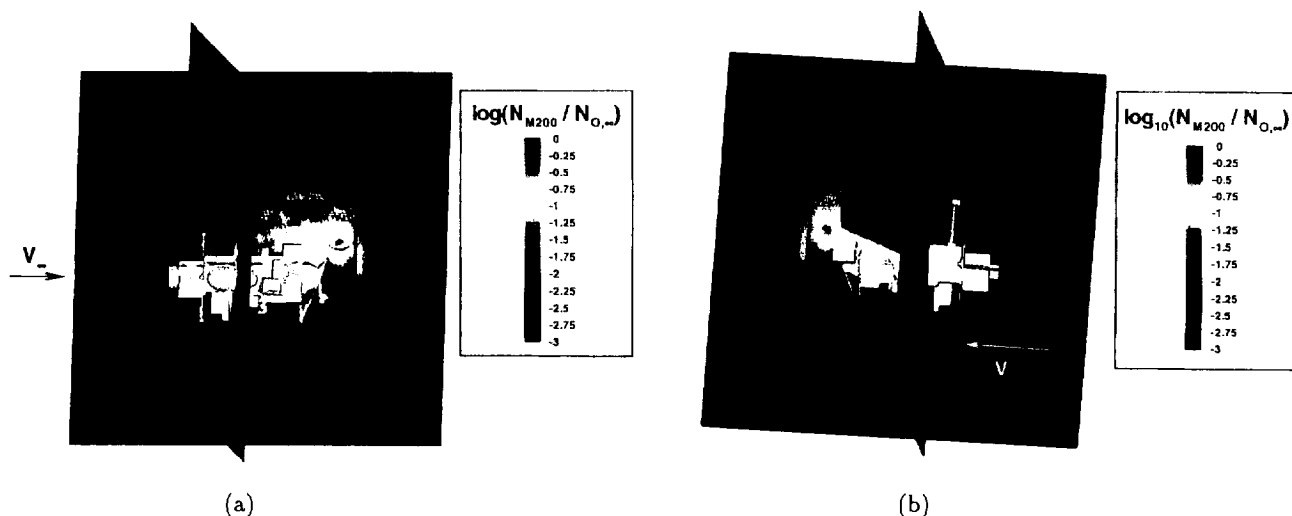


Figure 12. Case 1 number density contours of $GMW = 200$ outgassing species, logarithmic scale nondimensionalized by $[O]_\infty$: (a) $+Z$ side, (b) $-Z$ side.

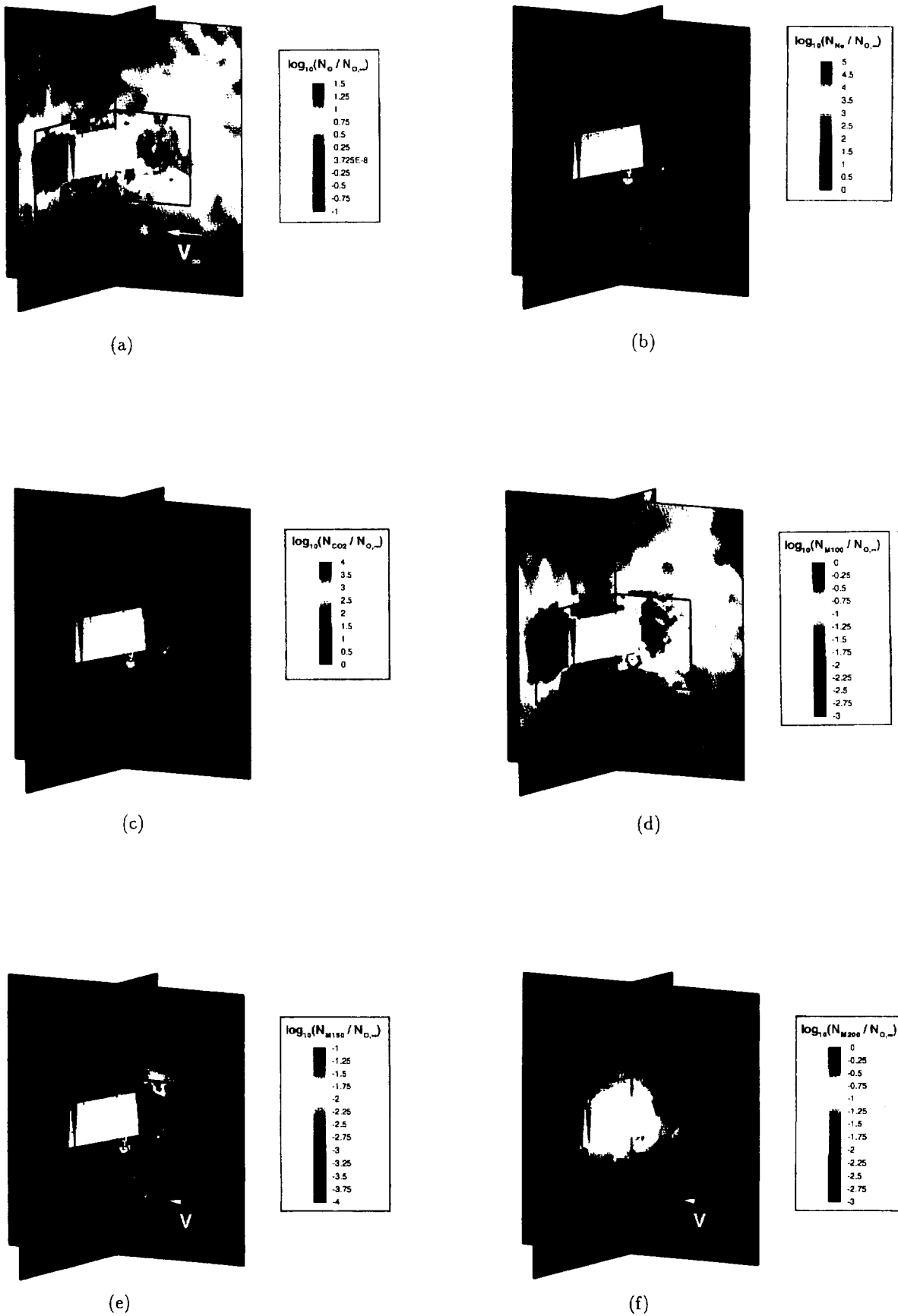


Figure 13. Case 1 species number density contour maps emphasizing the HALOE aperture environment. Logarithmic scale nondimensionalized by freestream number density $[O]_{\infty}$: (a) monatomic oxygen, (b) neon, (c) carbon dioxide, (d) $GMW = 100$ species, (e) $GMW = 150$ species, and (f) $GMW = 200$ species.

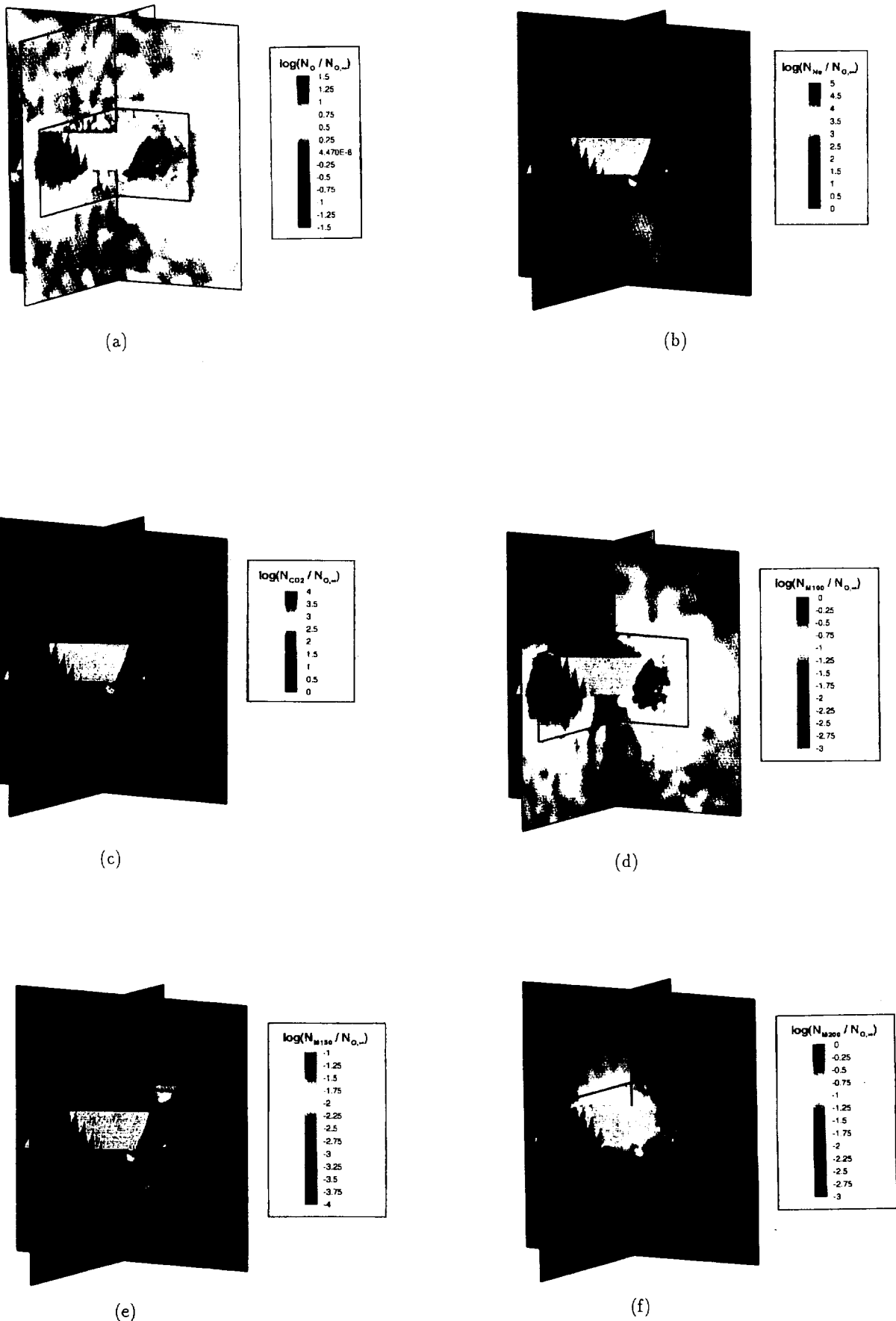


Figure 14. Case 2 species number density contour maps emphasizing the HALOE aperture environment. Logarithmic scale nondimensionalized by freestream number density $[O]_{\infty}$: (a) monatomic oxygen, (b) neon, (c) carbon dioxide, (d) $GMW = 100$ species, (e) $GMW = 150$ species, and (f) $GMW = 200$ species.

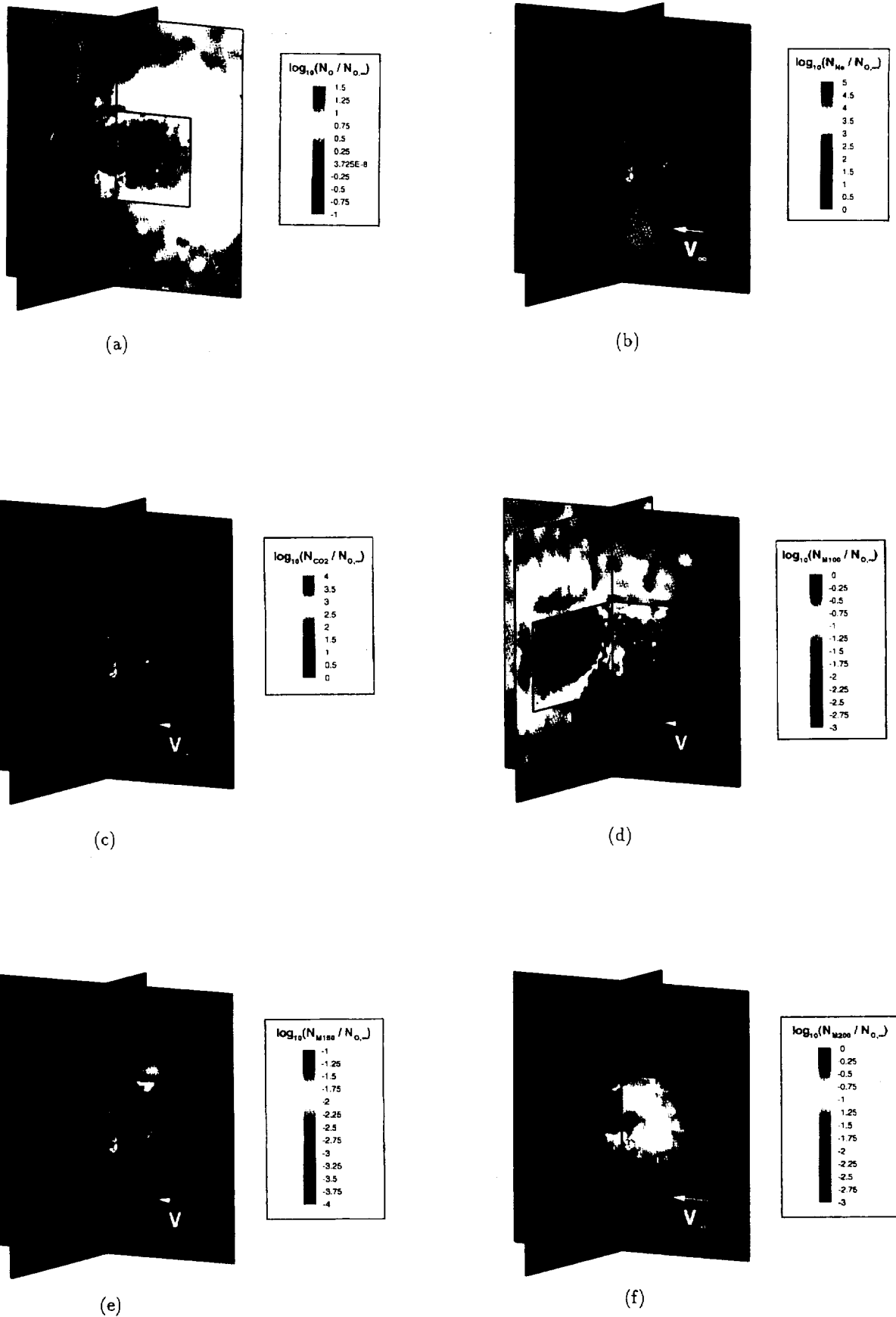
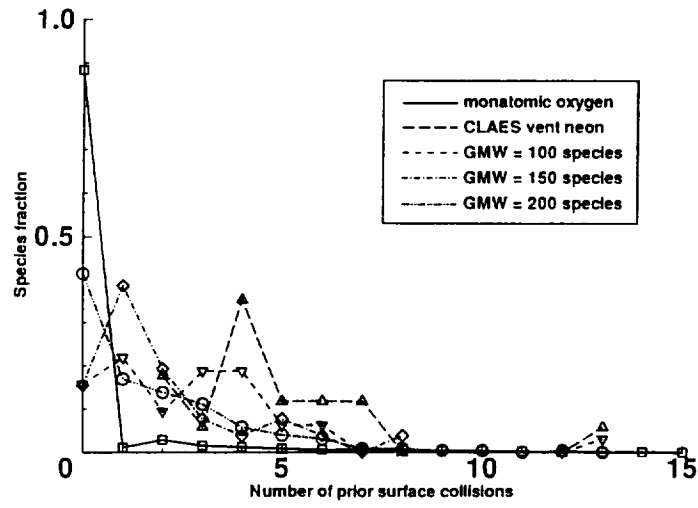
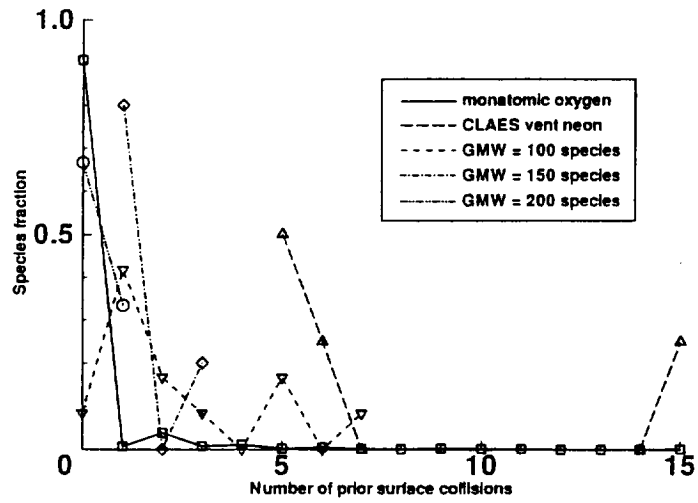


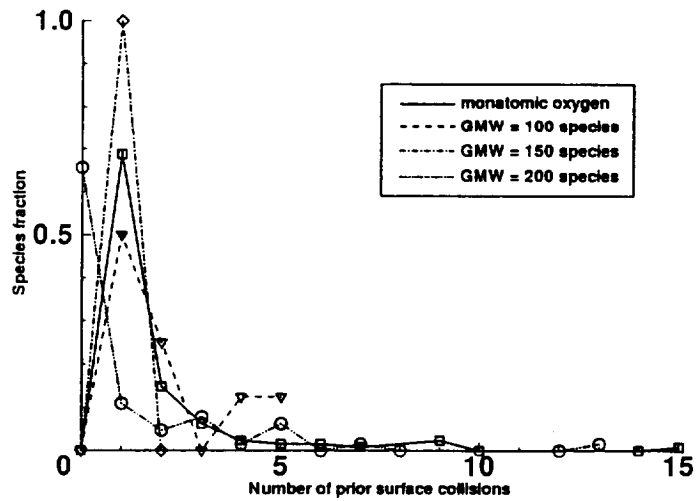
Figure 15. Case 3 species number density contour maps emphasizing the HALOE aperture environment. Logarithmic scale nondimensionalized by freestream number density $[O]_\infty$: (a) monatomic oxygen, (b) neon, (c) carbon dioxide, (d) $GMW = 100$ species, (e) $GMW = 150$ species, and (f) $GMW = 200$ species.



(a)

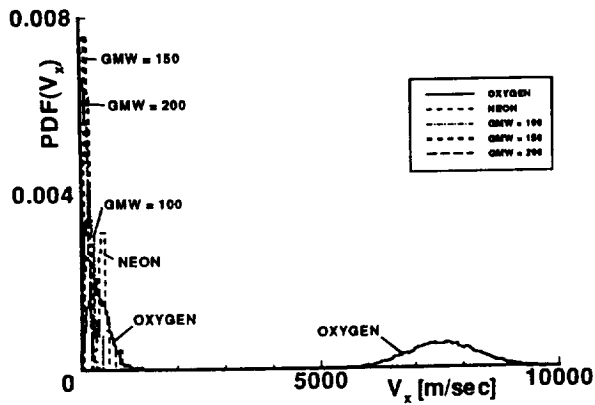


(b)

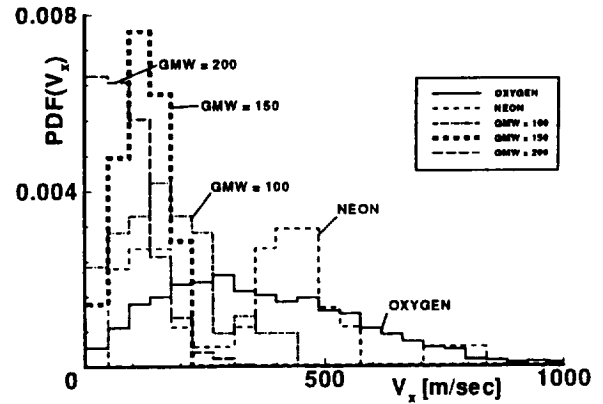


(c)

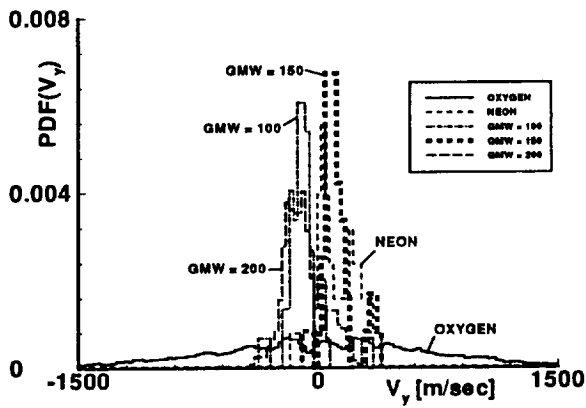
Figure 16. Number of surface collisions encountered by particles prior to striking the HALOE aperture: (a) Case 1, (b) Case 2, and (c) Case 3.



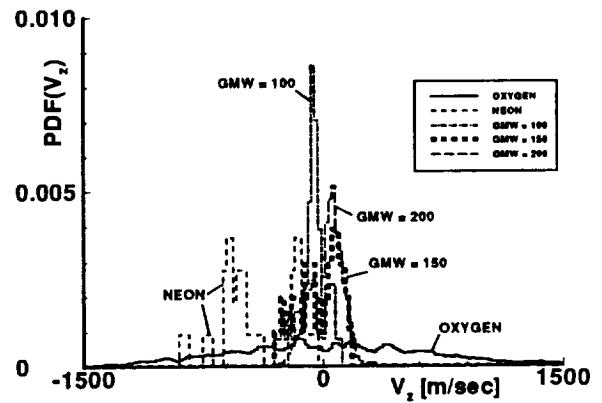
(a)



(b)

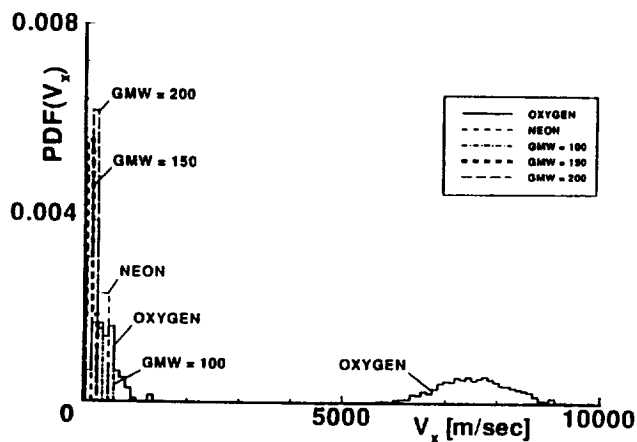


(c)

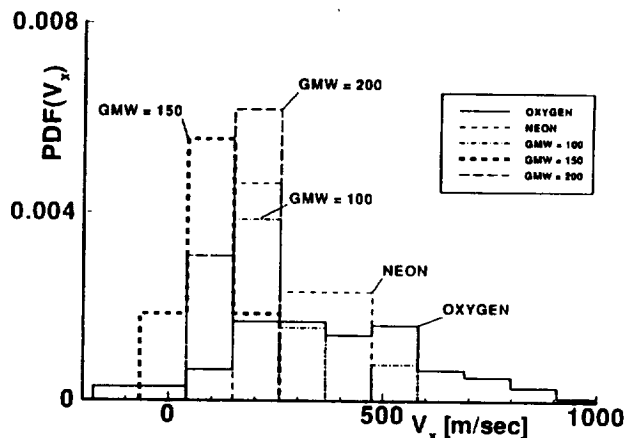


(d)

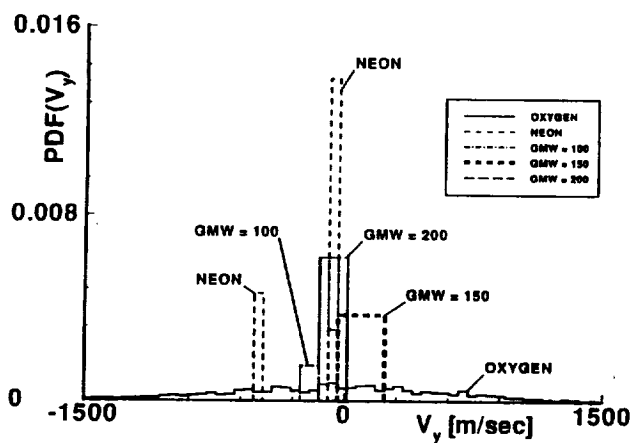
Figure 17. Case 1 histograms representing velocity distribution functions for particles striking the HALOE aperture: (a) X direction, (b) Y direction, (c) Z direction.



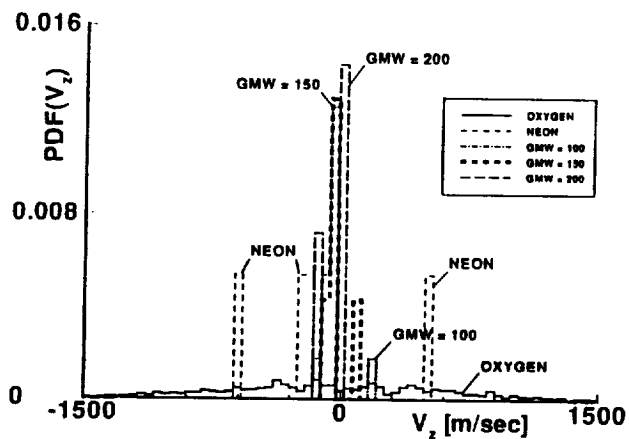
(a)



(b)

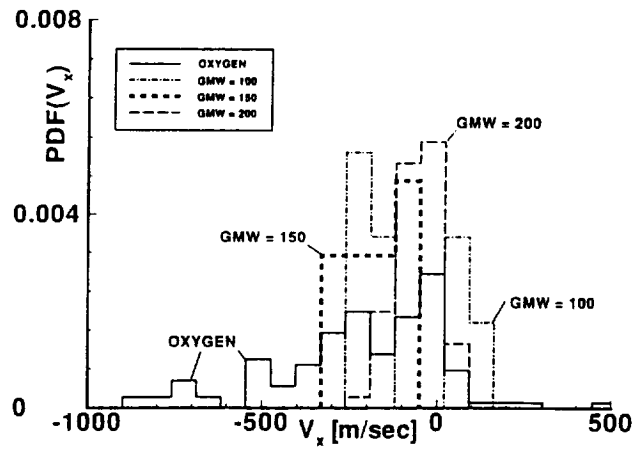


(c)

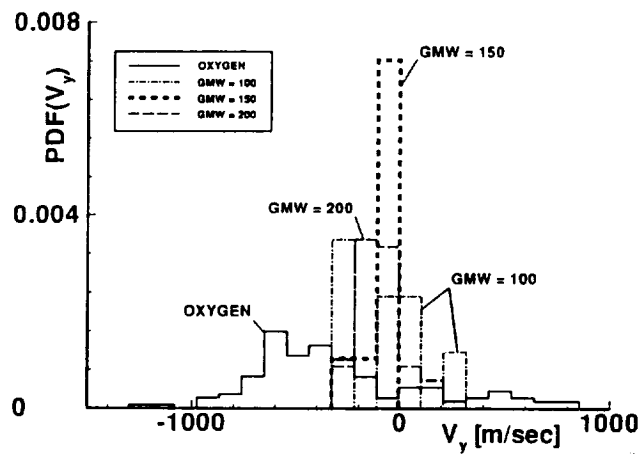


(d)

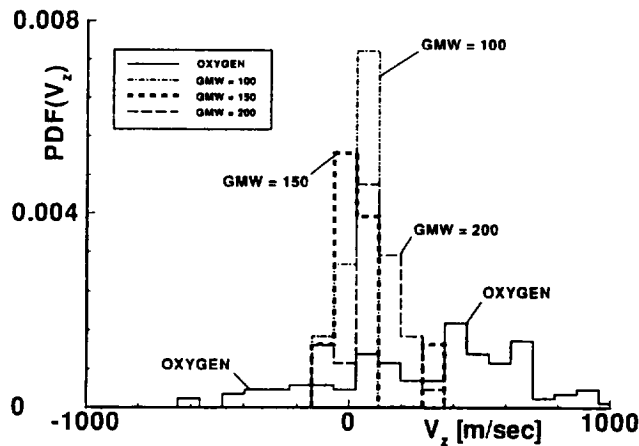
Figure 18. Case 2 histograms representing velocity distribution functions for particles striking the HALOE aperture: (a) X direction, (b) Y direction, (c) Z direction.



(a)

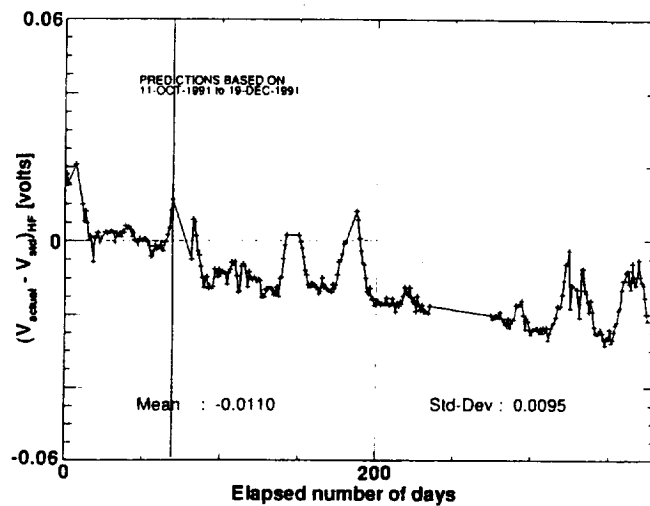


(b)

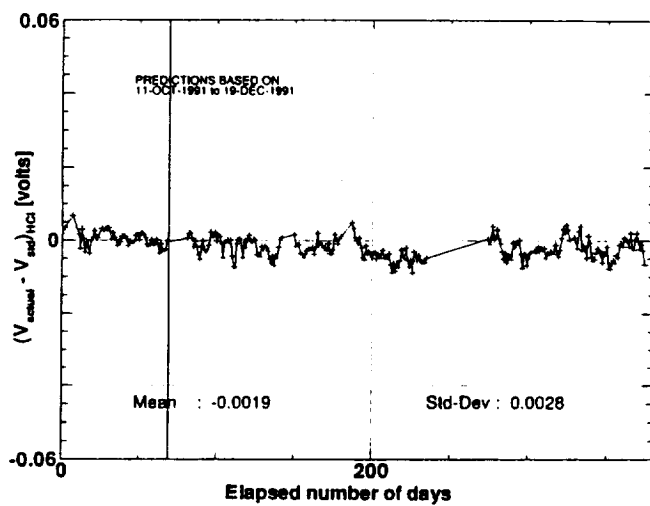


(c)

Figure 19. Case 3 histograms representing velocity distribution functions for particles striking the HALOE aperture: (a) X direction, (b) Y direction, (c) Z direction.



(a)



(b)

Figure 20. Actual HALOE signal attenuation measurements between October 11, 1991 and October 20, 1992 for (a) HF and (b) HCl species.

REPORT DOCUMENTATION PAGE

Form Approved
OMB No. 0704-0188

Public reporting burden for this collection of information is estimated to average 1 hour per response, including the time for reviewing instructions, searching existing data sources, gathering and maintaining the data needed, and completing and reviewing the collection of information. Send comments regarding this burden estimate or any other aspect of this collection of information, including suggestions for reducing this burden, to Washington Headquarters Services, Directorate for Information Operations and Reports, 1215 Jefferson Davis Highway, Suite 1204, Arlington, VA 22202-4302, and to the Office of Management and Budget, Paperwork Reduction Project (0704-0188), Washington, DC 20503.

1. AGENCY USE ONLY (Leave blank)		2. REPORT DATE August 1994	3. REPORT TYPE AND DATES COVERED Technical Memorandum	
4. TITLE AND SUBTITLE Direct Simulation Monte Carlo Prediction of On-Orbit Contaminant Deposit Levels for HALOE			5. FUNDING NUMBERS WU 232-01-04-04	
6. AUTHOR(S) Michael S. Woronowicz and Didier F. G. Rault				
7. PERFORMING ORGANIZATION NAME(S) AND ADDRESS(ES) NASA Langley Research Center Hampton, VA 23681-0001			8. PERFORMING ORGANIZATION REPORT NUMBER	
9. SPONSORING / MONITORING AGENCY NAME(S) AND ADDRESS(ES) National Aeronautics and Space Administration Washington, DC 20546-0001			10. SPONSORING / MONITORING AGENCY REPORT NUMBER NASA TM-109069	
11. SUPPLEMENTARY NOTES Woronowicz: ViGYAN, Inc., Hampton, VA and Rault: Langley Research Center, Hampton, VA.				
12a. DISTRIBUTION / AVAILABILITY STATEMENT Unclassified-Unlimited Subject Category 34			12b. DISTRIBUTION CODE	
13. ABSTRACT (Maximum 200 words) A three-dimensional version of the direct simulation Monte Carlo method is adapted to assess the contamination environment surrounding a highly detailed model of the Upper Atmosphere Research Satellite. Emphasis is placed on simulating a realistic, worst-case set of flow field and surface conditions and geometric orientations for the satellite in order to estimate an upper limit for the cumulative level of volatile organic molecular deposits at the aperture of the Halogen Occultation Experiment. A detailed description of the adaptation of this solution method to the study the satellite's environment is also presented. Results pertaining to the satellite's environment are presented regarding contaminant cloud structure, cloud composition, and statistics of simulated molecules impinging on the target surface, along with data related to code performance. Using procedures developed in standard contamination analyses, along with many worst-case assumptions, the cumulative upper-limit level of volatile organic deposits on HALOE's aperture over the instrument's 35-month nominal data collection period is estimated at about 13,350 A.				
14. SUBJECT TERMS direct simulation Monte Carlo, outgassing, satellite contamination, direct flux, return flux, Upper Atmosphere Research Satellite (UARS), and Halogen Occultation Experiment (HALOE)			15. NUMBER OF PAGES 113	
			16. PRICE CODE A06	
17. SECURITY CLASSIFICATION OF REPORT Unclassified	18. SECURITY CLASSIFICATION OF THIS PAGE Unclassified	19. SECURITY CLASSIFICATION OF ABSTRACT	20. LIMITATION OF ABSTRACT	